ANNUAL REPORT

Center for Experimental Nuclear Physics and Astrophysics
University of Washington
May, 2004

Sponsored in part by the United States Department of Energy under Grant #DE-FG02-97ER41020/A000.

Cover photos, clockwise from upper right:

1. A view into the SNO acrylic vessel showing the Remotely Operated Vehicle (ROV), which is used to install the Neutral Current Detectors (NCDs), some of which also appear in the picture. See Sec. 2.10. (Photo by John Amsbaugh)

2. Minesh Bacrania mounting targets in the 24” scattering chamber. See Sec. 3.3. (Photo by Derek Storm)

3. A torsion pendumum used for measuring gravity gradients. See Sec. 1.7. (Photo by Ki-Young Choi)

4. Joe Formaggio and Laura Stonehill operating the ROV while installing NCDs. See Sec. 2.10. (Photo by Jaret Heise)

INTRODUCTION

CENPA pursues a broad program of research in nuclear physics, astrophysics and related fields. Research activities are conducted locally and at remote sites. The current program includes "in-house" research on nuclear collisions and fundamental interactions using the local tandem Van de Graaff, as well as local and remote non-accelerator research on fundamental interactions and user-mode research on relativistic heavy ions at large accelerator facilities in the U.S. and Europe.

Our ^{7}Be(p,γ)^{8}B measurements have been completed and published. Three separate cross section measurements with 3 different (radioactive) targets are in excellent agreement, and determine the astrophysical S-factor to an experimental precision of $\pm$ 3% ($\pm$ 4% including theoretical extrapolation uncertainty). We have begun work on the $^{3}\mathrm{He}(\alpha,\gamma)^{7}\mathrm{Be}$ reaction, which is also very important in solar neutrino production.

The Gravity group has become a member of the LISA gravity wave detector project. The end masses of the LISA interferometer must be kept inertial at very delicate levels. An ultra-sensitive torsion balance instrument has been built to characterize small forces that may act on the end masses.

An initial broad survey of correlations and fluctuations in RHIC Au-Au and p-p collisions has been completed, revealing substantial evidence for a dissipative colored medium in central Au-Au collisions and several surprises relative to theoretical predictions. Among the findings: 1) p-p momentum distributions are precisely separated into soft and hard components, corresponding to string and minijet fragmentation respectively, which provide an essential reference for Au-Au collisions, 2) minijets in central Au-Au collisions are found to be strongly elongated along the collision axis and narrowed in azimuth, this trend being true for both angular correlations and transverse momentum correlations, and 3) the geometry of hadronization in central Au-Au collisions is demonstrated to be two-dimensional, in contrast to the previously-observed one-dimensional string fragmentation geometry in p-p.

The second phase of operation of the Sudbury Neutrino Observatory, in which salt was added to the heavy water to enhance sensitivity to the neutral-current interaction of solar neutrinos, was completed in September, 2003. An analysis of 254 live days of these data was released at the Topics in Astroparticle and Underground Physics international conference in Seattle. The new results have ruled out maximal mixing for solar neutrinos at more than 5 standard deviations, and disfavor the higher-mass "LMA-II" solution to the solar neutrino problem at greater than 99 % confidence level.

The salt has been removed from the SNO detector and 40 strings of ^{3}He counters have been installed to give SNO an event-by-event capability for discriminating neutral-current events from charged-current. Initial performance of the array is very satisfactory.

An integrated data-acquisition system has been commissioned to make possible the simultaneous collection of data from the photomultiplier array and the NCD array in SNO. The system integrates a new object-oriented realtime control and acquisition system, ORCA, with the existing SHaRC system, both developed at UW.

Design and construction of a grid to suppress backgrounds in the prespectrometer for the

KATRIN tritium beta decay experiment is nearing completion. The prespectrometer, the first module of this major new neutrino mass experiment, will be commissioned in 2004.

The emiT experiment collected over 350 million coincidences during its recently concluded data collection run at the NG-6 beamline at the NIST Center for Neutron Research (NCNR) in Gaithersburg, MD. Analysis of these data is underway, and should yield a statistical sensitivity to the time-violating coefficient "D" of 2×10^{-4}, which would exceed emiT's original design goal by about a factor of 1.5.

The source of Ultra-cold neutrons at LANL has been built, and the first production run successfully produced UCNs. We have started mounting the apparatus for measuring the beta-asymmetry from polarized-neutron decay and we expect to start taking data in October of 2004.

Using the Tandem, we have taken data that should yield the mass of the lowest T=2 state in ^{32}S to within $\Delta m/m \approx 10^{-8}$. We are currently analyzing the data and calculating systematic uncertainties.

In collaboration with the INT, we sponsored the Eighth International Workshop on Topics in Astrophysics and Underground Physics during September. This major conference is held every two years, and sponsoring such conferences is part of CENPA's mandate.

Initial exploration into the establishment of a Joint Institute for Advanced Detector Technology between the University of Washington and Pacific Northwest Laboratories received strong endorsement by the administrations of both institutions. A more detailed proposal is being pursued.

As always, we encourage outside applications for the use of our facilities. As a convenient reference for potential users, the table on the following page lists the capabilities of our accelerators. For further information, please contact Prof. Derek W. Storm, Executive Director, CENPA, Box 354290, University of Washington, Seattle, WA 98195; (206) 543-4080, or storm@npl.washington.edu. Further information is also available on our web page: http://www.npl.washington.edu.

We close this introduction with a reminder that the articles in this report describe work in progress and are not to be regarded as publications or to be quoted without permission of the authors. In each article the names of the investigators are listed alphabetically, with the primary author underlined, to whom inquiries should be addressed.

Derek Storm, Editor — Barbara Fulton, Assistant Editor

TANDEM VAN DE GRAAFF ACCELERATOR

A High Voltage Engineering Corporation Model FN purchased in 1966 with NSF funds, operation funded primarily by the U.S. Department of Energy. See W. G. Weitkamp and F. H. Schmidt, "The University of Washington Three Stage Van de Graaff Accelerator," Nucl. Instrum. Meth. **122**, 65 (1974). Recently adapted to an (optional) terminal ion source and a non-inclined tube #3, which enables the accelerator to produce high intensity beams of helium and hydrogen isotopes at energies from 100 keV to 5.5 MeV.

Some Available Energy Analyzed Beams

Ion	Max. Current (particle μA)	Max. Energy (MeV)	Ion Source
^{1}H or ^{2}H	50	18	DEIS or 860
^{3}He or ^{4}He	2	27	Double Charge-Exchange Source
^{3}He or ^{4}He	30	7.5	Tandem Terminal Source
^{6}Li or ^{7}Li	1	36	860
^{11}B	5	54	860
^{12}C or ^{13}C	10	63	860
$*^{14}$N	1	63	DEIS or 860
^{16}O or ^{18}O	10	72	DEIS or 860
F	10	72	DEIS or 860
* Ca	0.5	99	860
Ni	0.2	99	860
I	0.001	108	860

*Negative ion is the hydride, dihydride, or trihydride.

Additional ion species available including the following: Mg, Al, Si, P, S, Cl, Fe, Cu, Ge, Se, Br and Ag. Less common isotopes are generated from enriched material.
In addition, we are now producing a separated beam of 15-MeV ^{8}B at 6 particles/second.

BOOSTER ACCELERATOR

See "Status of and Operating Experience with the University of Washington Superconducting Booster Linac," D. W. Storm *et al.*, Nucl. Instrum. Meth. A **287**, 247 (1990). The Booster is presently in a "mothballed" state.

Contents

INTRODUCTION **i**

1 Fundamental Symmetries and Weak Interactions **1**

Weak Interactions **1**

1.1 Parity non-conserving neutron spin rotation in liquid helium 1

1.2 Progress on measuring the β-asymmetry in ultra-cold neutron decay 3

1.3 The completed second run of the emiT experiment 4

1.4 Search for a permanent electric dipole moment of ^{199}Hg 5

Torsion Balance Experiments **6**

1.5 Sub-mm test of Newton's inverse-square law 6

1.6 Spin pendulum update 7

1.7 A new equivalence-principle test 8

1.8 Small force measurements for LISA 9

1.9 The development of a torsion-pendulum based axion search 10

2 Neutrino Research **11**

SNO **11**

2.1 The Sudbury Neutrino Observatory 11

2.2 ^{16}N production by muons in SNO 13

2.3 Muon-induced neutrons at the Sudbury Neutrino Observatory
– refined and extended results plus new Monte Carlo capabilities 14

2.4 Atmospheric-neutrino-induced muons at the Sudbury Neutrino Observatory . 15

2.5 NUANCE: atmospheric-neutrino simulation in SNO 17

2.6 Estimation of the background to an $\overline{\nu}_e$ analysis of SNO data 18

2.7 Neutral-current results from the salt phase of SNO 19

2.8 The day-night measurement in the salt phase of SNO 20

SNO NCDs **21**

2.9 NCD backgrounds and data cleaning 21

2.10 Deployment of an array of Neutral Current Detectors (NCDs) in SNO 22

2.11 NCD analysis tools and electronics calibrations 23

2.12 PMT calibrations in SNO during the NCD phase 24

2.13 Upgrade to the NCD electronics for SNO 25

KATRIN **26**

2.14 The KATRIN neutrino-mass experiment 26

2.15 KATRIN electron gun testing of detector dead layers 27

2.16 KATRIN pre-spectrometer electrode 28

Majorana **29**

2.17 CENPA contributions to the Majorana experiment 29

2.18 A Joint Institute for Advanced Detector Technology 31

3 Nuclear Astrophysics **32**

3.1 Precise measurement of the ^{7}Be(p,γ)^{8}B S-factor 32

3.2 ^{3}He$(\alpha, \gamma)^{7}$Be γ-ray background analysis 33

3.3 Search for the ^{8}B$(2^{+}) \rightarrow {}^{8}Be(0^{+})$ ground state transition 35

4 Nuclear Structure **36**

4.1 $\beta - \nu$ correlation in A=8 and neutrino spectrum from ^{8}B 36

4.2 Response function of Si detectors for α particles 37

4.3 A Monte Carlo simulation of ^{35}Cl(n, γ) lines 38

4.4 A stringent test of the Isobaric Multiplet Mass Equation using ^{31}P(p, γ) . . . 39

5 Relativistic Heavy Ions **40**

5.1 Summary of event-structure analysis 40

5.2 Soft and hard components of inclusive p_t distributions from RHIC p-p collisions at $\sqrt{s} = 200$ GeV 41

5.3 Minimum-bias hard component (minijets) for inclusive p_t distributions from Pythia-V6.131 p-p collisions at $\sqrt{s} = 200$ and 630 GeV 42

5.4 Soft and semi-hard components of transverse-momentum-dependent two-particle correlations from p-p collisions at $\sqrt{s_{NN}} = 200$ GeV 43

5.5 Minijet structure of two-particle axial-momentum correlations in p-p collisions at $\sqrt{s} = 200$ GeV 44

5.6 Fluctuations, correlations and inverse problems 45

5.7 Charge-dependent n and $p_\perp$ correlations in Pythia and Hijing events 46

5.8 Charge-independent n and $p_\perp$ correlations in Pythia and Hijing events 47

5.9 n-$p_\perp$ covariances in Pythia and Hijing Monte Carlo events 48

5.10 Minijets as velocity structures: $\langle p_t \rangle$ fluctuation scaling and inversion to joint p_t autocorrelations from Au-Au collisions at $\sqrt{s} = 200$ GeV 49

5.11 Energy dependence of $\langle p_t \rangle$ fluctuations from $\sqrt{s_{NN}} = 10$ to 200 GeV 50

5.12 Minijet dissipation and transverse-momentum correlations in Au-Au collisions at $\sqrt{s_{NN}} = 130$ GeV 51

5.13 Minijet deformation on axial-momentum space and charge-independent number autocorrelations from Au-Au collisions at $\sqrt{s_{NN}} = 130$ GeV 52

5.14 Hadronization geometry and charge-dependent number autocorrelations on axial-momentum space in Au-Au collisions at $\sqrt{s_{NN}} = 130$ GeV 53

5.15 Overview of HBT physics at STAR 54

5.16 Pion opacity in RHIC collisions 55

5.17 Pion phase space density from STAR data 56

5.18 Pion entropy in RHIC collisions 58

5.19 Bichsel functions for particle tracks in STAR TPC 60

6 Electronics, Computing, and Detector Infrastructure **61**

6.1 PC-based data-acquisition developments at CENPA 61

6.2 Nanopore DNA sequencing . . . 62

6.3 Electronic equipment . . . 63

6.4 NSAC - a data-acquisition and control system for the parity non-conserving neutron spin-rotation experiment . . . 64

6.5 EötWash data-acquisition development . . . 65

6.6 Development of the ORCA DAQ system . . . 66

6.7 Laboratory computer systems . . . 67

7 Accelerator and Ion Sources **68**

7.1 Deck and ion sources . . . 68

7.2 Van de Graaff accelerator operations and development . . . 69

7.3 Progress toward UCN detectors with the 860 SpIS . . . 70

7.4 Removal of large pieces of the old cyclotron . . . 71

8 The Career Development Organization: year four **72**

9 CENPA Personnel **73**

9.1 Faculty . . . 73

9.2 Postdoctoral Research Associates . . . 73

9.3 Predoctoral Research Associates . . . 74

9.4 Research Experience for Undergraduates participants . . . 74

9.5 Professional staff . . . 75

9.6 Technical staff . . . 75

9.7 Administrative staff . . . 75

9.8 Part Time Staff . . . 76

10 Publications **77**

10.1 Degrees Granted, Academic Year, 2003-2004 . . . 87

1 Fundamental Symmetries and Weak Interactions

Weak Interactions

1.1 Parity non-conserving neutron spin rotation in liquid helium

E. G. Adelberger, A. García, B. R. Heckel and H. E. Swanson

We have undertaken a project to measure the PNC neutron spin rotation in a 50-cm long liquid-helium target to a precision of 10^{-7} rad and to explore the possibility of measuring the PNC interaction between bare neutrons and protons. This project has been supported by the NSF in addition to the support received from the DOE through CENPA. The collaboration for this project includes E. Adelberger, A. García, B. Heckel and E. Swanson from CENPA, M. Snow and C. Bass from Indiana University, and D. Markoff from TUNL.

Despite a considerable body of data of PNC measurements in nuclei, it has not been possible to extract a consistent picture of the weak force between nucleons. Uncertainties about the nuclear wave functions make it difficult to compare experiment to theory unambiguously. The weak isovector coupling constant, f_π, is of particular interest because it is strongly influenced by the neutral current Z^0 exchange, yet it has proven to be very difficult to measure.

We have proposed to measure f_π in PNC $n-\alpha$ scattering, a few-body nucleon system that may be calculated with relative confidence. The PNC rotation of the spin vector of a neutron beam as it traverses a liquid helium target, ϕ_{pnc}, provides a measurable observable:

$$\phi_{pnc}(n-\alpha) \quad \propto \quad +f_\pi + .33h^0_\rho + .23h^0_\omega - .11h^1_\rho - .23h^1_\omega - .02h'^1_\rho$$

where the coupling constants are the standard DDH amplitudes.[1] If f_π vanishes, then PNC p-α measurements, the isospin conjugate system to n-alpha, predict a value for ϕ_{pnc} of approximately 5×10^{-7} rad in a 50-cm long liquid-helium target, five times larger than the experimental limit we propose to achieve.

Cold neutrons, having de Broglie wavelengths longer than 0.4 nm, propagate through material targets as neutron waves. The target averaged interaction with the neutrons creates a neutron index of refraction. PNC neutron spin rotation arises from a term $G'\vec{\sigma}\cdot\vec{p}$ in the index of refraction that is generated by the weak interaction (where $\vec{\sigma}$ is the Pauli spin and $\vec{p}$ is the momentum of the neutron, and G' is proportional to the universal weak coupling constant.) The spins in a neutron beam whose polarization vector is transverse to $\vec{p}$ will experience a torque about $\vec{p}$, resulting in a total rotation angle of:

$$\phi_{pnc} \quad = \quad -4\pi NLRe(G')$$

independent of neutron momentum, where N is the number density of target nuclei and L the target length.

[1] V. F. Dmitriev, V. V. Flambaum, O. P. Sushkov and V. B. Telitsin, Phys. Lett. **125**, 1 (1983).

The experimental challenge is to distinguish the small PNC rotations from much larger neutron spin rotations due to residual magnetic fields. We have constructed a neutron spin polarimeter that includes a cryostat surrounding a liquid-helium target region and have performed the first measurement of the PNC neutron spin rotation in a liquid-helium target. The first data runs with the cryogenic polarimeter, taken at the NIST reactor, achieved a result of $\phi_{pnc} = (3.8 \pm 6.5) \times 10^{-7}$ rad, limited by count-rate shot noise.[2]

To achieve an additional factor of five in experimental sensitivity, we are in the process of rebuilding the polarimeter. There are three essential improvements. The first is to rebuild the cryostat so that superfluid helium can be used as a target. Superfluid helium has a density 20% higher than normal liquid helium; it will scatter 30% less neutrons out of the beam; and it provides better thermal conductivity to reduce systematic errors. The second improvement is to employ a long wavelength neutron filter in the beam to remove the longest wavelength neutrons. This is expected to increase the detected beam polarization by 50%. Finally, the beam collimation will be opened to allow a larger count rate.

In the past year, we have purchased the hardware required to rebuild the cryostat, our shops have machined new liquid-helium target chambers to be used in the cryostat, and our collaborators at Indiana University are in the process of assembling the rebuilt cryostat. A collaboration meeting was held at NIST in April 2004 and plans were made to test the cryostat at Indiana University in the summer of 2004 in preparation for data collection to begin at the NIST reactor at the end of 2004. In 18 weeks of beam time, we should have the statistics to measure ϕ_{pnc} at the level of 10^{-7} rad.

[2]D. Markoff, Ph.D. thesis, University of Washington, (1997).

1.2 Progress on measuring the β-asymmetry in ultra-cold neutron decay

A. García, S. A. Hoedl, A. L. Sallaska and S. K. L. Sjue

Ultra-high precision studies of neutron decay present a unique opportunity to improve the present uncertainty in V_{ud}, test the unitarity of the CKM matrix, and probe for physics beyond the standard model. We are members of the UCNA collaboration whose first goal is to measure the angular correlation between the electron momentum and the neutron spin five times better than the current uncertainty. Such a measurement, when combined with the presently known value of the neutron and muon lifetimes, will permit a determination of V_{ud} at the same level of precision as $0^+ \to 0^+$ decays without nuclear corrections.

The principal advantage of this experimental effort is the use of Ultra-Cold Neutrons (UCN). Since UCN reflect at all angles of incidence from most materials, they do not activate the experiment itself (in contrast to a cold neutron beam) and can be efficiently transported to a well-shielded low radiation environment. In addition, their low energy (E $\leq 2 \times 10^{-7}$ eV) permits a simple polarization scheme: passage through a 7-T magnet is sufficient to reject 100% of the wrong polarization state. Note that polarization has been the limiting systematic error in previous measurements of A. Our collaboration has built a new super-thermal solid deuterium source of UCN, which has recently been commissioned, and which we expect to achieve a world record density.

Our principal contribution over the past year has been the design and construction of UCN detectors and absorbers. Detectors monitor the UCN density in the fiducial volume, while absorbers confine UCN inside the fiducial volume. The detectors consist of a thin foil which converts UCN into energetic ($\sim 2-3$ MeV) ions which can be readily detected by a silicon surface barrier detector. The principal challenge was finding materials with small UCN reflectivity which could be readily manufactured at CENPA.

We developed two types of converter foils. In one type, we evaporated 300μg/cm^2 of natural isotopic abundance LiF onto 2000Å thick nickel foils. In this foil, the neutrons will be captured according to n+^{6}Li$\to$ α+^{3}H, with $\sigma = 4.7 \times 10^5$ Barns. The nickel serves as a strong substrate, which also has the added benefit of reflecting UCN and effectively doubling the path length of neutrons in the absorbing medium. Naturally occurring LiF has a low UCN potential (54.4 neV) and is easy to evaporate. In the other type, we implanted ^{10}B (see Section 7.3) into a 2000Å thick layer of V coated onto a 100Å adhesion layer of chrome in turn evaporated onto a 2000Å thick nickel foil. Neutrons are captured according to the reaction, n+^{10}B$\to$^{7}Li+α, with $\sigma = 1.8 \times 10^6$ Barns. V also has a low UCN potential (-7.2 neV) and can be e-beam evaporated.

We have also built two types of UCN absorbers. The challenge was finding material with a low UCN reflectivity which does not increase the radiation backgrounds. We have constructed absorbers consisting of TPX, which is a 3-methylpentene-1 based polyolefin with a nearly zero UCN potential, and LiF coated on stainless steel. TPX has a lower UCN potential; however, because n+H$\to$D+γ, it may produce higher backgrounds. We anticipate that both the absorbers and the detectors will be tested in calender year 2004.

1.3 The completed second run of the emiT experiment

H. P. Mumm, A. García, M. F. Wehrenberg and J. F. Wilkerson

The emiT experiment is a search for time-reversal (T) invariance violation in the beta decay of free neutrons. Current observations of CP(T) violation in the Kaon and B-meson systems can be accommodated within the standard model of particle physics. However, baryogenisis, as well as attempts to develop unified theories, indicate that additional sources are required. The standard model predicts T-violating observables in beta decay to be extremely small (Second order in the weak coupling constant) and hence are beyond the reach of modern experiments.[1] However, potentially measurable T-violating effects are predicted to occur in some non-standard models such as those with left-right symmetry, exotic fermions, or leptoquarks.[2] Thus a precision search for T-violation in neutron beta decay provides an excellent test of physics beyond the Standard Model.

The emiT experiment in sensitive to the T-odd P-even triple correlation between the neutron spin and the momenta of the neutrino and electron, $D\,\vec{\sigma}_n \cdot \vec{P}_e \times \vec{P}_\nu$, in the neutron beta-decay distribution. The coefficient of this correlation, D, is measured by detecting decay electrons in coincidence with recoil protons from a polarized beam of cold (2.7 meV) neutrons. Four electron detectors (plastic scintillators) and four proton detectors (large-area diode arrays) are arranged in an alternating octagonal array concentric with the neutron beam.

Following extensive upgrades, the emiT detector was moved from the University of Washington to NIST in June 2002. A number of set-up tasks were carried out from June until the start of production data taking in October of that year. Data was taken until December 2003. In all about two thousand data runs of up to four hours apiece were collected. These runs were of three types: coincidence runs used for extraction of the D coefficient, calibration runs, and Asymmetric beam Transverse Polarization (ATP) runs for understanding the dominant systematic effect in the experiment. In addition to a raw data stream, singles histograms were saved for the fast TDCs, QDCs, Shaper spectra, and proton energy versus delay time (summed over the entire detector). In total, approximately 350 million coincidence events were collected, involving approximately 78 Gb of data and resulting in an expected sensitivity of $D \approx 2 \times 10^{-4}$

Considerable effort has been put into understanding systematic uncertainties to at least the 10^{-5} level. Monte Carlo calculations suggest that the dominate systematic effect would be a combination of a beam asymmetry and a polarization misalignment. To fully understand this possibility, a series of 'ATP runs' were carried out. In these runs the polarization was intentionally misaligned in a variety of directions. This allows a probe of the ATP effect as well as verifying the scaling used to extract the experimental uncertainty. An initial assessment indicates $D_{ATP} < 3 \times 10^{-5}$. Monte Carlo calculations are also being used to understand the effects of backscattering and proton-recoil effects. These and all other systematic effects appear to be below 1×10^{-4}. A final result is expected by the end of 2004.

[1] M. Kobayashi and T. Maskawa, Prog. Theor. Phys. **49**, 652 (1973).

[2] P. Herczeg, *Progress in Nuclear Physics*, W.-Y. P. Hwang, ed., Elsevier Sciences Publishing Co. Inc. (1991) p. 171.

1.4 Search for a permanent electric dipole moment of ^{199}Hg

W. C. Griffith, M. D. Swallows,* M. V. Romalis† and E. N. Fortson*

An experimental effort is underway to improve the limit on, or possibly measure, a permanent electric dipole moment (EDM) of ^{199}Hg. The measurement of a non-zero EDM would likely reveal a new source of CP-violation, and would represent possible experimental evidence for supersymmetry. Our previous measurement[1] obtained a limit of $|d(^{199}\mathrm{Hg})| < 2.1\times10^{-28}\,e\,\mathrm{cm}$ by comparing the ^{199}Hg spin-precession frequencies in a stack of two Hg-vapor cells in a common magnetic field and oppositely directed electric fields. We are currently working on a version of the experiment using a stack of four vapor cells, where the two additional cells have zero electric field applied to them, and are used as magnetometers to improve statistical sensitivity and our understanding of systematic effects.

As of one year ago, we were attempting to begin dedicated data taking toward the new measurement. However, multiple instances of EDM-like false signals over the next several months led us to shift all of our efforts to trying to understand and eliminate the source of this systematic effect. In our experiment, the signature of an EDM would be a shift in the ^{199}Hg spin-precession frequency correlated with the electric field direction, and the most dangerous systematic effects are caused by high voltage correlated changes in the magnetic field observed by the vapor cells. The false signals we have generally observed would correspond to a local magnetic field change of 20 pG, or an EDM of $2 \times 10^{-27}\,e\,\mathrm{cm}$, an order of magnitude larger than our previous limit. Besides the large size of the false signals, we are certain that they are not evidence of an actual EDM because the frequency shifts do not appear as symmetrically opposite shifts in the 2 cells with opposite electric fields, and they often occur in the magnetometer cells.

In the course of our investigation we have ruled out several leading suspects. The measured steady-state electrical currents are much too small to cause the effect through direct magnetic field generation, even if all of the current maliciously flowed in a complete loop around a vapor cell. It is still a possibility that short current bursts due to high voltage sparks might lead to magnetic orientation of ferromagnetic contaminants, though. Cell movement due to an electric field induced force (e.g. piezoelectric) in the existing magnetic field gradient would lead to an EDM-like effect, but when the magnetic field gradient was increased to about 5 times its normal size there was no increase in the signal. This makes cell motion an unlikely culprit, although motion of a nearby magnetized material is still a possibility. The fact that the occurrence of false signals has been much more frequent with the 4-cell setup compared to the previous 2-cell measurement led to the suspicion that one of the changes implemented in the apparatus has led to an increased vulnerability to a particular systematic effect. This was tested by resurrecting the former 2-cell setup, and the resulting data has been much more susceptible to false signals than it was during the original dataset, indicating that the false signals are not caused by a specific apparatus difference. The origin of the false signals is still unresolved, and understanding this systematic effect remains the focus of our efforts.

*Physics Department, University of Washington, Seattle, WA 98195.
†Department of Physics, Princeton University, Princeton, NJ 08544.
[1] M. V. Romalis, W. C. Griffith, J. P. Jacobs, and E. N. Fortson, Phys. Rev. Lett. **86**, 2505 (2001).

Torsion Balance Experiments

1.5 Sub-mm test of Newton's inverse-square law

E. G. Adelberger, T. S. Cook, J. H. Gundlach, B. R. Heckel, D. J. Kapner and H. E. Swanson

Our main systematic effects are associated with the rotation frequency of our motor that drives the short-range attractor. These effects are predominantly mechanical or magnetic. Normally, our gravitational signal of interest is at such a high harmonic of the rotation frequency that any effect from the motor is highly attenuated. By increasing the isolation between our vacuum vessel and the motor, adding flexible couplings for a potential misalignment of the motor, and stiffening our optical mounts, we have reduced the spurious signals at the motor frequency by greater than a factor of four. We also added additional layers of magnetic shielding around our motor.

These reductions are helpful in determining our absolute gravitational calibration, as that signal frequency is at the third harmonic of the motor (as opposed to the short-range signal, which is at the 21st.) This calibration is typically a measurement of a long-range, easily-calculated gravitational torque on the pendulum from the interaction of small pendulum spheres and larger spheres on a turntable. We redesigned the pendulum frame to have much lower multipole moments (up to a factor of 400 lower for m=4) that could couple spuriously to our calibration turntable. The new frame is shown in Fig. 1.5-1. This frame has three spheres permanently mounted at a large distance from the short-range plate, to provide a continuous gravitational calibration, important for accounting for detector non-linearities.

To increase our sensitivity, we need to reduce the vertical separation between our pendulum and attractor disks. This separation is comprised of the thickness of our electrostatic shield ($10\mu m$) the separation between the attractor and the shield (previously $17\mu m$) and the separation between the pendulum and the shield (previously $70\mu m$.) We have recently reduced the latter to at least $40\mu m$ with the construction of a new shield and diligent dust-removal. We are set to take data with our new improvements in the next month.

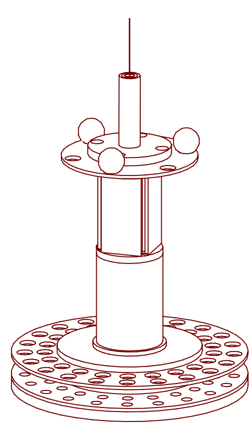

Figure 1.5-1. The new short-range frame and 21-fold symmetric disk.

1.6 Spin pendulum update

B. R. Heckel, T. S. Cook, E. G. Adelberger and H. E. Swanson

The next-generation spin pendulum has been assembled and is currently mounted in the original rotating Eöt-Wash torsion balance for the purpose of searching for new forces that couple to spin. The spin pendulum is a torsion balance that utilizes the magnetic properties of Alnico and SmCo to produce a spin-polarized test body.[1] By accurately measuring the affinity of the test body for a prefered direction in space (or lack thereof), the pendulum puts limits on possible simultaneous Lorentz and CPT symmetry violation as described by Colladay and Kostelecky.[2] Over the past year, a number of design improvements have been implemented to increase the overall sensitivity to such a symmetry violation.

Smaller - Lighter: The diameter of the pendulum has been reduced while maintaining the same active mass as previous pendulums. In the past, pendulums were built with an aluminum harness to place rectangular magnets into an octagonal ring. For the new pendulum, the magnets are precision machined into trapezoidal wedges to form the octagonal ring. The maximum diameter of a ring has been reduced from 1.67" to just 1.04". This reduced geometry requires less inert mass to support the ring structures, lowers the torsion moment of the pendulum and, due to the decreased mass, allows the inclusion of a magnetic shield on the pendulum while still using a 30-μm diameter suspension fiber.

Improved Optics: The angular position of the pendulum is monitored with an auto-collimator that reflects a laser off a mirror attached to the pendulum. The spin pendulum experiments run in the old Eöt-Wash apparatus which is designed for a single reflection off the pendulum mirror. However, one can double the angular resolution by double reflection: reflecting the light to an auxiliary mirror and then back to the pendulum mirror before returning it to the auto-collimator. We have refitted the old Eöt-Wash apparatus to accommodate a double reflection system.

As may be expected, the attenuation of all magnetic "leakage" fields from the pendulum is essential to performing a precise measurement. A magnetic coupling between the pendulum and the earth's field or any ambient laboratory fields could overwhelm a potential signal or even produce a false signal. To ascertain the strength of our leakage fields accurately, we have constructed a stepper-motor driven turntable and data acquisition system to read data from a 3-axis hall probe as the pendulum is rotated. With this system we have been able to measure the fields at any given radius from the pendulum to less than 50 μG.

Data with the new spin pendulum have been taken for six months. There is no evidence for magnetic coupling of the pendulum to the environment and the new angular reflection system is working well. An unknown systematic signal has been observed that appears to be associated with the torsion fiber pre-hangar and magnetic damper at the top of the torsion fiber. Measurements are being made to understand and eliminate this error before undertaking a search for new spin-coupled forces.

[1] M. G. Harris, Ph.D. thesis, University of Washington, 1998.

[2] D. Colladay and V. A. Kostelecky, Phys. Rev. D **55**, 6760 (1997); *ibid.* **58**, 116002 (1998).

1.7 A new equivalence-principle test

E. G. Adelberger, K. Choi, J. H. Gundlach, B. R. Heckel, S. Schlamminger and H. E. Swanson

We are testing the weak equivalence principle using a rotating torsion balance. A composition dipole, consisting of titanium, beryllium, or aluminum test bodies, is suspended from a torsion fiber inside a vacuum chamber. The vacuum chamber is hanging from a constantly rotating turntable. A violation of the equivalence principle would result in a periodic differential acceleration of the two materials directed towards a large variety of sources. We will be able to test the equivalence principle for Yukawa ranges from 1 m to ∞. In particular we can test for differential accelerations between the two different materials toward the Sun and the center of our Galaxy. By combining our measurement toward the Sun with lunar laser-ranging results, we will set new limit for the Strong Equivalence Principle. Since about 25% of the acceleration towards the center of the Galaxy is caused by dark matter, the measurement toward the center of our Galaxy allows us to test for the Equivalence Principle for the galactic dark matter.

During the past year we built a new gradiometer pendulum (Fig. 1.7-1) to measure the strength of the Q_{21}, Q_{31} and Q_{41} gravity gradient fields at the location of the pendulum. The gradiometer pendulum consists of four equally spaced aluminum disks, which have chamfered holes to seat titanium balls. By changing the position of 16 titanium balls, we can create large q_{21}, q_{31} and q_{41} moments of this pendulum. In all three formations the moment of interest is maximized, while the other moments vanish by design. Thus we can measure each of the Q_{21}, Q_{31} and Q_{41} ambient gravity-gradient fields independently. We compensated the fields with Q_{21}, Q_{31} gravity-gradient compensators masses so that their strength[1] was about 3% and 4% the uncompensated strength, respectively. Small tuning screws on the EP-pendulum were adjusted to reduce the q_{21} and q_{31} moments. The residual coupling due to gravity gradients is calculated to be less than 1 nrad. Other systematic effects, which include tilt, magnetics, thermal and etc. are highly reduced.[2]

Our current differential acceleration sensitivity is 1.3×10^{-14} m/s^2 per day measurement which corresponds to an angle of 2 nrad. We plan to start a long data run in the near future with the goal of achieving a sensitivity of 1.0×10^{-15} m/s^2 for accelerations toward the Sun and the center of our Galaxy.

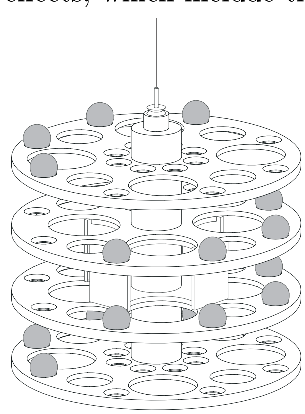

Figure 1.7-1. Gradiometer pendulum. Shown is the q_{31}-configuration for the measurement of the Q_{31} gravity gradient.

[1]The fields change slowly due to rainfall about 2 % seasonally.

[2]CENPA Annual Report, University of Washington (2003) p. 13.

1.8 Small force measurements for LISA

E. G. Adelberger, R. C. Carr, T. Cook, J. H. Gundlach, B. R. Heckel, M. J. Nickerson, B. R. Osting, S. Schlamminger and H. E. Swanson

The scientific goal of the Laser Interferometer Space Antenna, LISA,[1] a joint project of the ESA and NASA, is to observe gravitational waves in the frequency range of 10^{-4} to 10^{-1} Hz. The interferometer is formed by three identical spacecrafts $5,000,000$ km apart at the corners of an equilateral triangle. Each spacecraft carries two freely floating cubical masses (gravitational reference sensors), which define the ends of the interferometer arms. The spacecraft is servoed to maintain a constant distance of 2 to 4 mm between the sensor housing and the sensor. Major concerns of the mission are small spurious forces acting on the small masses, caused by e.g. patch effects, which limit the performance of LISA by introducing additional noise at low frequencies.

In order to investigate these effects we have built a sensitive torsion balance. The torsion pendulum consists of a gold coated glass plate (38.1 mm $\times$ 38.1 mm $\times$ 1 mm) and two gold coated aluminum cylinders mounted perpendicular to the plate at top and bottom of the glass. These cylinders compensate the q_{22} moment of the plate and therefore minimize the sensitivity to moving masses in the lab. Adjacent to the pendulum, a gold coated glass plate can be moved near to the pendulum plate. This setup allows us to test for forces that may arise between the LISA housing and the proof mass.

We have developed a new capacitive method to measure the position of the pendulum. To avoid large deflection of the pendulum from the equilibrium position, only small voltages can be applied between the grounded plate and the pendulum. The capacitor formed by the pendulum and the plate is part of a low-pass filter. The phase shift of a small (2 mV) AC signal caused by this filter is detected with a lock-in amplifier and measured for various plate positions.

In the course of the last year we have improved the torque noise of the apparatus by various measures. We have added a magnetic shield to reduce coupling to magnetic fields. In order to minimize vibrational couplings, the thermal insulating house was mechanically isolated from the concrete foundation. To increase the torque sensitivity of the pendulum, we have employed a thinner torsion fiber (diameter 12.7 μm). Finally, we have improved the magnetic damper, a device used to damp out the swing motion of the pendulum and excess vertical vibrations of the pendulum. As a result of these improvements, the measured noise of the torsion pendulum is at the thermal limit, see Fig. 1.8-1.

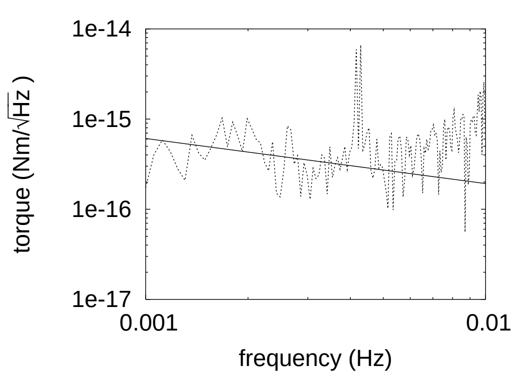

Figure 1.8-1. Measured torque noise (dotted line) and thermal limit (solid line) of the torsion pendulum at 11 mm separation between the attractor plate and the pendulum.

[1] http://lisa.jpl.nasa.gov/.

1.9 The development of a torsion-pendulum based axion search

E. G. Adelberger, B. R. Heckel, S. A. Hoedl, F. V. Marcoline and H. E. Swanson

We have designed a torsion-pendulum search for the axion which offers an improvement of 10^{18} over the most recent measurement[1] for an axion mass of $\sim$ 200 μeV. The axion is the result of the hypothesized Peccei-Quinn symmetry and is a favored cold dark matter candidate.[2] The mass is constrained by the known flat geometry of the universe to be heavier than 1 μeV ($\lambda_a < 20$ cm), and is constrained by the neutrino flux from SN1987A to be lighter than 1000 μeV ($\lambda_a > 0.02$ cm). Note that microwave cavity searches probe for light axions (1.2 μeV $< m_a <$ 12.4 μeV).

A torsion-pendulum based search is possible because the axion mediates a macroscopic pseudo-scalar potential between polarized and unpolarized fermions. The axion pendulum (see Fig. 1.9-1) will consist of four 4×4 cm planes of 250 μm thick germanium. In each quadrant defined by the germanium planes will be placed a quarter piece of a toroidal electro-magnet. The pole faces of these magnets will be positioned 100 μm away from the germanium planes, and will have a maximum field strength of 20 kG. When energized, the oriented electron spins in the ferromagnetic core provide the source of polarized fermions. The nucleons in the germanium provide the source of unpolarized fermions. By reversing the magnetization orientation at a fixed frequency, the pendulum will feel an axion-mediated torque at that frequency. After 100 days of measurement time, we anticipate a limit on the axion coupling as a function of the axion Compton wavelength as presented in Fig. 1.9-1. An unexplained positive signal for an axion can be rigorously identified as a systematic error. The axion torque scales as e^{-h/λ_a}, where h is the distance between a pole face and the germanium. Magnetic systematic errors (i.e. due to fixed electron spins in the germanium) will have a much slower fall off with h.

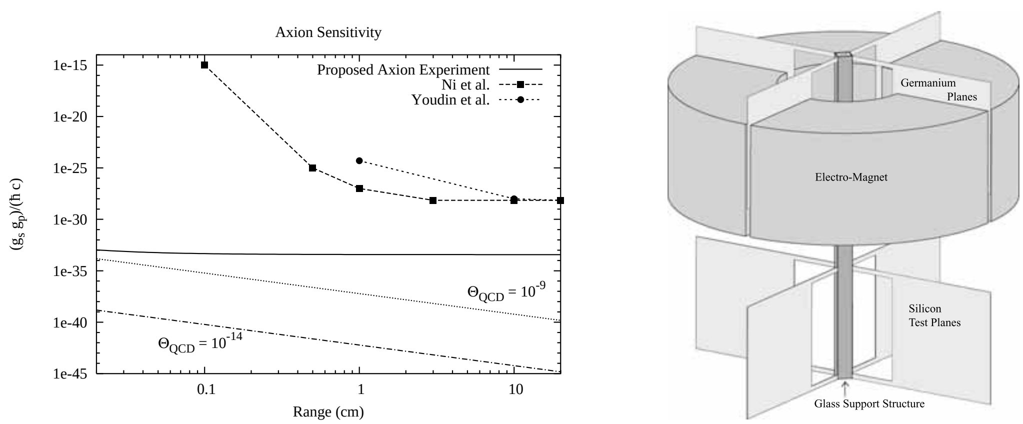

Figure 1.9-1. The axion pendulum and our expected sensitivity to the axion electron-nucleon coupling as a function of the axion Compton wavelength compared with recent experimental searches and the expected coupling for different values of Θ_{QCD}.

[1] W. T. Ni *et. al.* Phys. Rev. Lett. **82**, 2439 (1999).
[2] L. J. Rosenberg and K. A. van Bibber, Phys. Rep. **325**, 1 (2000).

2 Neutrino Research

SNO

2.1 The Sudbury Neutrino Observatory

J. F. Amsbaugh, T. H. Burritt, G. A. Cox, P. J. Doe, C. A. Duba, J. A. Formaggio, G. C. Harper, M. A. Howe, K. K. S. Miknaitis, S. McGee, A. W. Myers, N. S. Oblath, J. L. Orrell,* K. Rielage, R. G. H. Robertson, M. W. E. Smith and L. C. Stonehill

The Sudbury Neutrino Observatory (SNO) is a heavy water Čerenkov detector that was designed to study the flux, spectrum, and oscillation characteristics of ^{8}B neutrinos from the Sun. Previous solar-neutrino experiments, able to detect primarily electron neutrinos, have observed a deficit in the flux of solar neutrinos relative to the predictions of solar models. This discrepancy between the observed flux of electron neutrinos and the expected flux is known as the Solar-Neutrino Problem. The use of heavy water as a target medium in SNO allows sensitivity not only to electron neutrinos, but also to muon and tau neutrinos, through the neutral current (NC) reaction of neutrinos on deuterium. The three primary reactions through which we detect solar neutrinos are

$$\nu_x + {}^2\mathrm{H} \rightarrow \nu_x + p + n \quad \text{Neutral Current (NC)} \tag{1}$$
$$\nu_e + {}^2\mathrm{H} \rightarrow e^- + p + p \quad \text{Charged Current (CC)} \tag{2}$$
$$\nu_x + e^- \rightarrow \nu_x + e^- \quad \text{Elastic Scattering (ES)} \tag{3}$$

where x denotes any of the three active neutrino flavors. A comparison of SNO's measured CC and NC rates has shown that solar electron neutrinos are oscillating into muon and tau neutrinos prior to reaching our detector. SNO's results over the past two years have thus provided strong evidence for the oscillation of solar neutrinos and solved the long-standing puzzle of the missing solar neutrinos.

A wide range of activities has taken place in the past year for the Sudbury Neutrino Observatory. At the Summer TAUP'03 Conference, SNO announced first results from data taken during the salt phase of the experiment. The 254-day data set provided a more sensitive measurement of the neutral-current-neutrino flux from the sun. Results were consistent with SNO's previous analyses and helped restrict the solar mixing parameters solely to the Large Mixing Angle solution (see Fig. 2.1-1). In October 2003, the salt was extracted from the D_2O, paving the way for the third and final phase of the experiment, known as the neutral-current phase. An array of discrete neutral-current detectors (NCDs) is installed to provide an independent means of detecting the NC neutrons. The array deployment commenced and was successfully executed this past winter. It is anticipated that the data from this NCD phase, along with data from the previous phases, will significantly enhance our understanding of the properties of neutrinos.

*Presently at Pacific Northwest National Laboratory, Richland, WA 99352.

The University of Washington has played a major role in the experiment. Primary activities include analysis of the data from the salt phase of the experiment, coordination and installation of the neutral current detectors and development of the data acquisition system for the main SNO detector.

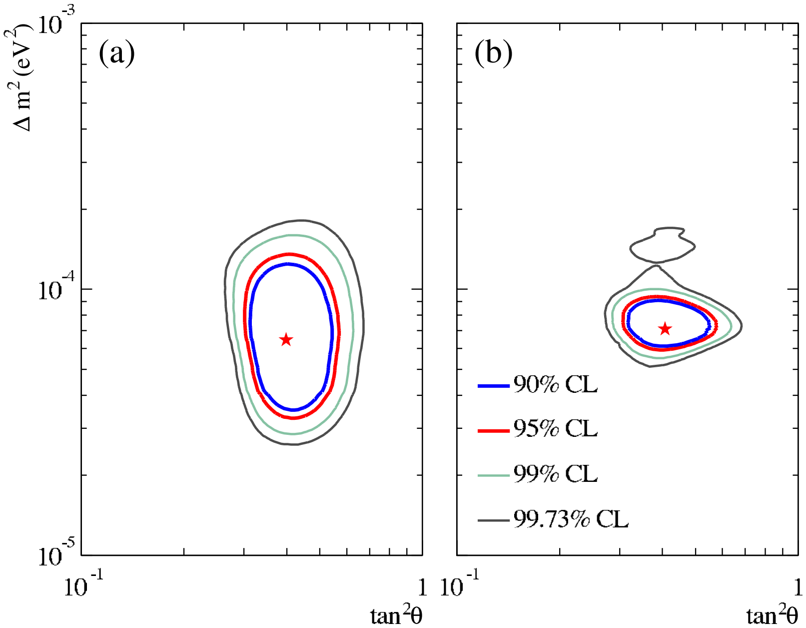

Figure 2.1-1. Global neutrino oscillation contours. (a) Solar global: D_2O day and night spectra, salt CC, NC, ES fluxes, SK, Cl, Ga. The best-fit point is $\Delta m^2 = 6.5 \times 10^{-5}$, $\tan^2\theta = 0.40$, $f_B = 1.04$, with χ^2/d.o.f. $= 70.2/81$. (b) Solar global + KamLAND. The best-fit point is $\Delta m^2 = 7.1 \times 10^{-5}$, $\tan^2\theta = 0.41$, $f_B = 1.02$. In both (a) and (b) the ^{8}B flux is free and the hep flux is fixed.

2.2 ^{16}N production by muons in SNO

N. S. Oblath, J. L. Orrell* and R. G. H. Robertson

Any ^{16}N that is produced in SNO would be a significant background to the charged current (CC) neutrino signal. ^{16}N decays via a 6.13-MeV γ and an electron with an energy of up to 4 MeV, or by a 10 MeV electron. The resulting spectrum resembles the CC spectrum. ^{16}N is produced primarily by muons through spallation or capture on ^{16}O, or by fast-neutron interactions with ^{16}O, where the fast neutrons come from cosmic ray interactions in the water.

An efficient method for identifying muons has been developed by John Orrell for his work on solar antineutrinos. We used his list of muons and searched for evidence of the decay of ^{16}N in a time window after each muon. The minimum edge of the time window was chosen to exclude the high multiplicity of free neutrons that are created by muons. The neutron capture time during the salt phase is 4 ms. Therefore, after 1 second all of the neutrons will have been captured. The time window extended to 50 seconds after each muon. The half-life of ^{16}N is 7.13 s, so the time window extends to 7 times the half-life, and should include almost any ^{16}N which is produced by a muon.

Two other cuts were used to reduce backgrounds. The radial fiducial volume cut was chosen to be the same as that used for SNO's published results. We also made a cut on the minimum number of PMT hits. This reduced the low-energy background, but sacrificed approximately 16% of any ^{16}N events.

The analysis was performed on SNO's 400-day salt-phase data by fitting an exponential with the appropriate decay constant, plus a flat background, to the data in the post-muon time window. The fit is shown in Fig. 2.2-1. The actual value for the initial activity is negative: $N_0 = -0.57 \pm 1.34$ s^{-1}. This is consistent with zero ^{16}N produced by muons in SNO. Analyses at other SNO institutions of D_2O-phase data have shown that a small

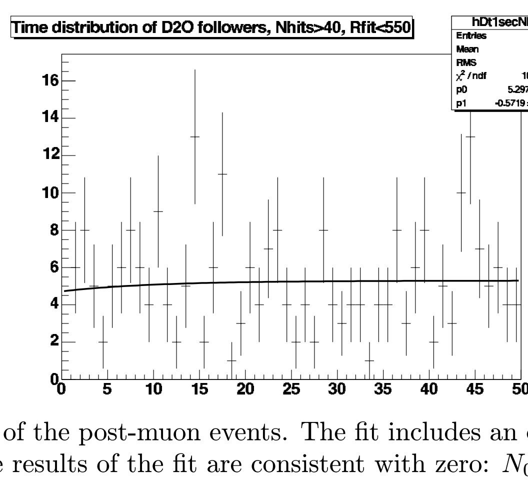

Figure 2.2-1. The fit of the post-muon events. The fit includes an exponential decay plus a flat background. The results of the fit are consistent with zero: $N_0 = -0.57 \pm 1.34$ s^{-1}.

amount of ^{16}N may have been produced by several high-energy muons. We hope to perform an analysis of the D_2O-Phase data to check those results in the near future.

*Presently at Pacific Northwest National Laboratory, Richland, WA 99352.

2.3 Muon-induced neutrons at the Sudbury Neutrino Observatory – refined and extended results plus new Monte Carlo capabilities

J. A. Formaggio and J. L. Orrell*

In a previous Annual Report[1] we presented an analysis of the events following within one-half second of the passage of a cosmic-ray muon through the Sudbury Neutrino Observatory (SNO) detector. These events are predominately spallation neutrons. Of particular interest[2] is the number of neutrons produced by a single muon, succinctly, the neutron multiplicity. Fig. 2.3-1 presents the results of a refinement of the method presented in the previously mentioned Annual Report. Data from both the D_2O and salt phases of the SNO experiment

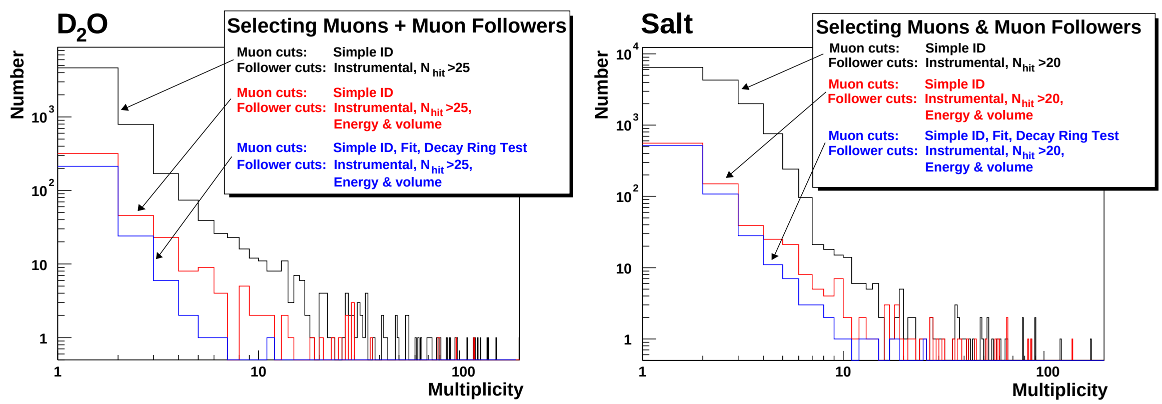

Figure 2.3-1. The multiplicity of spallation neutrons following a muon for different selection criterion on the muons and muon followers. In each plot, the lowest curve is predominately below a multiplicity of 10 while the two higher curves extend above a multiplicity of 100.

have now been analyzed. The results clearly show muons with neutron multiplicities over 100. However, the decay ring test[1] shows high- and low-multiplicity cases can be partitioned by looking for high-energy Čerenkov events following within 11 microseconds after a muon.

In conjuction with the analysis shown above, work has proceeded so as to properly simulate photoneutron production from high-energy muons. Photoneutron production involves the exchange of a virtual photon as the muon passes through matter. Theoretically, it is possible to calculate the muon photonuclear cross-section by use of the Equivalent Photon Approximation. This technique, originally proposed by Fermi[3] and later developed by C. F. Weizsäcker[4] and E. J. Williams,[5] relates the real photonuclear cross-section to the virtual cross-section. Other processes that are responsible for neutron production, such as secondary interactions, are also included. Comparisons of the experimental data against theoretical predictions are underway and should provide useful information to next-generation deep-underground experiments.

*Presently at Pacific Northwest National Laboratory, Richland, WA 99352.
[1]CENPA Annual Report, University of Washington (2003) p. 20.
[2]Y.-F. Wang *et al.*, Phys. Rev. D **64**, 013012 (2001).
[3]E. Fermi, Physik Z. **29**, 315 (1924).
[4]C. F. Weizsäcker Z. Phys. **88**, 612 (1934).
[5]E. J. Williams *et al.*, Kgl. Dan. Vidensk. Selsk. Mat. Fys. Medd.**XIII**, 4 (1935).

2.4 Atmospheric-neutrino-induced muons at the Sudbury Neutrino Observatory

J. A. Formaggio, N. S. Oblath and J. L. Orrell*

High energy muons and neutrinos are produced constantly by the interaction of primary cosmic rays with nuclei of the Earth's upper atmosphere. These primary interactions produce mesons (e.g. π, K and short-lived charmed D mesons) which decay into neutrinos and muons.

$$p + {}^{14}\mathrm{N} \rightarrow \pi^+(K^+) + X \quad (1)$$
$$\pi^+(K^+, D^+) \rightarrow \mu^+\nu_\mu \quad (2)$$
$$\mu^+ \rightarrow e^+\nu_e\bar{\nu}_\mu \quad (3)$$

At the depth of 2092 meters, where the Sudbury Neutrino Observatory (SNO) is located, only muons and neutrinos are able to penetrate. SNO is currently in a unique position amongst world experiments located underground. At the depth of over 6-km water equivalent, it is the deepest underground laboratory currently in operation. The vertical flux intensity at this depth is $4.1 \times 10^{-10}\mu/\mathrm{cm}^2\cdot\mathrm{s}\cdot\mathrm{sr}$, which corresponds to a rate of about 3 muons/hour.

SNO can make two important measurements with respect to muons present in the detector. First, SNO is sensitive to the downward-muon rate coming from primary cosmic ray interactions. The muon rate is expected to fall rapidly as a function of depth:

$$I_\mu(h) = A_\nu(\frac{h_0}{h})^\alpha \exp{(-\frac{h}{h_0})} \quad (4)$$

where h is the depth of rock, and h_0 is the scale height. By measuring the muon flux as a function of zenith angle, it is possible to test predictions regarding the energy dependence of the muon flux at the surface, as well as the transport mechanism of extremely high-energy muons.

Second, SNO's unprecedented depth allows for an unprecedented measurement of atmospheric neutrinos (via the detection of neutrino-induced muons) at inclinations as large as $\cos{(\theta_{\mathrm{Zenith}})} \simeq 0.4$. These atmospheric-muon neutrinos can interact with the rock around SNO. They produce penetrating muons that travel up to 10 km w.e. The predicted rate of neutrino-induced muons is about 120 muons/year and, as such, it is mainly a measurement limited by statistics. This rate is small compared with the downward muon rate, but SNO's angular resolution is sufficient to make a clean separation at an angle of $\cos{(\theta_{\mathrm{Zenith}})} \leq 0.4$. This feature is very important; all comparable experiments are at a much shallower depth than SNO and, thus, cannot distinguish neutrino-induced muons above the horizon. SNO's unique niche allows it to make important model-independent checks of atmospheric neutrino oscillations.

*Presently at Pacific Northwest National Laboratory, Richland, WA 99352.

SNO is progressing in completing measurements of both the downward and upward cosmic-ray muons. The neutral-current detectors do not add to the measurement of such muons, but the additional running time greatly improves the measurement, especially for neutrino-induced muons. A total dataset of 1000 days (an additional 300 live days from the NCD phase) would mean a total data set of 360 neutrino-induced muons, or a $\sim 5\%$ measurement (statistics only). SNO is currently exploring a number of ways to also improve the systematic errors associated with muon identification.

SNO is also sensitive to atmospheric-neutrino interactions that are contained within the fiducial volume of the detector itself and to measure the neutron flux induced from cosmic rays. SNO's sensitivity to these reactions is currently being explored.

2.5 NUANCE: atmospheric-neutrino simulation in SNO

J. A. Formaggio, N. S. Oblath and J. L. Orrell*

NUANCE is an atmospheric-neutrino simulator. The code was written by David Casper, and it is used as a stand-alone program with links to the CERN libraries. NUANCE simulates six categories of scattering interactions: quasi-elastic, resonance, coherent, diffractive, deep-inelastic and elastic. Also, it simulates neutral-current and charged-current interactions, as well as neutrino oscillations and matter effects. In the end, kinematic information is provided for each vertex.

NUANCE takes as its inputs information about the neutrino flux and information about the detector geometry. The flux inputs can be in the form of an arbitrary beam, or a histogrammed flux. We have used a flux which is specific for SNO, as determined in 1996 by the Bartol group.[1] The low-energy flux ($<$ 10 MeV) is particular to Sudbury due to geomagnetic effects, while the high-energy flux is a general flux.

The geometric input is a simple description of SNO built up with concentric spherical shells of specified materials. At the center is a 6-m radius sphere of heavy water. Surrounding that is a 5-cm thick shell of acrylic, and then a 2.5-m thick shell of light water.

NUANCE is now being used as the atmospheric-neutrino generator for SNO Monte Carlos. The output of NUANCE is a file which contains kinematic information about the vertices that result from the atmospheric-neutrino interactions. This file is then converted into a format which can be read by the Monte Carlo program, SNOMAN. By running the NUANCE output through SNOMAN, we can study the effects of atmospheric neutrinos in SNO.

We have studied the systematics of the NUANCE simulation based on the uncertainties of eight parameters: the axial mass in quasi-elastic scattering, Pauli suppression in oxygen, uncertainties in the resonance channels, neutrino oscillation parameters (θ_{12},θ_{23}, Δm^2_{12}, Δm^2_{23}), and the uncertainty in the total atmospheric neutrino flux. We found that for neutral-current interactions there is a 28% uncertainty, and for charged-current interactions there is a 30% uncertainty. Table 2.5-1 shows a summary of the systematics.

Systematic	CC % Error	NC % Error
θ_{12}	$^{+1.49}_{-5.91}$	N/A
Δm^2_{12}	+1.77	N/A
θ_{23}	+4.37	N/A
Δm^2_{23}	$^{+2.11}_{-1.31}$	N/A
Axial Mass	$^{+9.23}_{-6.44}$	$^{+9.22}_{-9.39}$
Pauli Suppression	$^{+14.42}_{-15.37}$	$^{+19.35}_{-19.18}$
Resonance Uncertainty	±6.78	±7.31
Total Flux	±20.00	±20.00
Total	$^{+27.71}_{-27.58}$	$^{+30.24}_{-30.22}$

Table 2.5-1. Listing of NUANCE systematics.

*Presently at Pacific Northwest National Laboratory, Richland, WA 99352.

[1]V. Agrawal, T. K. Gaisser, P. Lipari and T. Stanev, Phys. Rev. D **53**, 1314 (1996).

2.6 Estimation of the background to an $\overline{\nu}_e$ analysis of SNO data

J. L. Orrell*

Work done at CENPA is, in large part, responsible for the estimation of the background to an electron-antineutrino ($\overline{\nu}_e$) analysis of the pure heavy-water phase of the Sudbury Neutrino Observatory (SNO) experiment. The electron-antineutrino analysis of SNO is a low-signal, low-background analysis employing extensions to the well known Feldman & Cousins[1] method of confidence level determination for signals and limits on signals. A reported result using a Feldman & Cousins style confidence level determination *requires* an estimation of the background, hence the importance of this work.

The electron-antineutrino analysis of SNO data is a continuing effort[2] to measure or limit the conversion of ^{8}B solar electron neutrinos (ν_e) into electron antineutrinos ($\overline{\nu}_e$), comparable to recent results[3,4] from other subterranean neutrino detectors. This conversion ($\nu_e \to \overline{\nu}_e$) is a possibility for massive, Majorana-type neutrinos via an interaction between a neutrino magnetic moment and solar magnetic fields.[5] A measured signal would provide new insight into the properties of massive neutrinos, while a limit on the conversion mechanism implies limits on the combination of the magnitude of the neutrino magnetic moment and the maximum magnitude of solar magnetic fields.

Table 2.6-1 presents a preliminary estimation of the background to a search for a solar electron-antineutrino signal. Note that electron antineutrinos are detected by coincidences of events produced by any of the three product particles in the reaction $\overline{\nu}_e + d \to e^+ + n + n$. The estimated number of coincidences reported is for the pure heavy-water phase of the experiment composed of data recorded between 2 November 1999 and 28 May 2001. Separate Annual Reports provide further details of the reactor[6] and atmospheric neutrino (See Section 2.5) calculations. The SNO group at CENPA has played an important role in bringing the electron antineutrino analysis closer to publication.

$\overline{\nu}_e$ background		Non-$\overline{\nu}_e$ background	
Source	Coincidences	Process	Coincidences
Atmospheric	≤ 0.072	Atmospheric ν	1.46
Reactor	< 0.019	^{238}U: spontaneous fission	< 0.79
Diffuse supernova	≤ 0.005	Accidental coincidences	0.13

Table 2.6-1. Estimated number of background coincidences in a search for a solar electron antineutrino signal. Smaller, non-$\overline{\nu}_e$ induced backgrounds are not shown.

*Presently at Pacific Northwest National Laboratory Richland, WA 99352.

[1] G. J. Feldman and R. D. Cousins, Phys. Rev. D **57**, 3873 (1998).

[2] CENPA Annual Report, University of Washington (2003) p. 21.

[3] K. Eguchi *et al.* (KamLAND Collaboration), Phys. Rev. Lett. **92**, 071301 (2004).

[4] Y. Gando *et al.* (Super-Kamiokande Collaboration), Phys. Rev. Lett. **90**, 171302 (2003).

[5] E. Kh. Akhmedov, S. T. Petcov and A. Yu. Smirnov, Phys. Rev. D **48**, 2167 (1993).

[6] CENPA Annual Report, University of Washington (2003) p. 22.

2.7 Neutral-current results from the salt phase of SNO

J. A. Formaggio, K. K. S. Miknaitis, R. G. H. Robertson, J. F. Wilkerson and the SNO Collaboration

The Sudbury Neutrino Observatory is sensitive to solar neutrinos through three interactions of neutrinos with the heavy water in the detector volume:

$$\begin{array}{lrcl} \text{Charged Current (CC) Reaction:} & \nu_e + \mathrm{d} & \longrightarrow & \mathrm{p} + \mathrm{p} + e^- \\ \text{Elastic Scattering (ES) Reaction:} & \nu_x + e^- & \longrightarrow & \nu_x + e^- \\ \text{Neutral Current (NC) Reaction:} & \nu_x + \mathrm{d} & \longrightarrow & \mathrm{p} + \mathrm{n} \end{array} \quad (1)$$

Here, ν_e indicates electron-flavor neutrinos, and ν_x indicates neutrinos of any flavor. SNO's sensitivity to both the CC and the NC interactions has allowed the experiment to probe flavor change in solar neutrinos.

In September of 2003, the Sudbury Neutrino Observatory released first results from the second phase of the experiment.[1] In this phase of the experiment, ultra-pure salt (NaCl) was added to the D_2O in the detector to enhance sensitivity to the NC reaction. Neutron capture on ^{35}Cl has a higher cross section than neutron capture on deuterium, and the gamma cascade emitted has a higher energy (8.6MeV). A consequence of the gamma cascade is that light emitted in salt neutron-capture events is distributed more isotropically around the detector than the characteristic distribution of light from Čerenkov-radiating electrons from the CC or ES interactions. The difference in isotropy of the light emitted in neutron and electron interactions in the detector allowed a statistical separation of CC and NC fluxes that did not require any assumptions about the incoming neutrino spectrum.

Using 254.2 days of data taken between July 26, 2001 and October 10, 2002, the extracted neutrino fluxes reported were (in units of $10^6\mathrm{cm}^{-2}\mathrm{s}^{-1}$):

$$\begin{aligned} \phi_{\mathrm{CC}} &= 1.59^{+0.08}_{-0.07}(\mathrm{stat.})^{+0.06}_{-0.08}(\mathrm{syst.}) \\ \phi_{\mathrm{ES}} &= 2.21^{+0.31}_{-0.26}(\mathrm{stat.}) \pm 0.10(\mathrm{syst.}) \\ \phi_{\mathrm{NC}} &= 5.21 \pm 0.27(\mathrm{stat.}) \pm 0.38(\mathrm{syst.}) \end{aligned}$$

These results, which were obtained without constraints on the incoming-neutrino spectrum, allowed maximal mixing in the solar neutrino sector to be ruled out to 5.4σ. The best-fit neutrino-oscillation parameters in a global fit of all solar-neutrino data including the salt results were:

$$\begin{aligned} \Delta m^2 &= 7.1^{+1.0}_{-0.3} \times 10^{-5}\mathrm{eV}^2 \\ \theta &= 32.5^{+1.7}_{-1.6}\mathrm{degrees} \end{aligned}$$

Progress is being made on analysis of the remaining portion of the salt data.

[1] S. N. Ahmed and the SNO Collaboration, Phys. Rev. Lett. **92**, 181301 (2004).

2.8 The day-night measurement in the salt phase of SNO

J. A. Formaggio, K. K. S. Miknaitis and the SNO Collaboration

Thanks to results from SNO, we now know that electron-type neutrinos from the sun are oscillating into mu- and tau-type neutrinos prior to reaching the earth. This is explained through matter-enhanced neutrino oscillations (the so-called MSW effect) taking place inside the interior of the sun. In the same way that matter effects can change the flavor composition of neutrinos passing through the sun, matter effects could also affect the flavor of neutrinos passing through the earth. We can look for this effect by comparing the flavor composition of solar neutrinos detected during the night, after they have traveled through the earth, to solar neutrinos detected during the day. If we were to detect a day-night asymmetry in the flavor composition of solar neutrinos, this could be a direct test of MSW physics.

To search for a day night effect, we can construct an asymmetry parameter for electron-type neutrinos:

$$A_e = 2\frac{\Phi_{e,N} - \Phi_{e,D}}{\Phi_{e,N} + \Phi_{e,D}} \tag{1}$$

where $\Phi_{e,N}$ and $\Phi_{e,D}$ are the night and day electron-neutrino fluxes, respectively. Detecting a positive day-night asymmetry in the electron-neutrino flux would be direct evidence for MSW physics. Neutrino-oscillation parameters in the currently favored region predict electron-neutrino day-night asymmetries between 2% and around 7%. In the first phase of SNO we measured $A = 7.0 \pm 4.9(\text{stat.}) \pm 1.3(\text{syst.})\%$. This measurement is statistically limited, so we look forward to adding the additional data from the salt and NCD phases.

We are currently in the process of analyzing the salt-phase data for a day-night asymmetry. The first step in this measurement is an accurate determination of our day and night livetime, accounting for all data cleaning cuts. SNO's livetime is measured using a 10MHz GPS-synchronized clock, which is then checked using a 5Hz pulsed global trigger. Since we do not have the ability to do regular calibrations of the SNO detector during the night, determination of systematic uncertainties in diurnal stability of the detector response must be done using in-situ techniques. By studying the differences in rates and characteristics of signals that are always present in our detector, we can limit systematic variations in parameters such as energy scale or resolution day and night that could affect the asymmetry measurement. Classes of events that are used for these studies include a slightly radioactive "hot spot" on the acrylic vessel, low-energy backgrounds in the detector materials, and spallation neutrons due to cosmic-ray muon interactions. The muon follower events are a particularly attractive event class for these studies, because they mimic the NC signal.

SNO Neutral Current Detectors (NCDs)

2.9 NCD backgrounds and data cleaning

G. A. Cox, H. Deng,* P. J. Doe, S. R. McGee, K. Rielage, R. G. H. Robertson, L. C. Stonehill and J. F. Wilkerson

Now that the SNO NCD array has been deployed, efforts are shifting towards analysis activities such as background identification and rejection. This is a two-step process, where first non-physics backgrounds must be rejected and then the signal must be separated from physics backgrounds, such as alphas from the U- and Th-decay chains. Many non-physics backgrounds have been identified by hand-scanning through data taken during the cool-down phase and during NCD deployment. Based on the types of non-physics events, cuts are being developed to remove them. One major tool for rejecting backgrounds is the fact that the NCD system has different triggers in the shaper and digitized data paths. The shaper trigger integrates the pulse over several microseconds, so it is effectively a charge threshold, whereas the digitized data trigger has a very short integration time, so it is effectively a current amplitude threshold. Physics events will trigger both paths but many different types of non-physics events will trigger only one or the other. For example, oscillatory noise may have large amplitudes but integrate to small or zero charge. Similarly, HV related events such as microdischarge may also carry a small charge, due to the short duration of the discharge. By requiring that all candidate events pass both triggers, many non-physics backgrounds can be rejected. Other types of non-physics backgrounds require special cuts, which are being developed here and by SNO collaborators. For example, cuts are being developed to reject microphonic noise induced by blasting and seismic activity in the mine where SNO is housed.

Once the non-physics backgrounds are removed from the NCD data, most of the remaining events should be signal neutrons and U- and Th-chain alpha-particle emission from the NCD walls. The NCDs detect thermalized neutrons via the ^{3}He(n,p)^{3}H reaction. The neutron capture efficiency is such that we expect of order 1000 captures per year in the entire NCD array from solar-neutrino neutral-current interactions with SNO's heavy water. In addition to the main array of 36 ^{3}He strings, there are 4 strings filled with ^{4}He-CF$_4$ gas to assess non-neutron backgrounds. Data taken from the NCDs before their deployment into SNO indicates that the intrinsic alpha background rates are on the order of 100 events per day in the entire NCD array. A substantial number of these background events can be eliminated by energy cuts, since the ^{3}He(n,p)^{3}H reaction deposits 764 keV of energy in the NCD and the alpha backgrounds can range up to about 9 MeV. In addition, many more of these background events can be cut using pulse-shape analysis of the digitized current pulses from the NCDs. A technique using pulse duration vs. energy scatter plots to separate neutrons from physics backgrounds is the default pulse-shape analysis, although other techniques are being developed, such as a semi-analytic pulse-shape fitter.

*Department of Physics and Astronomy, University of Pennsylvania, Philadelphia, PA 19104-6396.

2.10 Deployment of an array of Neutral Current Detectors (NCDs) in SNO

J. F. Amsbaugh, J. Banar,* T. A. Burritt, G. A. Cox, P. J. Doe, D. Earle,†
J. A. Formaggio, G. C. Harper, J. Heise,* A. Krueger,‡ A. Krümins,§ I. T. Lawson,¶
K. Lesko,‖ S. McGee, B. Morrisette,† A. W. Myers, R. W. Ollerhead,¶ K. R. Rielage,
R. G. H. Robertson, M. W. E. Smith, L. C. Stonehill, T. D. Van Wechel, B. L. Wall,
J. F. Wilkerson and J. Wouters*

An array of 40 proportional counters has been installed in the heavy water volume of SNO. This array consists of 36 ^{3}He filled counters and four ^{4}He filled counters (as controls) arranged on a 1-m square grid about the center of SNO's acrylic vessel (AV).

The NCDs are 9 to 11 m long and are comprised of combinations of at least three counter sections of 2, 2.5 or 3 m in length welded with an Nd-YAG laser designed at UW.[1] Each NCD has an open-ended electrical configuration with an 80-nsec roundtrip delay line contained within a housing which terminates the NCD string and at least 9-m of readout cable required to run the length of the neck of the AV to reach the NCD data acquisition system.[2] Constraints imposed by the size of the cavity in which SNO sits limited the length of sections that could be deployed at one time to 5.5 m. This meant that at least one weld per string was needed at the time of deployment.

After the final weld was done over the neck of the AV, but before being flown to its final position with the Remotely Operated Vehicle (ROV),[3] a 60-Hz AmBe neutron source was placed near the center of each counter section of the NCD. The gain, resolution and total number of neutrons detected for each section was compared to known pre-deployment values to insure each NCD was functioning properly.

The first NCD was successfully deployed on December 2, 2003. Extensive monitoring of each NCD's data quality was conducted throughout the entire deployment period. Setbacks led to the extraction, testing and redeployment of a handful of the NCDs and caused the deployment schedule to run beyond its original end-date. The deployment phase officially ended on April 21, 2004 with the removal of the ROV from the AV.

The addition of NCDs begins phase III of the SNO experiment and allows for event-by-event separation of the neutral current (NC) measurement from that of the charged current (CC). This effectively makes phase III a different experiment from the earlier phases of SNO and puts it in the unique position of being able not only to make an improved NC/CC measurement but also to confirm its own previous results.

---

*Los Alamos National Laboratory, Los Alamos, NM 87545.
†Sudbury Neutrino Observatory, Lively, Ontario, Canada P3Y 1M3.
‡Laurentian University, Sudbury, Ontario, Canada P3E 2C6.
§Queens University, Kingston, Ontario, Canada, K7L 3N6
¶University of Guelph, Guelph, Ontario, Canada N1G 2W1.
‖Lawrence Berkeley National Laboratory, Berkeley, CA 94720.

[1] CENPA Annual Report, University of Washington (2001) p. 37.
[2] CENPA Annual Report, University of Washington (2003) p. 28.
[3] CENPA Annual Report, University of Washington (2001) p. 30.

2.11 NCD analysis tools and electronics calibrations

G. A. Cox, P. J. Doe, A. L. Hallin*, M. A. Howe, S. McGee, K. R. Rielage, R. G. H. Robertson, L. C. Stonehill, B. Wall and J. F. Wilkerson

The NCD data readout system has undergone a major change within the last year. While the hardware remained essentially unchanged, our data-acquisition software migrated from SHaRC to ORCA.[1] Both programs are similar in function, but ORCA has improved capabilities, integrates the NCD data acquisition system with the SNO PMT system, and runs on Mac OS X. Integration with the PMT system required a significant change in the methods used to access our data. There is a two–step process where the data from ORCA are processed through two programs called "ncdbuilder" and "snobuilder." (There is also a "pmtbuilder" program for the PMT data.) These programs combine information from the various hardware components in the NCDs (and PMTs) and reformat the "raw" data stream from ORCA into a ZDAB format that is readable by various analysis tools. There are four main programs that read ZDAB data files and produce useful information for the SNO detector operators and analysis teams: SNOSTREAM, NCDMonitor, SNOMAN, and XSnoED. NCDMonitor and SNOMAN are the programs that have been used by the NCD group for data analysis tasks. The NCDMonitor displays events and allows one to "hand–scan" the data to look for anomalous events. Our past ROOT macros are as useful as before because we use SNOMAN to process our ZDAB data files into ROOT–readable files.[2] Using ROOT's C–interpreter and a set of libraries built exclusively for SNO and NCD data, event rates, energy spectra, pulse width versus energy plots, data-acquisition efficiencies, and other information from NCD data can be extracted.

The multiplexer (MUX) logarithmic amplifier (logamp) must be calibrated in order to properly analyze the data. Events of sufficient amplitude are amplified by the logamp and then digitized by the oscilloscopes. The recorded pulses must be "de–logged" to retrieve the original event pulse. The logamp transforms the pulse according to

$$V_{out} = a \cdot \log\left(1 + \frac{V_{in}}{b}\right) + c. \tag{1}$$

Calibration of the MUX logamps is performed by injecting a known waveform into the current preamplifier at the front–end of the electronics system and performing a χ^2 minimization of the digitized pulse compared to the expected transformation, V_{out}. The values of a, b, and c are found in this way. Inverting this transformation allows original pulses to be retrieved from the digitized pulses. The calibration pulse is generated by a Hewlett Packard 33120A Function Generator and is distributed to all NCD electronic channels by our custom–built Pulser Distribution System. An offset single sine wave has been chosen to be the calibration pulse since it can have a large range in amplitudes and is a smooth function that is unrestricted by bandwidth constraints of the preamplifiers. The calibration of the logamp has been demonstrated to work, but is still being developed into a more automated routine. Calibration of the gain and thresholds of shaper/ADC cards has not yet been done in SNO.

*Department of Physics, Queen's University, Kingston, ON K7L 3N6.

[1] CENPA Annual Report, University of Washington (2002) p. 70.

[2] CENPA Annual Report, University of Washington (2003) p. 25

2.12 PMT calibrations in SNO during the NCD phase

A. Hallin,* I. Lawson,† N. S. Oblath and R. G. H. Robertson

The purpose of the SNO Photomultiplier Tube array is to measure the timing and number of photons within SNO. Naturally, the ability of the PMTs to make those measurements needs to be calibrated. This is done using a pulsed nitrogen/dye laser system. A 10-cm diameter diffuser ball is placed near the center of the detector. The light provided by the diffuser ball (laserball) is nearly isotropic (to $\approx$10%). With the laserball at the center of the detector, the light travel time to each PMT is the same, and refraction effects at the boundaries between the heavy water and the acrylic, and between the acrylic and the light water can be ignored. The intensity of the laser pulses is reduced so that, at most, only one photon is detected by any PMT.

In the NCD phase, the PMT calibrations are complicated by the fact that the NCDs cast shadows on the PMT array. This problem is solved by performing the calibration with the laserball at multiple locations. The goal is that every PMT will be illuminated by the laserball when it is at one or more of the positions.

Having the laserball off-center requires making a timing correction in the calibration software, since the distances between the laserball and the PMTs are not equal. Furthermore, the light spends different amounts of time in the heavy water and light water regions, depending on the exact path between the laserball and the PMT. The correction consists of determining the timing change between light traveling from the center of the detector to the PMT and light traveling from the off-center laserball to the PMT, and that time is subtracted off the PMT signal time before the calibration is made. Fig. 2.12-1 shows the result of the timing correction test. The laserball was 75 cm from the center of the detector. It is also

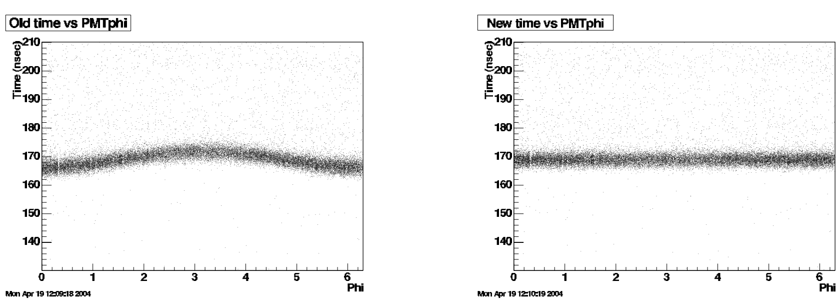

Figure 2.12-1. The prompt light peak of the PMT signals as a function of azimuthal angle before and after the timing correction.

necessary to determine which combinations of laserball positions allow for all of the PMTs to be calibrated in the shortest amount of time. We have written a 2-dimensional simulation to find the ideal combination of two laserball runs where the laserball is within 1 m of the center along the x-axis of the detector. The preliminary result shows that placing the laserball at +45 cm and −45 cm, with a tolerance of approximately 4 cm, provides the greatest overall coverage of the detector.

*Queens University, Kingston, Ontario, Canada K7l 3N6.
†University of Guelph, Guelph, Ontario, Canada, N1G 2W1.

2.13 Upgrade to the NCD electronics for SNO

G. A. Cox, S. McGee, A. W. Myers, K. Rielage, R. G. H. Robertson, L. C. Stonehill, T. D. Van Wechel and J. F. Wilkerson

A number of upgrades have been made to the SNO NCD electronics since original commissioning underground.[1] The electronics for the NCDs are composed of two main systems: a digitized data path utilizing 40 multiplexer channels that can be sent to two different oscilloscopes and 40 shaper channels that return a total integrated charge for the event.

The NCD cable connections to the electronics channels must be able to withstand significant strain during deployment as the NCDs are moved into position. All forty of the deployed NCD cables' dryend connections were replaced in November 2003 with a newly designed connector to ensure both excellent mechanical strength and electrical grounding. These replacements also lowered the overall noise pickup in these cables.

A new NCD preamp was designed in Summer 2003. This new design utilizes several additional JFETs in parallel and allows for the preamp to have an impedance match to the NCD cable. This close impedance match results in a signal with much lower noise. The new design also increased the bandwidth by a factor of three. These changes result in a much cleaner neutron signal compared to the older design as shown in Fig. 2.13-1. Fifty-five new preamps were constructed and tested and are now in use on the SNO NCD system.

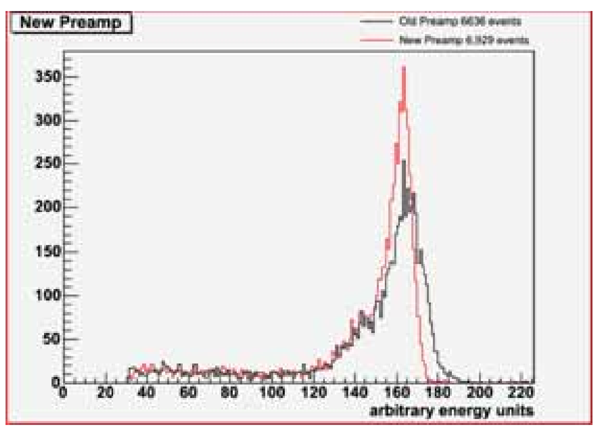

Figure 2.13-1. NCD neutron source spectrum with old preamp compared to new preamp

An NCD trigger card was also designed and constructed to allow the NCD events to be integrated into the SNO master trigger card with unique global trigger numbers. Several other modifications were made to high voltage readback electronics, multiplexer controller boards and multiplexer threshold readback electronics. An improved NCD trigger card is currently being designed to include a 10-MHz clock for timing information when the SNO master trigger card is offline. Other future upgrades include the replacement of all non-commercial electronics boards.

[1] CENPA Annual Report, University of Washington (2002) p. 33.

KATRIN

2.14 The KATRIN neutrino-mass experiment

T. H. Burritt, P. J. Doe, G. C. Harper, J. A. Formaggio, M. A. Howe, M. Leber, S. R. McGee A. W. Myers, K. R. Rielage, R. G. H. Robertson, T. D. Van Wechel and J. F. Wilkerson

The **KA**rlsruhe **TRI**tium **N**eutrino (KATRIN) experiment[1] is a next-generation tritium β-decay experiment designed to measure the mass of the neutrino with sub-eV sensitivity. The experiment should be an order of magnitude more sensitive than the best terrestrial measurements carried out to date, and hence should both improve our understanding of neutrino properties as well provide important constraints on models of nuclear and particle physics, cosmology, and astrophysics. With the current design, KATRIN expects a sensitivity to neutrino mass of 0.20 eV (90% CL) and would expect to observe a neutrino mass with a mass of 0.35eV at the 5 sigma significance level.

The experiment will be constructed adjacent to the Tritium Laboratory Karlsruhue at the Forschungszentrum Karlsruhe (FZK). The current goal is for the KATRIN to become operational during 2008. The University of Washington in collaboration with FZK intends to provide the primary detector system as well as the real-time data acquisition system.

During the past year, research and development at UW has progressed on several fronts, with emphasis on the pre-spectrometer system which is expected to begin operation in 2004.

- We are designing and fabricating the pre-spectrometer inner electrode system.
- A high-vacuum detector test stand was assembled and commissioned. The stand includes a UV photoemissive monoenergetic electron gun that can produce electrons with energies up to 30 keV. Preliminary backscattering studies have been completed.
- A Monte Carlo simulation effort to investigate energy loss and backscattering issues has been initiated.
- An interim electronics and data-acquisition system for the KATRIN pre-spectrometer, was delivered to FZK last fall. This system consists of 64 channels of peak detect, shaper ADCs based in a VME bus. For the shaper ADCs we used a slightly modified design from our custom emiT/NCD electronics. The data-acquisition software is built in our recently developed Macintosh OS X Object-oriented Real-time Control and Acquisition (ORCA) system.

In the coming year we expect our efforts on KATRIN to increase as our SNO NCD construction and deployment efforts have ended. We will concentrate on detector development, with some additional work on issues concerned with calibration and the accurate characterization of potential systematic uncertainties.

[1]The present collaboration: Univ. of Bonn; CCLRC Daresbury Laboratory; Joint Institute for Nuclear Research, Dubna; Univ. of Applied Sciences (FH) Fulda; Forschungszentrum Karlsruhe; U. of Karlsruhe; Johannes Gutenberg-Univ., Mainz; Institute for Nuclear Research, Moscow; Nuclear Physics Institute, Prague; Rutherford Appleton Laboratory; University of Wales Swansea; Center for Experimental Nuclear Physic and Astrophysics, Univ. of Washington.

2.15 KATRIN electron gun testing of detector dead layers

P. J. Doe, T. Gadfort,* J. A. Formaggio, G. C. Harper, M. A. Howe, M. Leber, S. McGee, K. Rielage, R. G. H. Robertson, J. F. Wilkerson and the KATRIN Collaborators

The KATRIN[1] (KArlsruhe TRItium Neutrino) experiment will measure the electron energies from tritium beta decay. By examining the endpoint of the electron energy spectrum near 18.6 keV for any deviation, an upper limit of 0.35 eV can be placed on the neutrino mass (or detection at the 5σ level). The experiment consists of a tritium source, a small pre-spectrometer followed by a 10-m diameter retarding-field magnetic-electrostatic analyzer, and a large (approximately 10 cm x 10 cm) silicon detector. The UW group is responsible for several aspects of this experiment including the DAQ system, the design and building of electrodes for the pre-spectrometer, and the design and characterization of the detector and associated front-end electronics. This section discusses the progress of the detector development and characterization.

In order to determine the deviation at the electron energy-spectrum endpoint with small systematic uncertainty it is necessary to utilize a detector that is well characterized. Some of the most crucial pieces of information needed are the accurate determination of the detector's dead layer and the number of events backscattering off the detector. To perform these measurements a monoenergetic electron gun was built[2] capable of producing electrons with energies up to 30 keV. These electrons can be used to determine the dead layer of various sold state detectors by using the tilt method.[3]

The electron gun is complete and has used to test several small silicon photodiode detectors including the Hamamatsu S3204-9. This detector has a 1.8 cm x 1.8 cm active window. The dead layer was measured to be 107 ± 10 nm. A second detector (Hamamatsu S3590-09 windowless Si PIN photodiode) with an active area of 1.0 cm x 1.0 cm was used to examine electrons scattered off the first detector as a function of electron angle of incidence.

Currently the detector test set-up is being redesigned to accommodate detectors up to 10 cm x 10 cm in size. A precision X-Y translation stage is being purchased capable of operating via stepper motors in the high-vacuum environment of the electron gun. This translation stage will be capable of rotating around the axis of the detector to perform dead-layer measurements at any location on the detector. The cooling system for larger detectors is also being designed to operate the detectors below 0° C. In addition, the electronics and data acquisition systems are being upgraded to support a Firewire to VME connection for communication between the two systems. A full 64-element detector will be tested and characterized for use during the testing of the KATRIN pre-spectrometer scheduled for late 2004 at Karlsruhe.

---

*Dept. of Physics, UW

[1] CENPA Annual Report, University of Washington (2002) p. 44.

[2] CENPA Annual Report, University of Washington (2003) p. 34 and p. 65.

[3] R. L. Williams and P. P. Webb, IEEE Trans. Nucl. Sci., **NS-9** (Number 3), June 1962, pp. 160-166.

2.16 KATRIN pre-spectrometer electrode

T. H. Burritt, P. J. Doe, R. G. H. Robertson and J. F. Wilkerson

Both the pre-spectrometer and the main spectrometer vacuum vessels are equipped with an internal electrode. The purpose of this electrode is to prevent electrons, originating from the walls of the vacuum vessel, from entering the spectrometer and constituting a source of background. These electrons may be produced by cosmic rays or natural radioactivity in the vessel walls. It is necessary that the internal electrode have very low mass and be compatible with the ultra high vacuum requirements of the spectrometer. The University of Washington will provide the internal electrode for the pre-spectrometer shown in Fig. 2.16-1.

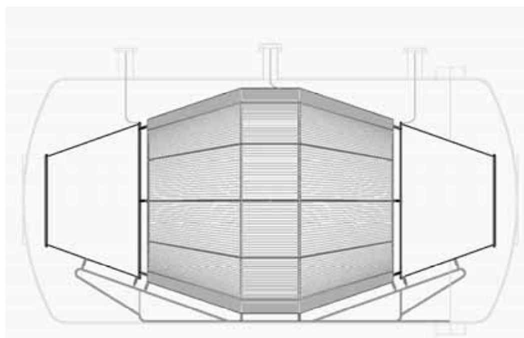

Figure 2.16-1. The Pre-Spectrometer Electrode, resting on its cradle in the pre-spectrometer vacuum vessel.

The electrode consists of a central, low mass, wire barrel. At each end of the barrel is a cone made of thin sheet metal. These cones are located in high field regions where the use of wires could result in breakdown.

The electrode must be capable of surviving bake-out to 350° C and be compatible with vacua of 10^{-11} Torr. In order to test the design concepts, a test electrode has been built to study the various fabrication concepts and techniques proposed for the final pre-spectrometer electrode. This electrode is shown in Fig. 2.16-2.

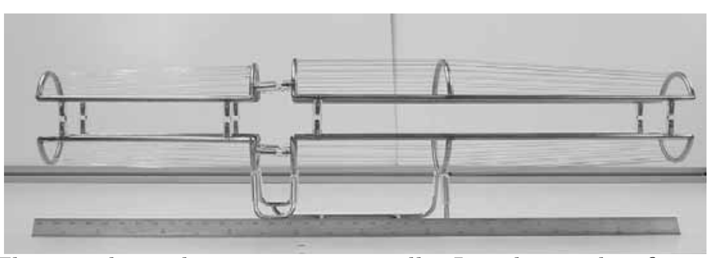

Figure 2.16-2. The test electrode resting on its cradle. It is designed to fit in the Karlsruhe vacuum test chamber.

The test electrode has shown that it is capable of withstanding the bake-out temperatures and maintaining wire tension and dimensional tolerance. It is being shipped to Karlsruhe to be subjected to vacuum tests. The fabrication drawings for the pre-spectrometer are undergoing final review. It is expected that the electrode will be shipped to Karlsruhe in late October 2004.

Majorana

2.17 CENPA contributions to the Majorana experiment

P. J. Doe, V. M. Gehman,* K. Kazkaz, R. G. H. Robertson and J. F. Wilkerson

The Majorana experiment[1] is a ^{76}Ge-based search for neutrinoless double-beta ($0\nu\beta\beta$) decay. In the past, CENPA has been involved with construction of related experiments, development of the data-acquisition system, and shielding simulations.[2] This year we have built on those projects and extended our involvement with the wider collaboration.

The construction of MEGA[3] has continued over the past year at Pacific Northwest National Laboratory. One two-pack is fully assembled, and the parts for the second two-pack are in hand. CENPA is developing an automated evaluation system for the two-packs as well as a system for monitoring state-of-health of the installed detector.

Two preamplifiers have been evaluated for their use in the Majorana experiment: the PGT-RG11 and the Amptek A250. The preamps are evaluated on the basis of various criteria, including response time, quality of the response curve, exponential return to baseline, intrinsic resolution, FET power dissipation, linearity of energy dependence, and bandwidth. Both of these preamps display acceptable performance, though the A250 has much cleaner response, with no real overshoot or ringing. It also has better intrinsic resolution. Three more preamps remain to be evaluated.

The simulation work done last year has been absorbed by a larger, all-encompassing simulation effort organized by Lawrence Berkeley National Laboratory. The Majorana collaboration has decided to adopt the GEANT4[4] simulation package. The simulation has been broken down into five primary efforts: database, background models and event generation, signal output, geometry, and the physics list. The last two of these efforts are the responsibility of CENPA.

The first geometry that is being created within the Majorana simulation framework is of what is known as a "clover detector," manufactured by Canberra. The clover simulation is used as a simple first case to determine how the various parts of the simulation will cooperatively interact. The simulation data will initially include event generators for both ^{232}Th and ^{68}Ge, and will be compared to experimental data obtained from the clover detector at Los Alamos National Laboratory.

The GEANT4 physics list incorporates low-energy electromagnetic and neutron interactions applicable to a low-background environment, as well as high-energy hadronic interactions resulting from cosmic-ray spallation. Our tuning of the physics list takes place using

*Presently at Los Alamos National Laboratory Los Alamos, NM 87545.

[1] http://majorana.pnl.gov

[2] CENPA Annual Report, University of Washington (2003) p. 32.

[3] K. Kazkaz *et al.*, MEGA: A Low-Background Radiation Detector, *IEEE Transactions on Nuclear Science*, accepted for publication June, 2004.

[4] http://wwwasd.web.cern.ch/wwwasd/geant4/geant4.html

a very simple single-crystal simulation with a thorium source. We compared the simulation data to data taken by a coaxial germanium surface detector completely encompassed by a six-inch lead shield in Seattle. The experimental setup is not considered "low-background", *e.g.,* no measures were taken to reduce either ^{40}K contamination or radon within the shield.

Fig. 2.17-1 shows the comparison between the simulated and experimental data. The two spectra have been normalized by the integrated counts in the well-modeled region between 1800 keV and 2640 keV. The curves do not match in the entire spectrum as a result of a deficiency of peaks in the simulation event generator. The validation of the physics list, however, comes about by comparing peak-to-Compton ratios, observing the existence of single- and double-escape peaks, and comparing the height of the annihilation peaks between curves. In this sense, the physics list is deemed trustworthy. The quality of the simulated hadronic interactions resulting from high-energy muons and fast neutrons has not yet been evaluated.

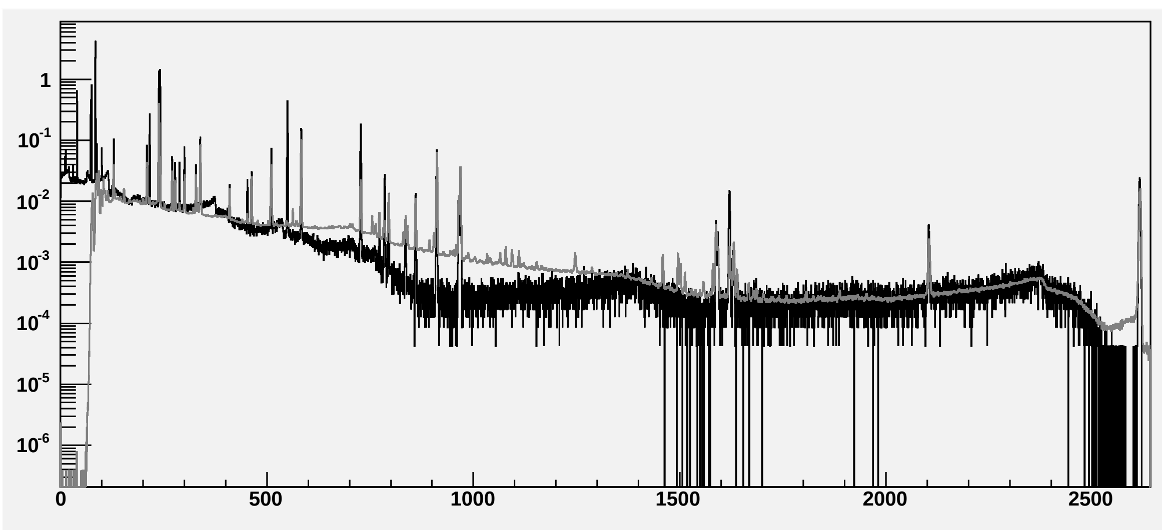

Figure 2.17-1. Spectra from simulated and experimental data from ^{232}Th. The lighter grey curve is the experimental data, and is narrower because of higher statistics. The vertical axis is an arbitrary scale resulting from the renormalization.

2.18 A Joint Institute for Advanced Detector Technology

P. J. Doe, J. H Gundlach, H. S. Miley,* R. G. H. Robertson and J. F. Wilkerson

The University of Washington (UW) and Pacific Northwest National Laboratory (PNNL) have a history of successful collaborations. At the institutional level, a Joint Board has been established between UW and PNNL to facilitate and foster such collaborative efforts. This board oversees and governs official Joint Institutes and Programs that the institutions have identified as meriting strategic support.

For the past four years our Electroweak Interactions group at CENPA and the PNNL Radiological and Chemical Sciences group have been collaborating together on a number of projects, including the Majorana next generation double-beta decay experiment and the investigation of advanced ultra-low background counting capabilities one would need at a Deep Underground Science and Engineering Laboratory (DUSEL). In March of 2004 we presented the concept of a new UW-PNNL Joint Institute for Advanced Detector Technology to a meeting of the Joint Board. This idea was extremely well received and the Board has requested that we submit a detailed formal proposal at its next meeting.

We have identified three main thrusts for this Joint Institute (JI):

- Developing Advanced Detectors for both applied (National and Homeland security) and basic physics (next-generation double-beta decay, and dark matter) experiments. There is a surprisingly large amount of overlap between these two research areas. It is envisioned that the JI would quickly reach beyond the initial core groups and engage experts in engineering, materials science, and chemistry. It is expected that this area will grow into a strong interdisciplinary effort.
- Developing a DOE proposal for an Underground Ultra Low Background Counting Facility (LBCF). This would be an effort aimed at developing a national facility based at DUSEL. Such a facility would support research into both next-generation basic physics detectors and national and homeland security applications. We envision that this proposal will have additional partners from both universities and other national laboratories, such as LBNL, LANL, and LLNL. The LBCF is currently a key component of our DUSEL - Cascades proposal.
- Working cooperatively to build the Majorana double beta decay detector. Both PNNL and UW have significant expertise in this area. UW brings knowledge on building and operating experiments in a clean, ultra-low background underground environment, most recently having deployed the specially fabricated neutral-current detectors at SNO. The PNNL group has extensive experience with germanium detectors, double beta decay, and ultra sensitive underground counting experiments.

We anticipate submitting a detailed proposal to the Joint Board in the fall of 2004.

---

*Pacific Northwest National Laboratory, Richland, WA 99352.

3 Nuclear Astrophysics

3.1 Precise measurement of the ^{7}Be(p,γ)^{8}B S-factor

A. R. Junghans,* E. C. Mohrmann, K. A. Snover, T. D. Steiger,† E. G. Adelberger, J. M. Casandjian,‡ H. E. Swanson, L. Buchmann,§ S. H. Park,§ A. Zyuzin§ and A. M. Laird§

We have completed our precision measurements of the ^{7}Be(p,γ)^{8}B cross section at astrophysically interesting energies.[1] Results were obtained with 3 different targets, spanning the center-of-mass energy range E = 116 to 2460 keV. Our latest results, obtained with a 340-mCi ^{7}Be target, incorporated several improvements over our previously published experiment.[2] Our new measurements lead to $S_{17}(0) = 22.1 \pm 0.6$(expt) $\pm$ 0.6(theor) eV b based on data from $\bar{E}_{\mathrm{c.m.}} = 116$ to 362 keV, where the central value is based on the theory of Descouvemont and Baye, and the theoretical error estimate is based on the fit of 12 different theories to our low-energy data. This result is in excellent agreement with our previously published value.

We find that all modern direct results for $S_{17}(0)$ are mutually compatible. We recommend a "best" value, $S_{17}(0) = 21.4 \pm 0.5$(expt) $\pm$ 0.6(theor) eV b, based on the mean of all modern direct measurements below the 1^+ resonance. We also present S-factors at 20 keV which is near the center of the Gamow window: the result of our measurements is $S_{17}(20) = 21.4 \pm$ 0.6(expt) $\pm$ 0.6(theor) eV b, and the recommended value is $S_{17}(20) = 20.6 \pm 0.5$(expt) $\pm$ 0.6(theor) eV b.

$S_{17}(0)$ values have also been determined using indirect techniques; namely Coulomb dissociation and peripheral heavy-ion transfer. Mean values determined from these indirect measurements lie lower than the mean determined from direct experiments. In addition the slope (energy dependence) of S(E) versus E inferred from Coulomb dissociation is steeper than the slope observed in the direct measurements.[1] These differences represent an important unresolved problem.

Recently, we refit the region of the 3^+, E = 2183 keV resonance with an improved (quadratic polynomial) background, and determined $\Gamma_\gamma = 101 \pm 51$ meV for the ground-state transition, corresponding to a reduced transition strength B(M1) = 0.38 $\pm$ 0.19 W.u. (Weisskopf units). The reduced M1 strength for the ground-state transition from the 1^+, E = 630 keV resonance is 2.66 $\pm$ 0.13 W.u. (see Table IV of ref.1). These estimates, made assuming pure M1 decay (and negligible resonance inelasticity) may be compared to 0.29 $\pm$ 0.13 W.u. and 2.8 $\pm$ 0.9 W.u. for the mirror transitions in ^{8}Li, respectively.[3]

*Permanent address: Forschungszentrum Rossendorf, Dresden, Germany
†Present address: Cymer, Inc., San Diego CA 92127.
‡Present address: GANIL, Caen, France.
§TRIUMF, Vancouver, Canada.
[1] A. R. Junghans *et al.*, Phys. Rev. C **68**, 065803 (2003).
[2] A. R. Junghans *et al.*, Phys. Rev. Lett. **88**, 041101 (2002).
[3] http://www.tunl.duke.edu/nucldata/ourpubs/p08_2002.shtml. The shell model predicts small isoscalar matrix elements for these transitions (D. J. Millener, private comm.).

3.2 ^{3}He$(\alpha,\gamma)^{7}$Be γ-ray background analysis

C. Bordeanu, J. Manor,* P. N. Peplowski, K. A. Snover and D. W. Storm

We are planning a precision measurement of the ^{3}He$(\alpha,\gamma)^{7}$Be cross section by detecting both the prompt capture γ-rays and the delayed γ-rays from ^{7}Be decay, using an α beam incident on a ^{3}He gas cell. Before the gas cell can be constructed, it is necessary to test materials for possible use as the entrance foil, cell liner and beam stopper. Due to the small ^{3}He$(\alpha,\gamma)^{7}$Be cross section, it is important to limit both the prompt and delayed γ-ray background coming from interactions of the beam with materials in the gas cell. We irradiated Ni, Co, Cu, Nb, Ta, Pt and Au test materials from Goodfellow (labelled 'G') and Alfa Aesar (labelled 'A'), and measured both prompt and delayed γ-ray backgrounds.

Prompt γ-ray background resulting from the α beam interacting with the entrance foil and/or beam stopper can cause difficulties if it interferes with the ^{3}He$(\alpha,\gamma)^{7}$Be capture γ-ray peaks. Prompt background measurements were analyzed to determine which materials have the lowest background in the energy range of the ^{3}He$(\alpha,\gamma)^{7}$Be primary and secondary capture γ-rays. Gamma-ray spectra were measured in the range E_{γ} = 0.5 - 5 MeV, with results for selected energy bins shown in Fig. 3.2-1.

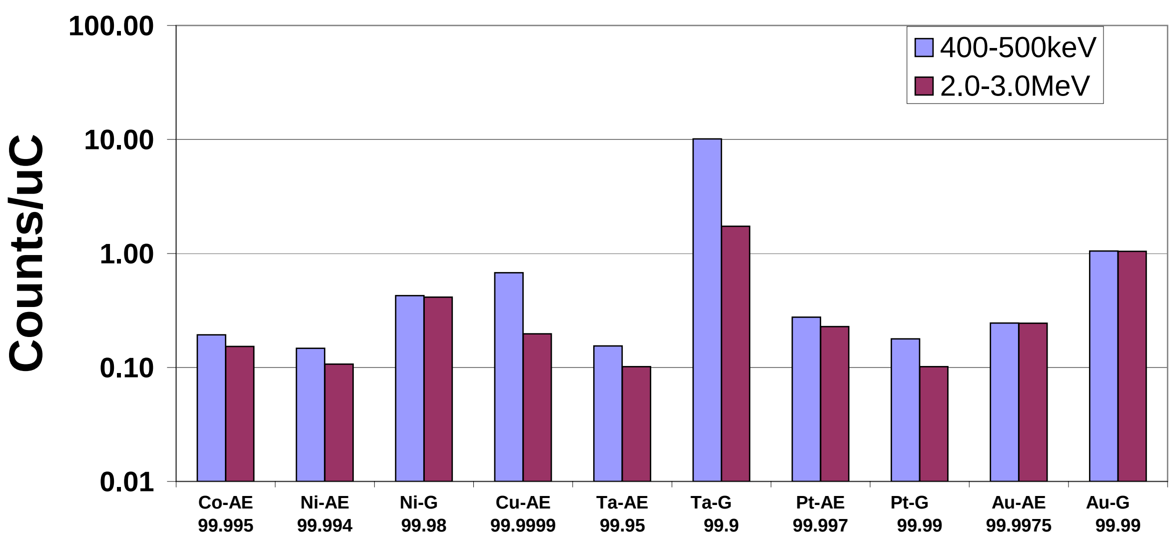

Figure 3.2-1. Prompt γ-background from 3.5 MeV α-bombardment of various materials, observed in a 50% Ge detector 3 cm from the target. Yields in Counts per μC of ^{4}He^{+} are shown for energy bins E_{γ} = 400 - 500 keV and 2.0 - 3.0 MeV.

Delayed γ-ray background from ^{7}Be decay may result from contamination reactions.[1] For a ^{4}He beam, contaminant ^{7}Be production can occur via ^{6}Li(d,n)^{7}Be and ^{10}B(p,α)^{7}Be, if there is a proton or deuteron contaminant in the beam and Li or B in the ^{3}He gas cell stopper or

*Graduated in March 2004.

[1] M. Hilgemeier, H. W. Becker, C. Rolfs, H. P. Trauvetter and J. W. Hammer, Z. Phys. A **329**, 243 (1988).

liner. Since the cross sections for these contamination reactions are five orders of magnitude larger than the cross section for ^{3}He(α, γ)^{7}Be, small amounts of contamination may result in significant ^{7}Be production.

We performed tests with our terminal ion source to determine the molecular p and d contamination in our 3 MeV ^{4}He beam using the accelerator 90° analyzing magnet. A small satellite beam at slightly higher rigidity than ^{4}He$^+$ was observed, corresponding to D_2^++DH_2^+. The presence of deuterium in this satellite was verified by observing β-delayed α-particles from the ^{7}Li(d,p)^{8}Li reaction. The intensity of this satellite peak was 0.1% to 1% of the ^{4}He$^+$ beam, depending on the preparation of the ion source. This satellite beam was intermittently transmitted to the target chamber by small downward fluctuations in the accelerator voltage.

In separate measurements, we determined the ^{7}Be production from 0.75-MeV proton and 1.5-MeV deuteron irradiation of our test materials, shown in Fig. 3.2-2. On the basis of these measurements, we should be able to avoid contaminant ^{7}Be production and achieve low prompt γ-background during α-bombardment by using a Ni, Co or Ta gas cell stopper.

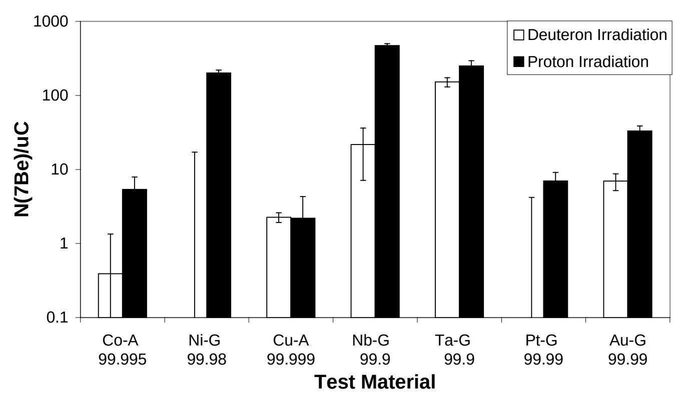

Figure 3.2-2. Number of ^{7}Be atoms N(^{7}Be) produced per μC of irradiated 0.75 MeV proton and 1.5 MeV deuteron beam on various test materials. Error bars indicate statistical uncertainty. Error bars with no histogram indicate upper limits.

3.3 Search for the ^{8}B(2^+) → ^{8}Be(0^+) ground state transition

M. K. Bacrania, D. Crompton, R. G. H. Robertson, D. W. Storm and S. Uehara

SNO and Super-Kamiokande are sensitive to high-energy (> 5 MeV) solar neutrinos produced by the decay of ^{8}B. The decay of ^{8}B proceeds primarily through the allowed $2^+ \rightarrow 2^+$ transition to the 3-MeV broad excited state in ^{8}Be. The resulting neutrino spectrum has an endpoint energy of approximately 14 MeV. It is also possible for ^{8}B to decay to the ground state of ^{8}Be through a second-forbidden transition ($2^+ \rightarrow 0^+$) with an endpoint of approximately 17 MeV. Solar neutrinos produced via this decay branch would be a background to both measurements of ^{8}B neutrino spectrum shape and measurements of the *hep* neutrino spectrum. This branching ratio is expected to be very small, but to date, no experimental verification has been published.

As reported last year,[1] we produce beams of 15-MeV ^{8}B by irradiating a ^{3}He gas target with a 36-MeV ^{6}Li beam. The ^{8}B is magnetically separated and implanted into a 500μm silicon PIN detector. The ^{8}B decay produces a β^+ and the prompt decay of ^{8}Be produces a pair of α particles. The β^+ is detected in a scintillator, providing a coincidence trigger. For ^{8}Be excitation energies below 7 MeV, both α particles come to rest inside the Si detector. Decay via the $2^+ \rightarrow 2^+$ branch results in a broad α-energy spectrum centered around 3 MeV, and decay to the ground state results in a line centered at 92 keV.

In 2003, we improved beam collimation and detector positioning in order to reduce backgrounds from stray ^{8}B deposited near the detector. We also improved our ^{6}Li ion source which allowed us to produce higher beam currents over a longer period of time. Our current limit (1σ) for the branching ratio of the ^{8}B(2^+) →^{8}Be(0^+) is $< 1 \times 10^{-4}$. This limit was obtained by subtracting from our ^{6}Li + ^{3}He spectrum a ^{6}Li + ^{4}He spectrum obtained under identical conditions, and dividing the net number of counts in a 60-100 keV region of interest by the total number of detected ^{8}B decays. Our limit is an order of magnitude smaller than the value which would affect solar neutrino measurements.

We are currently studying the response of our PIN photodiode detector to low-energy alpha particles. We scattered alpha particles with incident(scattered) energies between 300(130) keV and 1000(440) keV from a carbon foil into our detector. To correct for the detector dead layer, measurements were made with the detector at different angles relative to the incident alpha particles. The detector was calibrated using 30-keV x-rays and 81-keV gamma rays from a ^{133}Ba source. Based on the measured alpha peak shape and position, we hope to be able to determine the pulse-height defect and peak-shape parameters as a function of alpha-particle energy in order to better define our low-energy region of interest.

While we are able to detect alpha particles coming from the $2^+ \rightarrow 2^+$ transition, our current PIN detector calibration is not precise enough for us to determine the ^{8}B neutrino spectrum from this data. We are currently investigating whether alpha particles from the reaction ^{29}Si(n,α)^{26}Mg can be used as a precise *in situ* calibration for our PIN detector in the 3-5 MeV energy range.

[1] CENPA Annual Report, University of Washington (2003) p. 37.

4 Nuclear Structure

4.1 $\beta - \nu$ correlation in A=8 and neutrino spectrum from ^{8}B

J.M. Couture,* A. García and S. Sjue

Due to the presence of gluon exchanges between quarks, the weak currents between nucleons are more complicated than the corresponding between leptons. The axial vector current between nucleons, for example, is:

$$(p|A_\mu|n) = i(u_p| - f_a\gamma_\mu\gamma_5 - \frac{f_t}{2M}\sigma_{\mu\nu}q_\nu\gamma_5 + i\frac{f_p}{2M}q_\mu\gamma_5|u_n) \quad (1)$$

The term with f_t is called Second Class Currents (SCCs) and should vanish if Time-Reversal Invariance and Charge Symmetry hold. Presently the limits on SCCs are still not very good: the recent fruit of > 20 years of work by a group at Osaka yields an upper limit of $|f_t/f_a| < 0.15$.[2] If enough accuracy could be reached to measure f_t/f_a at the $\approx 0.1\%$ level, the experiments would be sensitive to the up-down quark mass difference. In the $A = 8$ system SCCs show through the angular correlations in the decay, in which the dominant terms are:

$$W(\hat{e}, \hat{\nu}, \hat{\alpha}) \approx 1 - \frac{v_e}{c}\hat{e}\cdot\hat{\alpha}\hat{\nu}\cdot\hat{\alpha} \mp \frac{2}{3}\frac{E_e - E_\nu}{M}b/Ac(\hat{e}\cdot\hat{\nu}) + \frac{2}{3}\frac{E_e + E_\nu}{M}(d^I/Ac \pm f_t/f_a)(\hat{e}\cdot\hat{\nu}) \quad (2)$$

where the upper (lower) sign corresponds to $\beta^{-(+)}$ decays and b, c, and d^I are the weak-magnetism, Gamow-Teller, and first-class induced pseudotensor form factors.

We have measured the energy of the two alpha particles emitted following the β decays of ^{8}B and ^{8}Li. The data taking took place over the last couple of years at Notre Dame. J. Couture is presently doing calculations to properly calibrate the spectra and analyzing the data to extract the $\beta - \nu$ correlation. From the data we plan to extract limits on f_t/f_a and to get an improved measurement of the (first class) pseudo-induced tensor, d^I. On a separate report we describe ancillary calculations that are being done regarding the response function of the Si detectors (see Section 4.2).

In a previous experiment performed at Notre Dame[3] we deduced the shape of the ^{8}B neutrino spectrum from the alpha spectrum following the beta decay of ^{8}B. A later publication[4] claims disagreements on the shape of the alpha spectrum. Unfortunately the original data taken at Notre Dame and the tools for the analysis were lost. S. Sjue in collaboration with the rest of us has started calculations that will allow us to extract the neutrino spectrum from ^{8}B using the new data and calibrations obtained at Notre Dame.

---

*Department of Physics, University of Notre Dame, Notre Dame, IN 46556.
[2] Phys. Rev. C **65**, 015501 (2002).
[3] Phys. Rev. Lett. **85**, 2909 (2000).
[4] Phys. Rev. Lett. **91**, 252501 (2004).

4.2 Response function of Si detectors for α particles

H. Bichsel, J. M. Couture* and A. García

In order to extract the neutrino spectrum from ^{8}B and the beta-neutrino correlation in the decay of ^{8}Li and ^{8}B from the measured energy of the alpha particles (see Section 4.1) following the decays of ^{8}Li and ^{8}B, we need to understand the response of our α counters in the range $1\text{MeV} \leq E_\alpha \leq 9\text{MeV}$. We have made calibration determinations at $E_\alpha \approx 3.2$ and 5.5 MeV, but calculations are essential to interpolate between them.

We have performed Monte-Carlo simulations of the ionization function of our Si counters for α particles. We consider two effects which cause an asymmetry in this function: 1) energy losses in dead layers of detector and sources; and 2) energy transfered to Si atoms in nuclear collisions that does not generate further ionization.

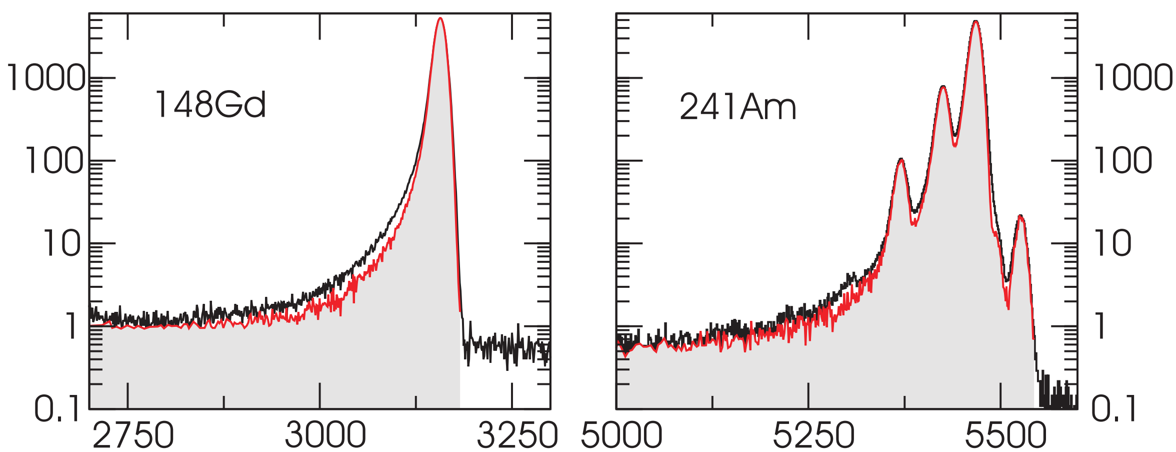

Figure 4.2-1. Measured versus simulated (shaded) response functions for ^{148}Gd and ^{241}Am sources.

Alpha particles are tracked through Si taking into account energy-loss straggling. The Rutherford scattering collisions that determine the tails for the ionization function occur near the end of the range of the alpha particle, when the cross section for nuclear scattering becomes significant compared to the cross section for electronic energy loss. The figure shows measured ionization functions using ^{148}Gd and ^{241}Am sources compared to our calculations where we assumed the cross section for nuclear scattering is twice the value given by the Rutherford cross section. We are still working on understanding the differences.

*Department of Physics, Notre Dame University, Notre Dame, IN 46556.

4.3 A Monte Carlo simulation of ^{35}Cl(n, γ) lines

A. García, G. J. Hodges, S. A. Hoedl and S. Triambak

One of the calibration reactions in our quest to obtain the excitation energy of the lowest T = 2 state[1] in ^{32}S is ^{35}Cl(n, γ). A 200-nA beam of protons with incident energy E_p = 1.912 MeV from the Terminal Ion Source was incident on a thick Li_2O target ($\approx 500 \frac{\mu g}{cm^2}$) so that all the protons lost energy to below threshold[2] E_p = 1881 keV to produce neutrons via ^{7}Li(p, n). The neutrons are moderated by a 4 cm thick slab of paraffin before being absorbed by a $8{\times}10^3$ cm^3 volume of NaCl. The experimental setup is as shown in Fig. 4.3-1.

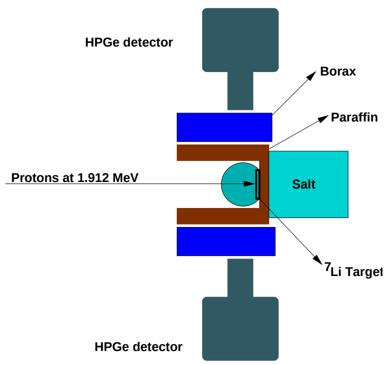

Figure 4.3-1. Experimental Setup.

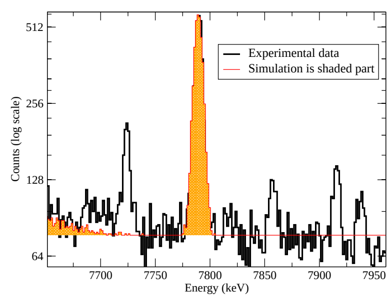

Figure 4.3-2. Peak at 7.79 MeV.

The neutrons moving towards the detector are absorbed by ≈ 15 cm of borax after being moderated by ≈ 8 cm of paraffin to protect the high purity Ge detectors from neutron damage.

A Monte Carlo simulation was performed to account for elastic scattering and absorption of the neutrons in the paraffin before capture on the ^{35}Cl nuclei. Following neutron capture, the moving compound nuclei emit gammas that are detected by the HPGe detectors. An additonal radiation transport program called PENELOPE[3] was used to simulate the interaction of the photons with the Ge crystal. Using both these simulations, we obtain the Doppler effects on the calibration lines as detected by the Ge detectors. Fig. 4.3-2 shows a comparision of simulation to actual experimental data. In addition, we compared the ratios of the areas of the primary peaks to their first and second escape peaks in the simulated spectra to the experimental data to check the geometry of the detector used in the simulations. The preliminary results are shown in the table below.

E_γ (MeV)	Sim. Ratio 1^{st}/Peak	Exp. Ratio 1^{st}/Peak	Sim. Ratio 2^{nd}/Peak	Exp. Ratio 2^{nd}/Peak
8.578	1.33	1.27	0.45	0.53
5.715	0.74	0.85	0.38	0.46

Our preliminary simulations show that the average Doppler shift on the 8.578 MeV line (highest gamma energy) is ≈ 0.16 keV.

[1] CENPA Annual Report, University of Washington (2003) p. 39.
[2] R. Ratynski and F. Käppeler, Phys. Rev. C **37**, 595 (1988).
[3] J. Sempau *et al.*, Nucl. Instrum. Methods in Phys. Res. B **132**, 377 (1997).

4.4 A stringent test of the Isobaric Multiplet Mass Equation using $^{31}\mathbf{P}(p,\gamma)$

E. G. Adelberger, A. García, G. J. Hodges and S. Triambak

The Isobaric Multiplet Mass Equation (IMME) relates the masses of the levels of a isospin multiplet in the following way:

$$M(T_z) = a + bT_z + cT_z{}^2$$

It has been known to work successfully for 21 of the 22 examined quartets, the only deviation being the A = 9 multiplet which required an additional cubic term and also happens to be the most accurately known one.[1]

Due to its success, the IMME has been widely used to deduce masses and level energies of members of multiplets where direct measurements are difficult, for example in determining the Doppler broadening of beta delayed protons and the $\mathcal{F}t$ value in the beta decay of ^{32}Ar, which is a member of the T = 2 quintuplet. In our effort to determine the mass of the lowest T = 2 state in ^{32}S $\approx$ 0.3 keV, we hope to be able to test the IMME up to its most stringent limits for T = 2 (since the masses of the other members are well known) and check the validity of the use of this equation to deduce masses at the levels of accuracy required.[2]

A proton beam from the Terminal Ion Source at $E_p = 3285$ keV impinged on our implanted ^{31}P water cooled target to populate the lowest T = 2 state in ^{32}S. We observed the decaying gammas in HPGe detectors positioned at $\pm 90°$ to the target to minimize Doppler effects on the gamma energies (which is the largest source of systematic uncertainties). For our energy calibration, two reactions, ^{35}Cl (n,γ) and ^{27}Al(p,γ) were used. These produce very precisely known gammas[3,4] in the energy range 0-8 MeV. In the former, the neutrons were produced by ^{7}Li(p,n) at $E_p = 1912$ keV. The protons were incident on a thick Li_2O target that was evaporated on a Ta backing. This produces a fairly collimated cone of neutrons[5] with energies upto $\approx$ 110 keV which were then slowed down by a 4-cm thick slab of paraffin before absorbing in $\approx 8 \times 10^3$ cm^3 volume of NaCl. Monte Carlo simulations are being performed to investigate Doppler and recoil effects in both these calibration reactions. In addition, at all times during data acquisition we used a 3.5-μCi ^{56}Co gamma source that emitted gammas in the range 0-3.5 MeV.

Our preliminary results for the excitation energy of the lowest T = 2 state gives us $E_X \approx$ 12046.02 keV $\pm$ 0.30 keV which disagrees with the previously measured[6] value of 12045 $\pm$ 0.4 keV.

[1] W. Benenson and E. Kashy, Rev. Mod. Phys. **51**, 527, (1979).
[2] CENPA Annual Report, University of Washington, (2003), p. 39.
[3] B. Krusche *et al.*, Nucl. Phys. **A386**, 245, (1982)
[4] P. M. Endt *et al.*, Nucl. Phys. **A510**, 209 (1990).
[5] W. Ratynski and F. Käppeler, Phys. Rev. C **37**, 595, (1988).
[6] M. S. Antony *et al.* in *Proceedings of the International Conference on Nuclear Physics*, Berkeley, 1980, Lawrence Berkeley Laboratory, Berkeley, CA, 1980, Vol. 1.

5 Relativistic Heavy Ions

5.1 Summary of event-structure analysis

T. A. Trainor

Event-structure analysis characterizes the evolution of heavy ion collisions from first contact to kinetic decoupling on the basis of final-state hadron fluctuations and correlations. From studies to date two central issues have emerged: 1) Dynamical evolution in A-A collisions of minimum-bias partons from initial production to final fragmentation, including different aspects of parton coupling to the produced color medium, and 2) local structure of the hadronization process in p-p and A-A collisions. In particular, understanding parton dynamics and coupling to the color medium in A-A has required a full study of minimum-bias partons and their hadron fragments (minijets) in p-p collisions as a reference system. The present elements of this program are

- Two-component soft/hard analysis of p_t distributions from p-p collisions
- Two-particle correlations on $y_t \otimes y_t$ and $\eta \otimes \phi$ in p-p collisions
- Minijets as velocity structures: $\langle p_t \rangle$ fluctuation scaling in Au-Au collisions
- Collision energy dependence of $\langle p_t \rangle$ fluctuations
- Minijet dissipation and two-particle p_t correlations in Au-Au collisions
- Minijet angular deformation on (η, ϕ) in Au-Au collisions
- Hadronization geometry in p-p and Au-Au collisions
- Charge-independent fluctuations and minijet structure
- Charge-dependent fluctuations and hadronization geometry
- Joint autocorrelations from fluctuation scaling by inversion

The principal results of this program are detailed characterization of soft and hard components of two-particle correlations in p-p collisions providing essential new information on *in vacuo* parton fragmentation, minijets in Au-Au collisions as velocity structures and the strong coupling of partons to an axially-expanding color medium in those collisions, a better understanding of the dominant role of minijets in producing the complex velocity structure we observe in A-A collisions at RHIC and evolution of hadronization geometry from 1D in p-p collisions to 2D in central Au-Au collisions. Centrality dependence of various correlation structures reveals an ordered sequence of dynamical changes with increasing A-A centrality: string melting, parton energy loss along the thrust axis, strong parton coupling of low-p_t partons to an expanding bulk medium. Those results have depended on the development of several novel analysis techniques including direct construction of precision pair-ratio autocorrelations, derivation of the integral equation that relates fluctuations to correlations and inversion of that integral equation to extract autocorrelation distributions from fluctuation scale dependence.

5.2 Soft and hard components of inclusive p_t distributions from RHIC p-p collisions at $\sqrt{s} = 200$ GeV

J. Gans* and T. A. Trainor

In the context of a two-component hard/soft model of p-p collisions we analyze the shapes of p_t distributions for several event-multiplicity classes from RHIC collisions at $\sqrt{s} = 200$ GeV. We find that those distributions can be decomposed into a soft component described by a Lévy distribution on transverse mass m_t or error function on transverse rapidity y_t and a semi-hard or minijet component described by a gaussian distribution on y_t. We obtain the average fraction of particles in the minijet component as a function of mean event multiplicity and the shape parameters of the soft and hard components, which are approximately independent of event multiplicity. We observed that p-p event multiplicity at this energy linearly determines the frequency of hard scatters in each event class. The two-component model function is then

$$1/p_t\, dN/dp_t \quad = \quad n_s(n_{ch})\, S_0(p_t) + n_h(n_{ch})\, H_0(p_t) \tag{1}$$

which represents such a factorization hypothesis, with soft and hard reference components $S_0(p_t)$ and $H_0(p_t)$ (independent of n_{ch} by hypothesis) both integrating to unity on p_t, hard fraction $n_h(n_{ch})/n_{ch} = \alpha(n_{ch} - n_0)$ (linearity assumption) and constraint $n_s(n_{ch}) + n_h(n_{ch}) = n_{ch}$. We transform to transverse rapidity $y_t \equiv \ln\{\sqrt{1 + (p_t/m_0)^2} + p_t/m_0\}$ as a velocity variable to provide a 'native' description of minijets as hadron fragments from a moving source.

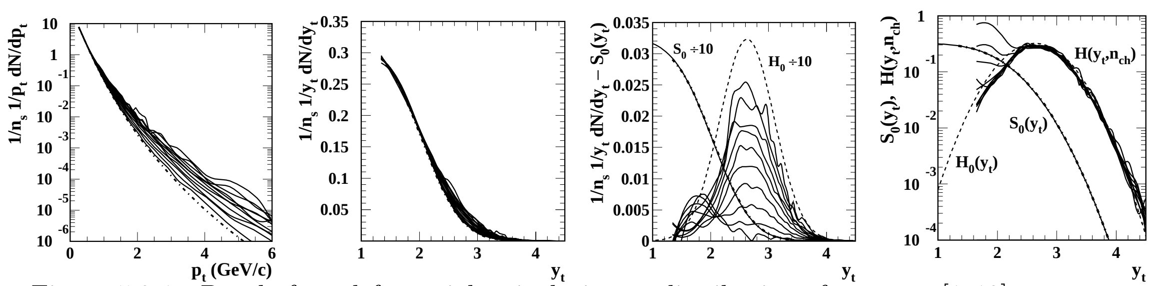

Figure 5.2-1. Panels from left to right: inclusive p_t distributions for $n_{ch} \in [1, 12]$, same on transverse rapidity y_t, soft reference S_0 subtracted to reveal hard components, hard components on logarithmic scale normalized to $n_h = 1$ and compared to hard reference H_0.

We observe in Fig. 5.2-1 that soft-component S_0 (string fragments) is well represented on transverse rapidity y_t by an error function (corresponding to a Lévy distribution on m_t), and hard component H_0 (minijet fragments) is represented by a gaussian distribution on y_t, each form approximately independent of event multiplicity and determined by two parameters. The minijet fraction at 200 GeV increases linearly with event multiplicity (a fifth parameter), and there is evidence for a small but significant third component at smaller y_t which *decreases* nonlinearly with increasing multiplicity. The stability of the minijet fragment distribution with event multiplicity indicates that the gaussian distribution on y_t is a valid minimum-bias minijet input for A-A collision models. This y_t dependence has not previously been observed and disagrees with the standard pQCD picture of a 'power-law' fragment distribution.

*Department of Physics, Yale University, New Haven, CT 06520.

5.3 Minimum-bias hard component (minijets) for inclusive p_t distributions from Pythia-V6.131 p-p collisions at $\sqrt{s} = 200$ and 630 GeV

C. Han and T. A. Trainor

Using the two-component analysis method described in Section 5.2 we extract minimum-bias hard-component (minijet) distributions on transverse rapidity y_t for p-p collisions simulated by the Pythia-V6.131 Monte Carlo at $\sqrt{s} = 200$ and 630 GeV. The properties of minijets are of considerable interest because they drive the early correlation structure of A-A collisions. Comparison of A-A minijet structure at kinetic decoupling with that observed in p-p collisions can reveal the dynamical properties of the color medium produced in HI collisions.

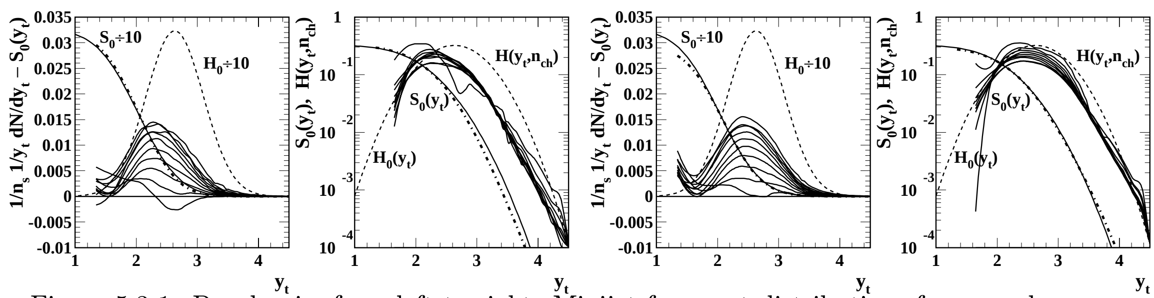

Figure 5.3-1. Panel pairs from left to right: Minijet fragment distributions for several n_{ch} classes on transverse rapidity, same normalized to equivalent hard-component multiplicity, both panels for $\sqrt{s_{NN}} = 200$ GeV; same panel pair for $\sqrt{s_{NN}} = 630$ GeV. H_0 hard-component model curves are for RHIC p-p data.

In Fig. 5.3-1 (left panels) we observe minijet fragment distributions on transverse rapidity y_t for several event multiplicity classes at $\sqrt{s} = 200$ GeV. Comparing to the same distributions from RHIC p-p collisions (Section 5.2) we observe that the minijet fragment yield from Pythia at 200 GeV is about half that observed in RHIC data at the same energy. The distribution is skewed, the maximum on y_t is shifted to lower y_t and the shape differs significantly from the gaussian shape observed for RHIC data. In the log plot we observe that at large y_t the Pythia distribution approaches a 'power law' trend ($\propto p_t^{-n}$), consistent with pQCD expectations but inconsistent with RHIC data in this p_t range. In Fig. 5.3-1 (right panels) we observe for 630 GeV trends expected with increasing $\sqrt{s}$: the fragment distribution shifts to larger y_t, and the power-law trend at larger y_t persists. The fragment number per event does not increase, and the high-y_t fragment yield at 630 GeV still falls well below RHIC data at 200 GeV.

The two-component decomposition is a sensitive probe of p_t distribution structure, revealing the minijet fragment distribution on y_t. The evolution of minijet structure with centrality in Au-Au collisions can reveal the dissipative properties of the color medium. However, precise study of color-medium properties requires a reliable characterization of p-p minijet structure. We observe in its single-particle distributions that Pythia-V6.131 does not represent p-p minijet structure correctly at RHIC energies. Further disagreement with RHIC p-p data is revealed in two-particle correlations studies (see Section 5.4). Improved phenomenological representation of p-p minijets would further the study of the color medium produced in RHIC Au-Au collisions.

5.4 Soft and semi-hard components of transverse-momentum-dependent two-particle correlations from p-p collisions at $\sqrt{s_{NN}} = 200$ GeV

R. J. Porter and T. A. Trainor

We have measured two-particle correlations of unidentified charged primary hadrons on transverse momentum p_t ($0.15 \le p_t \le 6.0$ GeV/c) from p-p collisions at $\sqrt{s_{NN}} = 200$ GeV. We observe strong large-scale correlation structures consistent with a model of p-p collisions as composites of soft (string) and semi-hard (minijet) components. Correlation features are more naturally depicted on transverse rapidity $y_t \equiv \ln(\sqrt{1 + (p_t/m_\pi)^2} + p_t/m_\pi)$, with pion mass assumed for all hadrons. This transformation reduces single-particle density excursions at larger p_t values, but y_t is more importantly motivated as a *velocity variable* equivalent to longitudinal rapidity y_z: particle production from parton fragmentation along the jet thrust axis may be similar to production from string fragmentation along the collision axis. The correlation measure is the difference between a two-particle or pair density of sibling pairs from same events and a reference density obtained by pairing particles from different (but similar) events. In two-particle (y_{t1}, y_{t2}) space we determine $C(y_{t1}, y_{t2}) = \rho_{sibling}(y_{t1}, y_{t2}) - \rho_{mixed}(y_{t1}, y_{t2})$, where each ρ is unit-normalized and $C(y_{t1}, y_{t2})$ integrates to zero by construction.

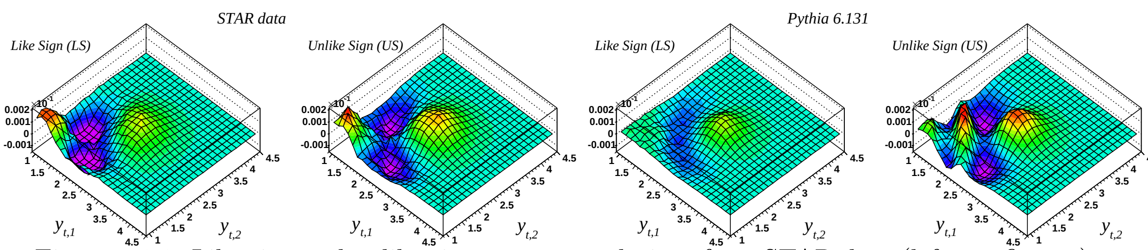

Figure 5.4-1. Like-sign and unlike-sign $y_t \otimes y_t$ correlations from STAR data (left two figures) and *Pythia* Monte Carlo simulations (right two figures).

Fig. 5.4-1 shows $C(y_{t1}, y_{t2})$ from *like-sign* (LS) and *unlike-sign* (US) charged-pairs for both STAR and Pythia Monte Carlo data. STAR data show two regions of positive correlation. At low y_t both LS and US distributions contain soft-component (string fragmentation) structures that fall off rapidly with increasing y_t, and LS data also contain HBT correlations. At higher y_t a positive correlation structure is centered around $y_{t1} = y_{t2} \simeq 2.6$ ($p_{t1} = p_{t2} \simeq 1.0$ GeV/c), which is attributed to correlated minijet fragments from semi-hard parton scatterings. Results from *Pythia* also reveal soft and semi-hard components. The minijet peak at larger y_t coincides approximately with STAR data. However, the soft component is quite different. There is little positive correlation in the low-y_t region for LS pairs (*Pythia* does not simulate HBT correlations and does not couple partons to the string), and the US distribution is dominated by a prominent ridge along $y_{t1} + y_{t2} \simeq 3.0$. Based on an invariant mass analysis we attribute this ridge to copious ρ^0-meson production: *Pythia* shows preference for ρ^0s in its string-fragmentation algorithm. The large ρ^0 component in Pythia is clearly inconsistent with STAR data. These distributions provide the first comprehensive view of minijet correlations on y_t from *minimum-bias* partons, and provide an essential reference for A-A collisions.

5.5 Minijet structure of two-particle axial-momentum correlations in p-p collisions at $\sqrt{s} = 200$ GeV

R. J. Porter and T. A. Trainor

We have measured projections of two-particle number distributions on axial-momentum components (η, ϕ) for charged primary hadrons in p-p collisions at $\sqrt{s} = 200$ GeV. Two-particle correlations on transverse rapidity $y_t \otimes y_t$ for interval $4.0 \leq y_{t,\Sigma} \equiv y_{t,1} + y_{t,2} \leq 9.0$, which is dominated by hadron fragments from jets, provided a cut space for further analysis. For each $y_{t,\Sigma}$ selection we constructed charge-independent *per-hadron* joint autocorrelations on axial difference variables $\eta_\Delta \equiv \eta_1 - \eta_2$ and $\phi_\Delta \equiv \phi_1 - \phi_2$ as pair-number ratio histograms

$$\bar{N} \times \frac{\Delta A}{A}(\eta_\Delta, \phi_\Delta) = \bar{N} \times \frac{\rho_{sibling}(\eta_\Delta, \phi_\Delta) - \rho_{mixed}(\eta_\Delta, \phi_\Delta)}{\rho_{mixed}(\eta_\Delta, \phi_\Delta)}, \tag{1}$$

where $\rho_{sibling}$ is the pair density from same events, ρ_{mixed} is a reference density obtained by pairing particles from different events and $\bar{N}$ is the mean event multiplicity.

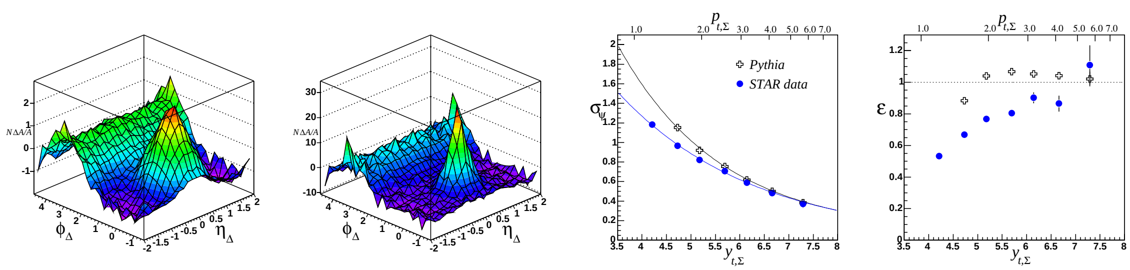

Figure 5.5-1. Left panels: autocorrelations on $(\eta_\Delta, \phi_\Delta)$ from STAR data ($p_{t,\Sigma} \sim 1.5$ and 4 GeV/c, respectively) and right panels: $y_{t,\Sigma}$-dependence of near-side peak widths and eccentricities for STAR data (filled circles) and Pythia Monte Carlo simulations (open crosses).

The left two panels in Fig. 5.5-1 contain autocorrelations from two $y_{t,\Sigma}$ selections (pair $p_{t,\Sigma} \sim 1.5$ and 4 GeV/c respectively) which reveal common features: a near-side peak symmetric about $\eta_\Delta = \phi_\Delta = 0$ and a broad η_Δ-independent away-side ridge about $\phi_\Delta = \pi$. Such features at larger $p_{t,\Sigma}$ are interpreted in terms of di-jet production: the near-side peak represents hadron fragments distributed about a common jet thrust axis, and the away-side band correlates those particles with an opposite $\vec{p}$-balancing jet. Persistence of those structures down to quite low hadron $p_{t,\Sigma}$ ($\simeq 1.0$ GeV or less) is interpreted to indicate that minimum-bias partons down to $p_t \sim 1$ GeV similarly fragment to 'minijets' of one or a few hadrons. The autocorrelations are well described by a near-side 2D gaussian on $(\eta_\Delta, \phi_\Delta)$ and an away-side 1D gaussian on ϕ_Δ. The right two panels in Fig. 5.5-1 show near-side gaussian peak widths and eccentricities extracted by fitting autocorrelations from STAR experimental data and from the Pythia Monte Carlo commonly used for modeling p-p collisions. Radial peak widths $\sigma_\psi \equiv \sqrt{\sigma^2_{\eta_\Delta} + \sigma^2_{\phi_\Delta}}$ for data and Pythia decrease exponentially with increasing $y_{t,\Sigma}$, widths from data being systematically smaller than those from Pythia. Same-side peaks for data also exhibit eccentricities $\epsilon \equiv \sigma_{\eta_\Delta}/\sigma_{\phi_\Delta}$ which fall well below 1 for $p_{t,\Sigma}$ below 5 GeV/c and which substantially differ from symmetric Pythia angular correlations. Such differences suggest an incomplete understanding of parton fragmentation over the statistically important low-p_t minijet region essential to understanding A-A collisions.

5.6 Fluctuations, correlations and inverse problems

R. J. Porter, D. J. Prindle and T. A. Trainor

Fluctuations in nuclear collisions can be measured as a function of momentum-space binning scale over an interval bounded below and above by detector two-track resolution and acceptance. Scale distributions are related to two-particle correlations by a Fredholm integral equation. The integral equation can be inverted by standard numerical methods to yield an *autocorrelation* distribution on difference variables, a projection of the full two-particle momentum distribution which retains most of the correlation information in a more compact form. Autocorrelation distributions are more easily interpreted in terms of physical models than fluctuation measurements. The Fredholm equation for a typical analysis application is

$$\Delta\sigma^2_{p_t:n}(m\,\epsilon_\eta, n\,\epsilon_\phi) \;\equiv\; 4\hat{p}_t^2 \sum_{k,l=1}^{m,n} \epsilon_\eta \epsilon_\phi\, K_{mn;kl}\, \Delta R_{kl}(p_t:n;\epsilon_\eta,\epsilon_\phi), \tag{1}$$

where $\Delta\sigma^2_{p_t:n}$ is a variance difference, $K_{mn;kl}$ is a kernel representing the binning process and ΔR_{kl} represents a joint autocorrelation difference (object − reference) on momentum difference variables. This is formally a matrix equation which can be exactly inverted algebraically. Such inversion however exaggerates short-wavelength noise on the image autocorrelation (differentiation as a 'high-pass' filter). Control of statistical noise in an inverse problem requires a regularization procedure: elements of the image autocorrelation are determined by a free χ^2 minimization which however includes an additional term sensitive to short-wavelength structure on the autocorrelation and controlled by a Lagrange multiplier.

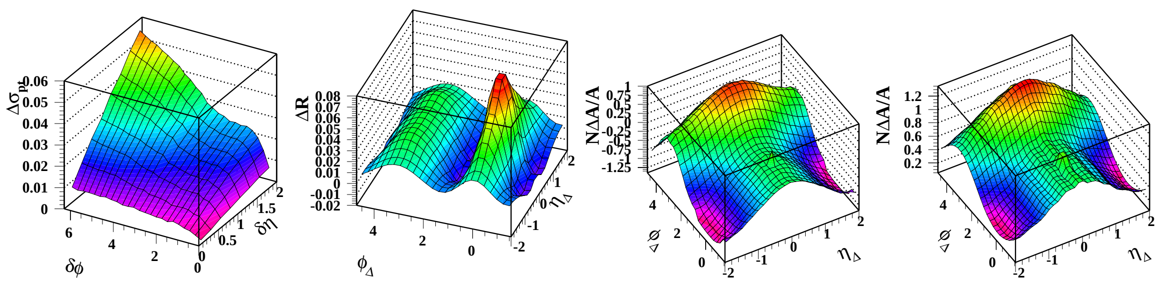

Figure 5.6-1. $\langle p_t \rangle$ fluctuation scale dependence, inverted p_t autocorrelation, Pythia number autocorrelation and Pythia number fluctuations inverted to corresponding autocorrelation.

Fig. 5.6-1 (left panel) shows $\langle p_t \rangle$ fluctuation scale dependence represented by $\Delta\sigma_{p_t:n} \equiv \Delta\sigma^2_{p_t:n}/2\sigma_{\hat{p}_t}$ for central Au-Au collisions at $\sqrt{s_{NN}} = 200$ GeV. The next panel shows the corresponding joint p_t autocorrelation on pseudorapidity and azimuth angle difference resulting from optimized inversion. The last two panels compare analyses of Pythia Monte Carlo data for 200 GeV p-p collisions. On the left is a joint *number* autocorrelation obtained directly from pair-number ratios. On the right is the same joint autocorrelation obtained by inverting multiplicity fluctuation scale dependence. The correspondence is excellent. Establishment of this exact connection between fluctuations and correlations permits precise interpretation of fluctuation results and provides the opportunity to employ an $O(n)$ computation (fluctuation inversion) rapidly to obtain information that would otherwise require an $O(n^2)$ computation (direct construction of pair ratios), especially important for central heavy ion collisions.

5.7 Charge-dependent n and $p_\perp$ correlations in Pythia and Hijing events

R. J. Porter, D. J. Prindle and T. A. Trainor

We have studied charge-dependent two-particle correlations at 200 A-GeV from Pythia and Hijing event generators, which simulate respectively p-p and Au-Au collisions. Pythia contains Lund-model axial string fragmentation and a pQCD model of parton scattering and fragmentation in p-p collisions. Hijing is essentially a Glauber-model superposition of Pythia nucleon-nucleon collisions but also contains a perturbative model of parton energy loss by gluon bremsstrahlung (jet quenching). These Monte Carlos illustrate manifestations of hard scattering in two-particle correlations and also provide a reference for STAR data.

We measure particle number n and transverse momentum $p_\perp$ charge-dependent (CD) fluctuations at axial-momentum scales (bin size) $(\delta\eta, \delta\phi)$ with measures

$$\Delta\sigma^2_{\delta n}(\delta\eta, \delta\phi) = \overline{(\delta n - \overline{\delta n})^2 / \overline{n}} - 1$$

and

$$\Delta\sigma^2_{\delta p_\perp}(\delta\eta, \delta\phi) = \overline{(\delta p_\perp - \delta n \hat{p}_\perp)^2 / n} - \sigma^2_{\hat{p}_\perp}$$

respectively, where $n = n^+ + n^-$, $\delta n = n^+ - n^-$ and $\delta p_\perp = p_\perp^+ - p_\perp^-$ are sums over all corresponding particles in a single bin, and the average is over all bins in all events. $\hat{p}_\perp$ is the inclusive single-particle mean $p_\perp$. We obtain corresponding autocorrelation as described in Sec. 5.6. Examples of autocorrelations for minimum-bias Pythia and central Hijing events are shown in Fig. 5.7-1. There is no dramatic centrality dependence for these CD correlations.

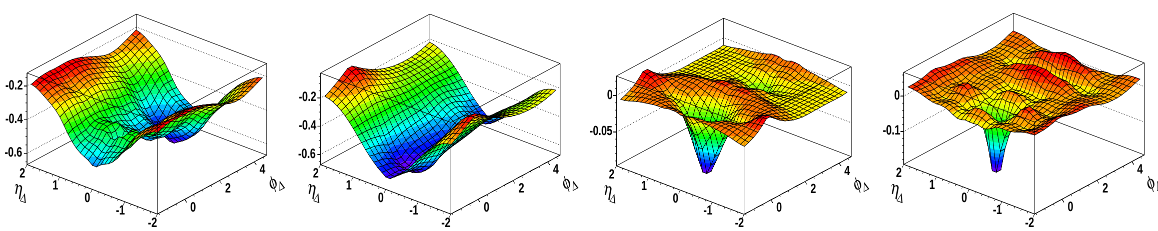

Figure 5.7-1. CD number and $p_\perp$ correlations for minimum-bias Pythia and Central Hijing. The first and third panels show the minimum-bias Pythia number and $p_\perp$ correlations. The second and fourth panels show the Central Hijing number and $p_\perp$ correlations.

Charge-dependent or net-charge correlations primarily measure hadronization effects. In the number correlations we see a weak ϕ_Δ dependence and a strong η_Δ dependence. The Gaussian shape on η_Δ reflects local charge conservation on space axis z mapped onto pseudorapidity η by strong longitudinal (Bjorken) expansion. Plus-minus charge pairs are nearest neighbors along the string due to canonical suppression of net charge. The η_Δ peak represents charge-pair separation on z divided by the Bjorken expansion rate. There is typically a small difference in the near side-away side relative correlation strength in all cases. CD $p_\perp$ correlations show a strong near-side negative correlation peak at (0,0) with much smaller away-side structure. The near-side peak changes shape from symmetric about zero on $(\eta_\Delta, \phi_\Delta)$ for central Hijing to strong elongation along η_Δ for Pythia p-p and peripheral Hijing Au-Au.

5.8 Charge-independent n and $p_\perp$ correlations in Pythia and Hijing events

R. J. Porter, D. J. Prindle and T. A. Trainor

We measure charge-independent (CI) two-particle correlations of hadrons produced in Hijing Au-Au and Pythia p-p simulated collisions at 200 A-GeV. Pythia models p-p collisions with Lund string fragmentation and pQCD hard parton scattering. Hijing is a superposition of Pythia nucleon-nucleon collisions with parton energy loss modeled by pertubative gluon bremsstrahlung. These Monte Carlos reveal manifestations of hard scattering in charge-independent two-particle correlations and provide a reference for STAR correlation analysis.

Particle number and $p_\perp$ fluctuations are related to two-particle correlations. CI fluctuation measures evaluated at scale (bin size) $(\delta\eta, \delta\phi)$ are

$$\Delta\sigma_n^2(\delta\eta, \delta\phi) = \overline{(n - \overline{n})^2}/\overline{n} - 1$$

and

$$\Delta\sigma_{p_\perp}^2(\delta\eta, \delta\phi) = \overline{(p_\perp - n\,\hat{p}_\perp)^2/n} - \sigma_{\hat{p}_\perp}^2$$

where $n = n_+ + n_-$ is the number of charged particles and $p_\perp$ the scalar sum of all transverse momenta in a bin, and the average is over all bins in all events. $\hat{p}_\perp$ is the inclusive mean $p_\perp$ and $\sigma_{\hat{p}_\perp}^2$ is the inclusive variance. Fluctuation scale dependence is inverted to obtain autocorrelations as described in Sec. 5.6. Autocorrelations for minimum-bias Pythia and Hijing central events are shown in Fig. 5.8-1.

We observe a smooth transition from minimum-bias Pythia through peripheral Hijing to central Hijing for both $p_\perp$ and n autocorrelations.

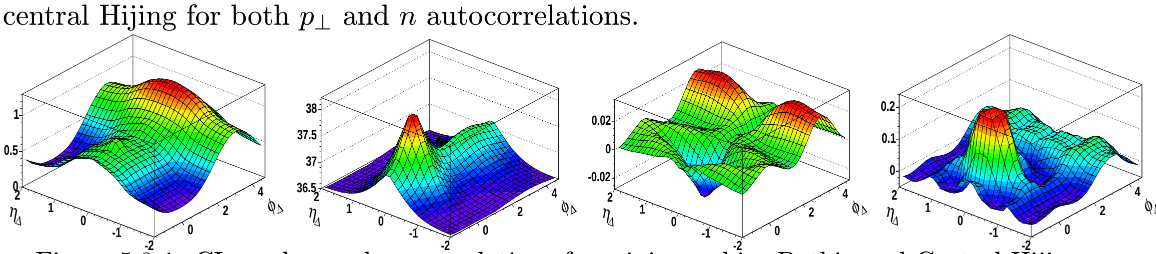

Figure 5.8-1. CI number and $p_\perp$ correlations for minimum-bias Pythia and Central Hijing. The first and third panels show the minimum-bias Pythia number and $p_\perp$ correlations. The second and fourth panels show the Central Hijing number and $p_\perp$ correlations.

The CI number correlations for minimum-bias Pythia are dominated by the initial conditions. The collisions are modeled as color-field strings stretched along the beam axis following the p-p interaction, locally conserving transverse momentum as they stretch and fragment: transverse momenta of nearest-neighbor hadrons tend to be opposed on azimuth ϕ. For more central Hijing collisions the fraction of particles being produced by hard scattering increases due to multiple N-N collisions. Struck partons emerging from the axial system can be characterized as strings at an angle to the beam axis. The produced hadrons are then fragments from a moving source boosted in the laboratory frame and emerge at small relative angles, giving rise to the 'near-side' peak in the $(\eta_\Delta, \phi_\Delta)$ autocorrelation. The width of this peak is a measure of the characteristic transverse momentum j_t relative to the parton momentum direction (jet thrust axis) divided by the momentum of the leading parton. CI $p_\perp$ correlations show a similar trend, but there is also a suppression of local $p_\perp$ correlations. Pythia and Hijing seem to impose this condition almost independently for differences on η and ϕ.

5.9 n-$p_\perp$ covariances in Pythia and Hijing Monte Carlo events

R. J. Porter, D. J. Prindle and T. A. Trainor

In this study we measure two-particle correlations of unidentified charged hadrons produced by Hijing and Pythia event generators simulating collisions at 200 A-GeV: p-p collisions from Pythia and Au-Au collisions from Hijing. Pythia p-p collisions include Lund string fragmentation and pQCD hard scattering to jets. Hijing is essentially a super-position of Pythia nucleon-nucleon collisions, but fast partons suffer energy loss in the color medium *via* pQCD gluon bremsstrahlung, which is expected to contribute to two-particle correlations. These Monte Carlo events provide examples of possible hard-scattering contributions to two-particle correlations and are important as references for STAR data analysis.

We measure fluctuations in number n *together with* transverse momentum $p_\perp$ which are related to corresponding two-particle correlations. CI and CD n-$p_\perp$ fluctuations measured (by *covariances*) at scale (bin size) $(\delta\eta, \delta\phi)$ are

$$\Delta\sigma^2_{n\text{-}p_\perp}(\delta\eta,\delta\phi) = \overline{(p_\perp - n\,\hat{p}_\perp)/\sqrt{n}\cdot(n-\overline{n})/\sqrt{\overline{n}}}$$

and

$$\Delta\sigma^2_{\delta n\text{-}\delta p_\perp}(\delta\eta,\delta\phi) = \overline{(\delta p_\perp - \delta n\,\hat{p}_\perp)/\sqrt{n}\cdot(\delta n-\overline{\delta n})/\sqrt{\overline{n}}}$$

where $n = n_+ + n_-$ is the number of particles, $p_\perp = p_{\perp +} + p_{\perp -}$ is the scalar sum of transverse momentum, $\delta n = n_+ - n_-$ is the number charge difference and $\delta p_\perp = p_{\perp +} - p_{\perp -}$ is the transverse-momentum charge difference in the bin. The average is over all bins of all events. $\hat{p}_\perp$ is the ensemble particle mean $p_\perp$. After measuring the scale dependence of these fluctuations we invert to obtain the corresponding autocorrelations as described in Sec. 5.6. Samples of autocorrelations for minimum-bias Pythia and central Hijing collisions are shown in Fig. 5.9-1.

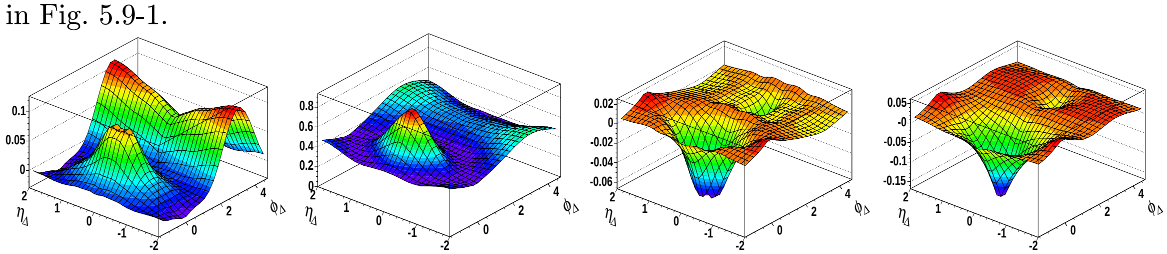

Figure 5.9-1. Number-$p_\perp$ CD and CI covariances for minimum-bias Pythia and Central Hijing. The first and second panels show the minimum-bias Pythia and Hijing CI number-$p_\perp$ covariances. The third and fourth panels show the minimum-bias Pythia and Hijing CD number-$p_\perp$ covariances.

We generally observe strong covariances between n and $p_\perp$. For CI n-$p_\perp$ the away-side ridge stays relatively constant with centrality while the near-side peak shows a strong increase in amplitude with increasing centrality. CD n-$p_\perp$ covariances have the same qualitative shape as the CD $p_\perp$ correlations, but there are quantitative differences in widths and centrality dependence. The physics that drives these n-$p_\perp$ covariances is an open question at this early stage. But since these covariances give a significant contribution to overall $p_\perp$ fluctuations and the inverted CI n-$p_\perp$ covariance is different from the n and $p_\perp$ autocorrelations, we anticipate the possibility of novel physics not otherwise accessible.

5.10 Minijets as velocity structures: $\langle p_t \rangle$ fluctuation scaling and inversion to joint p_t autocorrelations from Au-Au collisions at $\sqrt{s} = 200$ GeV

Q. J. Liu, D. J. Prindle and T. A. Trainor

We have measured the scale (bin-size) dependence of event-wise mean transverse momentum $\langle p_t \rangle$ fluctuations for Au-Au collisions at $\sqrt{s_{NN}} = 200$ GeV. We invert the scale distributions to construct joint p_t autocorrelations on pseudorapidity and azimuth angle difference variables which represent a correlated velocity/temperature distribution. The autocorrelations have near-side and away-side components which depend separately and strongly on collision centrality. The structure and centrality dependence of those components suggest that the principal origin is minijets, substantially altered by a dissipative color medium in the more central Au-Au collisions. We measure variance difference factor $\Delta\sigma_{p_t:n}$, related to the variance difference measure of nonstatistical p_t fluctuations by $\Delta\sigma^2_{p_t:n} \equiv 2\sigma_{\hat{p}_t}\Delta\sigma_{p_t:n}$. The variance difference is in turn related to the joint autocorrelation ΔR by integral equation

$$\Delta\sigma^2_{p_t:n}(m\,\epsilon_\eta, n\,\epsilon_\phi) \equiv 4\hat{p}_t^2 \sum_{k,l=1}^{m,n} \epsilon_\eta\epsilon_\phi\, K_{mn;kl}\, \Delta R_{kl}(p_t : n; \epsilon_\eta, \epsilon_\phi), \qquad (1)$$

In the left panel of Fig. 5.10-1 is the scale variation of $\langle p_t \rangle$ fluctuations up to the limiting STAR acceptance for central Au-Au collisions at $\sqrt{s_{NN}} = 200$ GeV. In the next panel is the corresponding joint autocorrelation on difference variables obtained by inverting Eq. (1), with a prominent near-side peak and away-side structure. That distribution in cylindrical format reveals necking on the azimuth difference variable ϕ_Δ. The autocorrelation summarizes the structure of multiple minijets averaged over many central Au-Au collisions. Based on that autocorrelation structure we simulate the velocity structure of a typical collision event in the right panel.

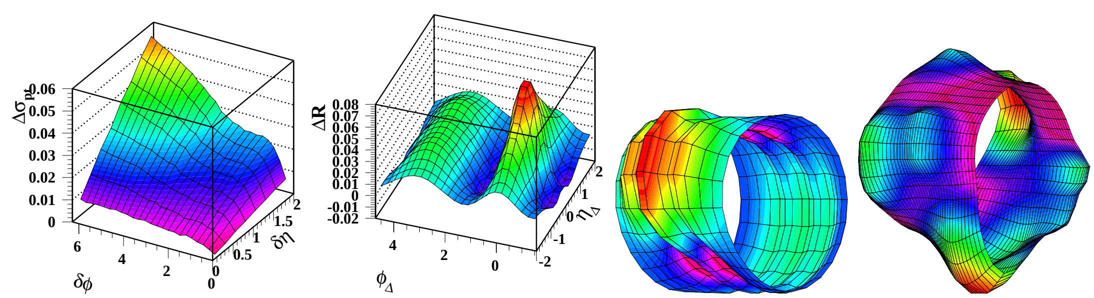

Figure 5.10-1. Fluctuation scale dependence, inverted p_t autocorrelation, same in cylindrical format and simulated event showing minijet structures consistent with p_t autocorrelation.

By inverting scale distributions of $\langle p_t \rangle$ fluctuations on $(\delta\eta, \delta\phi)$ to autocorrelation distributions on difference variables $(\eta_\Delta, \phi_\Delta)$, we obtain the event-wise two-point correlation structure of a spatially-varying parent p_t distribution, specifically a combination of velocity and temperature correlations. The inferred autocorrelations reveal complex correlation structure in Au-Au collisions at RHIC, including peaked structures attributed to minijets which vary strongly with collision centrality. Further studies with identified particles may separate the detailed velocity and temperature structures of heavy ion collisions, and by this means the interaction dynamics of counterpropagating color fluids.

5.11 Energy dependence of $\langle p_t \rangle$ fluctuations from $\sqrt{s_{NN}} = 10$ to 200 GeV

Q. J. Liu, D. J. Prindle and T. A. Trainor

Considerable controversy has emerged over the $\sqrt{s_{NN}}$ dependence of $\langle p_t \rangle$ fluctuations in heavy ion collisions from SPS to RHIC energies. Analysis in terms of autocorrelation amplitudes indicates a strong and monotonic increase with collision energy, with fluctuations appearing to drop below a threshold of observability near 10 GeV. Analysis in terms of 'temperature' fluctuations on the other hand suggests that $\langle p_t \rangle$ fluctuations are nearly independent of collision energy over this interval. Shown in Fig. 5.11-1 left panel is $\langle p_t \rangle$ fluctuation scale dependence on pseudorapidity bin size $\delta\eta$ at five energies, the lower two being CERES Pb-beam data at fixed-target beam energies 80 and 158 GeV/nucleon (labeled with corresponding cm energies) and the upper three being STAR data at cm energies 20, 130 and 200 GeV. The next two panels compare p_t autocorrelations from STAR data at 20 and 200 GeV, with same detector and analysis system in each case. The 200-GeV autocorrelation corresponds to the top-most data in the left panel. By either comparison there is evident a dramatic difference in fluctuations/correlations between SPS and RHIC energies.

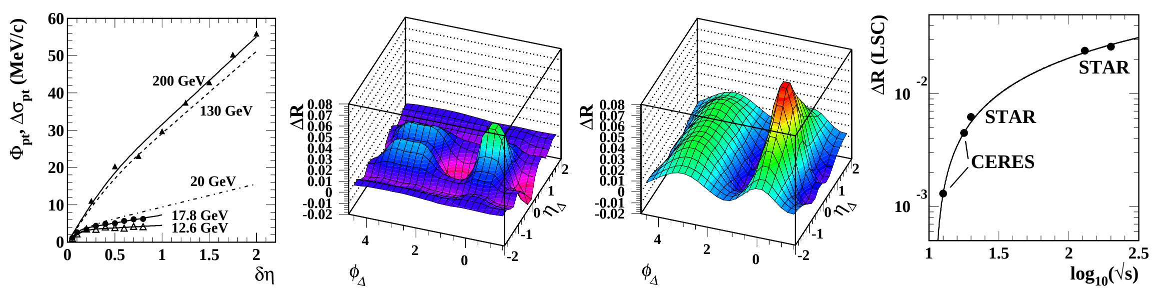

Figure 5.11-1. STAR and CERES p_t fluctuation η-scale dependence, p_t autocorrelation at 20 GeV, p_t autocorrelation at 200 GeV, energy dependence of large-scale correlations (LSC).

The right-most panel shows the trend on collision energy of the large-scale correlation (LSC) amplitude in autocorrelations at five energies. The LSC, determined as the autocorrelation amplitude at large difference variable η_Δ, is distinguished from the small-scale correlation (SSC) amplitude, which especially at SPS energies is dominated by HBT (quantum) and Coulomb correlations. Since we observe that the principal mechanism for $\langle p_t \rangle$ fluctuations at RHIC is minijets, the energy dependence of the LSC component is of considerable interest: what is the energy trend of hard scattering down to the lowest relevant energies?

An alternative analysis has been based on variable $\sigma^2_{p_t,dynamical} \sim \Delta\sigma^2_{p_t:n}/\bar{n}$, and defined as $\Sigma_{p_t} \equiv \sqrt{\sigma^2_{p_t,dynamical}/\hat{p}_t^2}$. This measure is motivated by the intent to measure 'global' temperature fluctuations in the form $\delta T/T_0 \sim \Sigma_{p_t}$. Whereas $\Delta\sigma^2_{p_t:n}$ is linearly related to the autocorrelation by an integral equation, $\sigma^2_{p_t,dynamical}$ acts as a *running average of the autocorrelation*. At lower energies this averaging acts to spread the SSC peak out to large difference-variable values as a systematic error contribution to LSC. The result is that Σ_{p_t} introduces an SSC 'contamination,' confusing contributions from hard scattering at higher energies and from soft physics at lower energies to reduce the *apparent* energy dependence. This comparison explains the apparent large discrepancy between the two methods.

5.12 Minijet dissipation and transverse-momentum correlations in Au-Au collisions at $\sqrt{s_{NN}} = 130$ GeV

A. Ishihara,* R. L. Ray* and T. A. Trainor

We have measured two-particle correlations on transverse momentum p_t for Au-Au collisions at $\sqrt{s_{NN}} = 130$ GeV. Significant large-momentum-scale correlation structures are observed for charged primary hadrons with $0.15 \le p_t \le 2$ GeV/c and pseudorapidity $|\eta| \le 1.3$ which were not predicted by theoretical collision models. The principal features in Fig. 5.12-1 can be described by two models, the first ('saddle' structure) based on local velocity/temperature fluctuations on (η, ϕ), the second (large-$X(p_t)$ peak) reflecting hard-scattering correlations. Fluctuating event-wise velocity/temperature structure $\beta(\eta, \phi)$ ($\beta = 1/T$ and/or v/c) is represented by distribution $g_1(\beta)$, with centroid β_0 and variance σ_β^2. Two-point β correlations are represented by peaked 2D distribution $g_2(\beta_1, \beta_2)$ from pairs of local velocity/temperature values sampled event-wise on (η, ϕ). The inclusive distribution on (p_{t1}, p_{t2}) is the convolution of thermal model distribution $\mathrm{e}^{-\beta_1 m_{t1} - \beta_2 m_{t2} + (\beta_1+\beta_2)\, m_\pi}$ with $g_2(\beta_1, \beta_2)$. If $g_2(\beta_1, \beta_2)$ is modeled by a 2D gamma distribution, the distribution on (p_{t1}, p_{t2}) is a 2D Lévy distribution

$$F_{sib} \propto \left(1 + \frac{\beta_0 m_{t\Sigma}}{2n_\Sigma}\right)^{-2n_\Sigma} \left[1 - \left(\frac{\beta_0 m_{t\Delta}}{2n_\Delta + \beta_0 m_{t\Sigma}}\right)^2\right]^{-n_\Delta} \tag{1}$$

on sum and difference transverse-mass variables $m_{t\Sigma} \equiv m_{t1} + m_{t2} - 2m_\pi$ and $m_{t\Delta} \equiv m_{t1} - m_{t2}$. $1/n_\Sigma$ and $1/n_\Delta$ represent relative variances $\sigma_\Sigma^2/\beta_0^2$, $\sigma_\Delta^2/\beta_0^2$ of $g_2(\beta_1, \beta_2)$ along sum and difference variables β_Σ and β_Δ respectively, and $(1/n_\Sigma - 1/n_\Delta) \equiv \Delta(1/n)_{tot}$ is the relative *covariance*, which measures velocity/temperature correlations on (η, ϕ). This distribution is used to fit the saddle structures in Fig. 5.12-1. Fit parameters are shown in the right-most panel of the figure. The third panel shows saddle-fit residuals consistent with fragments from *undissipated* minimum-bias partons which are fit with a separate modeling procedure.

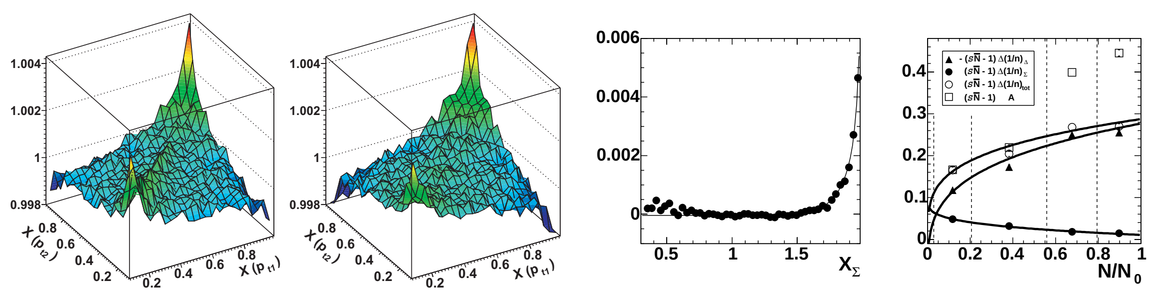

Figure 5.12-1. Two $p_t \otimes p_t$ correlations with saddles, fit residuals and saddle fit parameters.

The most prominent trend is monotonic increase of curvature measure $\Delta(1/n)_{tot}$ (open circles) with centrality. The corresponding β-correlation structure is then interpreted as the result of initial-state semi-hard parton scattering and subsequent fragmentation (minijets) in which most partons in the more central Au-Au collisions encounter strong in-medium dissipation. With increasing Au-Au centrality the two-particle fragmentation function is shifted to lower p_t and asymptotically approaches a form consistent with a structured velocity/temperature distribution (Lévy saddle) as part of an incomplete equilibration process.

*Department of Physics, University of Texas at Austin, Austin, TX 78712.

5.13 Minijet deformation on axial-momentum space and charge-independent number autocorrelations from Au-Au collisions at $\sqrt{s_{NN}} = 130$ GeV

A. Ishihara*, R. L. Ray* and T. A. Trainor

We have measured charge-independent joint number autocorrelations on momentum-space difference variables $\eta_1 - \eta_2$ (pseudorapidity) and $\phi_1 - \phi_2$ (azimuth) for primary charged hadrons with $0.15 \leq p_t \leq 2$ GeV/c and $|\eta| \leq 1.3$ from Au-Au collisions at $\sqrt{s_{NN}} = 130$ GeV. We observe large-scale isoscalar correlations associated with elliptic flow and minijets. In Fig. 5.13-1 left panels are autocorrelations for peripheral and central collisions with multipole components subtracted (conversion-electron pairs also contribute to (0,0) bins), revealing minijet-fragment angular distributions. The normally (η, ϕ)-symmetric p-p jet angular correlations, also symmetric in peripheral HI collisions (d), are severely distorted in central collisions (a). Joint autocorrelations for four centralities were fitted with model function

$$\begin{aligned} F &= A_{v_1} \cos(\phi_\Delta) + A_{v_2} \cos(2\,\phi_\Delta) + A_0\, e^{-\left(\frac{\eta_\Delta}{\sqrt{2}\sigma_0}\right)^2} \qquad (1) \\ &+ A_1\, e^{-\left\{\left(\frac{\phi_\Delta}{\sqrt{2}\sigma_{\phi_\Delta}}\right)^2 + \left(\frac{\eta_\Delta}{\sqrt{2}\sigma_{\eta_\Delta}}\right)^2\right\}} + A_2. \end{aligned}$$

Typical fits are illustrated by the projections on η_Δ (solid) and ϕ_Δ (open) in the third panel of Fig. 5.13-1, and fitted widths σ_η (dot) and σ_ϕ (triangle) are shown in the forth panel *vs* centrality measure ν, which estimates the mean participant path length in encountered nucleons.

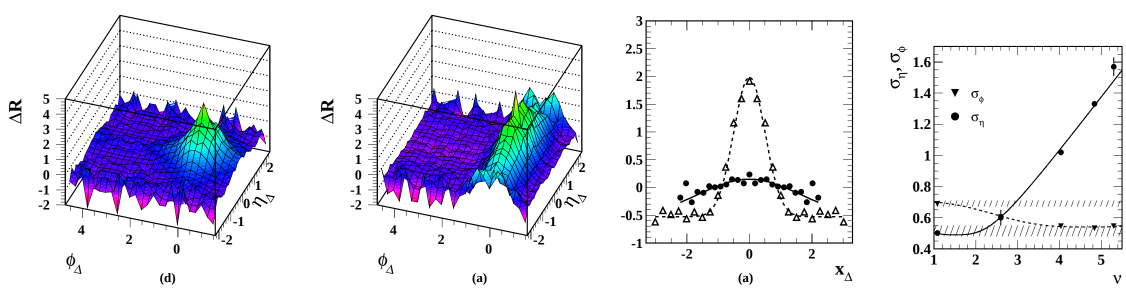

Figure 5.13-1. Joint autocorrelations with v_1, v_2 multipoles removed for peripheral (d) and central (a) events, 1D projections with fits for (a) and minijet width parameters *vs* centrality.

We observe that minijet peak structure varies in angular shape with centrality from a symmetric shape on $(\eta_\Delta, \phi_\Delta)$ for peripheral collisions to a highly asymmetric peak for central collisions. This trend can be interpreted as a transition from *in vacuo* jet fragmentation similar to p-p collisions in peripheral heavy ion collisions to strong coupling of minimum-bias partons with a longitudinally-expanding color medium in the more central collisions. These results are for charged particles with $p_t < 2$ GeV/c and reveal the state of *minimum-bias* parton fragments (minijets) at HI kinetic decoupling. We assert that minijets are optimal probes of bulk properties of the color medium produced in RHIC Au-Au collisions. The present result is certainly inconsistent with pQCD-based models of jet quenching but may favor some recombination models.

*Department of Physics, University of Texas at Austin, Austin, TX 78712.

5.14 Hadronization geometry and charge-dependent number autocorrelations on axial-momentum space in Au-Au collisions at $\sqrt{s_{NN}} = 130$ GeV

A. Ishihara,* R. L. Ray* and T. A. Trainor

We have measured charge-dependent (CD) joint number autocorrelations on axial momentum-space difference variables $\eta_\Delta \equiv \eta_1 - \eta_2$ (pseudorapidity) and $\phi_\Delta \equiv \phi_1 - \phi_2$ (azimuth) for primary charged hadrons with $0.15 \leq p_t \leq 2$ GeV/c and $|\eta| \leq 1.3$ from Au-Au collisions at $\sqrt{s_{NN}} = 130$ GeV. We observe large-momentum-scale correlation structures not predicted by theory but consistent with a change in the geometry of hadron emission with increasing centrality of Au-Au collisions. In p-p collisions charge-dependent correlations are dominated by a 1D gaussian on η_Δ indicative of charge-ordering on the axial string manifested on pseudorapidity through Bjorken expansion. In Au-Au collisions we observe that CD correlations are dominated by a central peak nearly exponential in shape and nearly symmetric on (η, ϕ) for the most central events. Fig. 5.14-1 left panel shows CD correlations for the most peripheral event class (d) in this study, in which the central 2D exponential peak and the 1D gaussian peak on η_Δ coexist. Joint autocorrelations for four centrality classes were fitted with a model function consisting of a 2D exponential with independent widths on η_Δ and ϕ_Δ, and a 1D gaussian on η_Δ. 1D projections of data and model functions are shown in the second panel. Fitted width parameters are shown in the last two panels on two centrality measures. Parameter ν measures the mean participant path length in number of encountered nucleons.

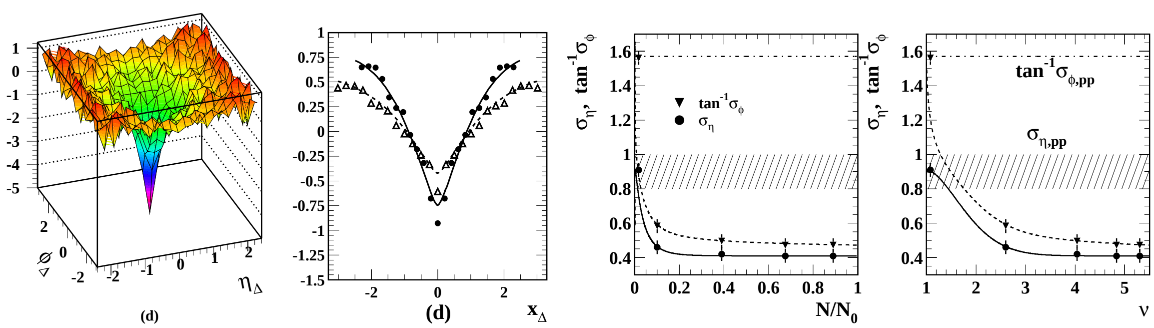

Figure 5.14-1. Charge-dependent joint autocorrelation for peripheral Au-Au collisions (d), corresponding 1D projections with fits and fitted model parameters on two centrality measures.

These data are generally consistent with local charge conservation or canonical suppression of net-charge fluctuations. We observe strong variation of correlation structure from p-p to peripheral Au-Au to central Au-Au which can be interpreted as follows. Hadronization geometry evolves from 1D color-string fragmentation in p-p collisions to exponentially-attenuated 2D charge-ordered emission from a hadron-opaque bulk medium in central Au-Au collisions. Those results are qualitatively inconsistent with standard collision models and predictions of QGP-related strong suppression of net-charge fluctuation. Charge-dependent autocorrelations provide unique access to the changing geometry of hadron production as the energy density and spatial extent of A-A collisions increase with centrality.

*Department of Physics, University of Texas at Austin, Austin, TX 78712.

5.15 Overview of HBT physics at STAR

J. G. Cramer and the STAR HBT Physics Working Group*

The STAR HBT[1] Physics Working Group (HBT PWG), active membership about 20 physicists led by conveyors Sergei Panitkin and Fabrice Retire, has made very significant progress in the past year in analyzing data from the first four years of operation of the STAR detector at RHIC. In 2001, the first STAR HBT paper reporting the initial pion correlation results at $\sqrt{s_{NN}} = 130$ GeV was published.[2] In the past year, a paper on three-pion correlations[3] and a paper on pion-kaon correlations[4] have been published in Physical Review Letters. In addition, a paper on azimuthally sensitive HBT in Au+Au collisions at $\sqrt{(}s_{NN}) = 200$ GeV has just been accepted for publication in PRL. Additional papers about aspects of STAR HBT physics are in various stages of preparation.

In the past year we at CENPA working in the HBT PWG have continued to refine our estimates of the pion phase-space density in Au + Au collisions at $\sqrt{s_{NN}} = 130$ GeV for 7 centrality intervals and 6 intervals of pair-average momentum. We have used these phase space density estimates to obtain corresponding estimates of the pion entropy per particle as a function of centrality. These results have added even more puzzling facts to the investigation of RHIC collisions. The estimate of total system entropy obtained from this analysis is found to be proportional to initial participant number, an indication that each initial participant contributes the same entropy to the system, whether the collision is peripheral or central. This suggests that no qualitative change in the reaction mechanism of the collisions occurs between peripheral and central collisions.

In addition, we have collaborated with G. A. Miller of the UW Nuclear Theory Group on a full quantum mechanical optical-model-based treatment of opacity effects in the transport of pions through the collision fireball, as they affect the HBT observables. This is the first application of quantum mechanical particle transport techniques to such phenomena.

In parallel with these investigations, other members of the STAR HBT Physics Working Group have continued investigations of a number of other aspects of the physics of correlations and interferometry, including HBT analysis of d+Au and p+p collisions and the correlations of other identical particles including protons, charged and uncharged kaons, and other strange particles.

In summary, the STAR HBT Physics Working Group has made considerable progress in analyzing the data from the first four years of RHIC operation. The initial HBT analysis has presented several theoretical puzzles that are now being addressed. We look forward in the coming year to further progress in data analysis and in theoretical understanding.

*See the HBT PWG web site at http://connery.star.bnl.gov/STAR/html/hbt_l
[1]HBT is a widely used abbreviation for Hanbury-Brown Twiss interferometry.
[2]C. Adler *et al.*, Phys. Rev. Lett. **87**, 082301 (2001).
[3]C. Adler *et al.*, Phys. Rev. Lett. **91**, 262301 (2003).
[4]C. Adler *et al.*, Phys. Rev. Lett. **91**, 262302 (2003).

5.16 Pion opacity in RHIC collisions

J. G. Cramer, G. A. Miller,* J. M. S. Wu† and Jin-Hee Yoon‡

In ultra-relativistic heavy ion collisions it is usually assumed that the medium resulting from the collision is transparent to emitted pions, so that the detector receives pions from all kinematically-allowed regions of the source. This leads to the prediction that the radius parameter towards the detector, R_O, is larger than the corresponding radius perpendicular to the detector, R_S. Under these assumptions these radii are related by the equation $R_O^2 = R_S^2 + \beta_0^2 \delta\tau^2$, were $\delta\tau$ is the duration of pion emission, $\beta_0 = p_T/m_T$ is the pion velocity in the direction of the detector, p_T is the transverse momentum of the pions, and $m_T = \sqrt{p_T^2 + m_\pi^2}$ is their transverse mass.

Experimentally these radii are extracted from the two-particle momentum correlation functions using HBT interferometry, and it is found[5] that for Au+Au collisions at RHIC, R_O is approximately equal to R_S. Moreover, it is observed[6] that at higher values of the average pion pair momentum $K_T = \frac{p_1+p_2}{2}$, R_O may actually be smaller than R_S. These observations contradict the theoretical expectations above, and they have been taken as an indication that the emission duration may be extremely short, i.e. that the pions freeze out quite suddenly.

We are investigating the alternative scenario that the medium following the collision is opaque to pions. Previous attempts to treat pion-source opacity have used high-energy approximations that are inappropriate and have produced results that fail in the $K_T = 0$ limit. As reported last year, we have formulated a quantum mechanical treatment of the effects of opacity that provides a proper treatment of pion emission at all energies, even in the presence of collective flow of the source. We solve the quantum mechanical wave equations for the pions in an opaque medium, using a fully relativistic optical model. The production code is now working reliably, and we are investigating its predictions. We find that at $K_T = 0$, $R_O = R_S$ as required and that, for a suitable choice of opacity strength and flow, we can reproduce all of the qualitative features of the HBT data. This work is continuing and should result in a publication in the next few months.

*Supported by the UW Nuclear Theory DOE Contract. Department of Physics, University of Washington, Seattle, WA 98195.

†Department of Physics, University of Washington, Seattle, WA 98195.

‡Department of Physics, Inha University, Inchon, 402-751, Korea.

[5] C. Adler *et al.* Phys. Rev. Lett. **87**, 082301 (2001).

[6] K. Adcox *et al.*, Phys. Rev. Lett. **88**, 192302 (2002).

5.17 Pion phase space density from STAR data

J. G. Cramer, J. M. S. Wu, and the STAR HBT Physics Working Group*

A fundamental quantum-statistical quantity probed by ultra-relativistic heavy ion collisions is the pion six-dimensional phase-space density $f(\vec{r},\vec{p}) \equiv f$, a local Lorentz scalar that gives the number of freeze-out pions in each six-dimensional phase-space cell of volume h^3. The source-averaged phase-space density $\langle f(\vec{p})\rangle$ can be extracted from charged-pion experimental observables, is readily calculated in many theoretical models, and sets the scale for multiparticle correlations. As first suggested by Bertsch[1] $\langle f(\vec{p})\rangle$ at a given vector momentum $\vec{p}$ can be written as:

$$\langle f(\vec{p})\rangle = \left[\frac{1}{E_\pi}\right]\left[\frac{d^2N}{2\pi m_T dm_T dy}\right]\left[\frac{V_p}{\sqrt{\lambda}}\right]; \tag{1}$$

$$V_p \equiv \int_{-\infty}^{\infty}\left[C_2(\vec{q})-1\right] d^3q = \left[\frac{\lambda(\hbar c\sqrt{\pi})^3}{R_O R_S R_L}\right]. \tag{2}$$

Here E_π, the pion total energy, forms a Jacobian preserving Lorentz invariance. The second bracketed quantity is the single-particle pion-momentum spectrum $d^2N/2\pi m_T dm_T dy$ for pions of a given charge emitted with transverse mass m_T and longitudinal rapidity y. The third quantity in brackets is V_p, the *momentum* volume occupied by the three dimensional Bose-Einstein correlation "bump", divided by $\sqrt{\lambda}$, assumed here to be the freeze-out fraction of observed pions. In (2) the quantity $C_2(\vec{q})$ is the Coulomb-corrected two-particle momentum correlation function of $\vec{q}$, the vector momentum difference of the pair. The last expression in (2), under the assumption that the source is Gaussian, gives V_p at midrapidity with azimuthal averaging in terms of the usual Pratt-Bertsch Hanbury-Brown Twiss (HBT) parameters[2] R_O, R_S, R_L, and λ.

The corrected momentum volume and pion spectra are combined to provide an estimate of the source-averaged charged-pion phase-space density $\langle f\rangle$. Fig. 5.17-1a shows $\langle f\rangle$-values at the bin-average momenta of the HBT analyses, using the spectrum global fit to interpolate spectrum values for the same momenta. The open crosses are $\langle f(p)\rangle$ values for NA49 at a centrality of 0-4% of σ_{tot}. The present analysis indicates that at low momenta the NA49 $\langle f\rangle$ values are exceeded by the RHIC $\langle f\rangle$ values by almost a factor of 2. We note, however, that in the present analysis the four most central bins (0-40%) have very similar phase-space densities, suggesting the onset of some limiting process.

Fig. 5.17-1b shows the average phase space density $\langle f\rangle$, with successive centralities reduced by factors of 1.5, calculated using the actual spectrum points and interpolated/extrapolated values of the corrected momentum volume $V_p/\sqrt{\lambda}$. The solid lines through these points use these fits.

---

*See HBT PWG web site at http://www.star.bnl.gov/STAR/html/hbt_l.

[1] G. F. Bertsch, Phys. Rev. Lett. **72**, 2349 (1994); Phys. Rev. Lett. **77**, 789(E) (1996).

[2] G. F. Bertsch, M. Gong and M. Tohyama, Phys. Rev. C **37**, 1896 (1988); G. F. Bertsch, Nucl. Phys. **A498**, 173c (1989).

[3] D. Ferenc, U. Heinz, B. Tomášik, U. A. Wiedemann, and J. G. Cramer, Phys. Letters **B457**, 347-352 (1999).

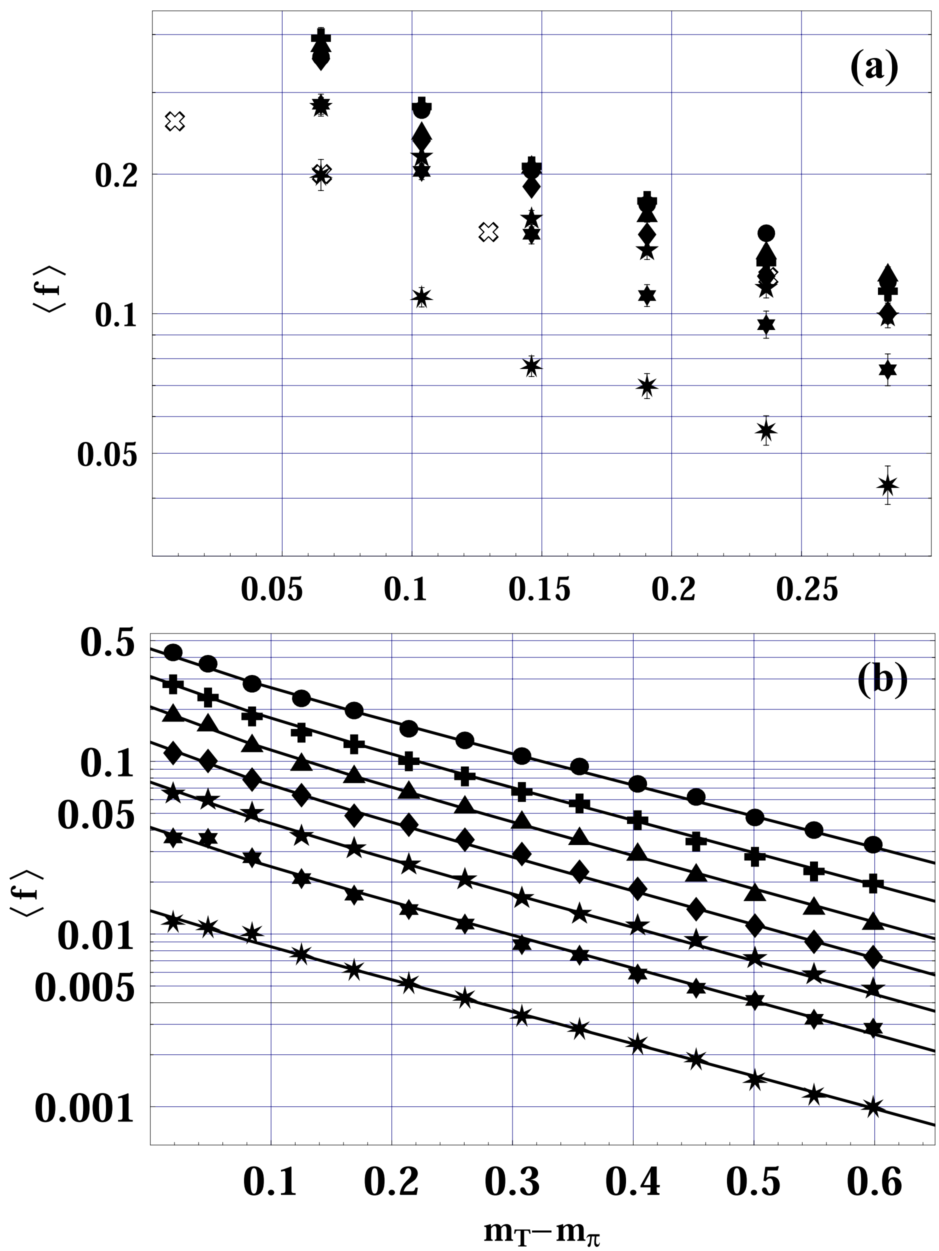

Figure 5.17-1. Source-averaged π^- phase-space density $\langle f\rangle$ for $\sqrt{s_{NN}}$=130 GeV Au+Au collisions in centrality intervals of 0-5% (circle), 5-10% (cross), 10-20% (triangle), 20-30% (diamond), 30-40% (5-pointed star), 40-50% (6-pointed star), and 50-80% (7-pointed star) of the total reaction cross section. **(a)** $\langle f\rangle$ calculated with $V_p/\sqrt{\lambda}$ in 6 momentum bins combined with interpolated spectrum values. Open cross symbols are $\langle f\rangle$ values taken from Ferenc[3]for $\sqrt{s_{NN}}$=17 GeV mid-rapidity Pb+Pb collisions at centrality 0-4% of σ_{Tot} using NA49 results. **(b)** $\langle f\rangle$ calculated from spectrum values in 14 momentum bins combined with $V_p/\sqrt{\lambda}$ values extrapolated from fit. To separate successive centralities, each is displaced downward by a factor of 1.5^{n-1} where n=1-7. The solid curves are calculated from the spectrum and correlation momentum volume fit functions.

5.18 Pion entropy in RHIC collisions

J. G. Cramer, J. M. S. Wu and the STAR HBT Physics Working Group*

The entropy is of considerable interest in RHIC collisions, because it is expected to be qualitatively larger for an initial quark gluon plasma than for an initial hadron gas. The average pion phase space density $\langle f \rangle$, estimated by combining the pion momentum spectrum and the HBT correlation function, can be used to estimate the entropy per particle S_π/N of the colliding system at freeze out. The relation for converting $f \equiv f(\vec{p}.\vec{r})$ to entropy per particle is:

$$S_\pi/N = \frac{\int [(f+1)\log(f+1) - f\log(f)]\, d\vec{r}\, d\vec{p}}{\int f\, d\vec{r}\, d\vec{p}} \tag{1}$$

To make use of this relation, we assume that $f(\vec{p},\vec{r})$ is proportional to $\langle f \rangle$ and has the radial shape and radial momentum dependence given by the HBT analysis, and that the source is azimuthally symmetric. We then need the functional dependence of $\langle f \rangle$ with respect to p_T for all values of p_T, and for this we use fits to the pion spectra and corrected momentum volume. We perform the integrals of Eqn. 1 to obtain the entropy per particle S_π/N for each centrality. These are shown in Fig. 5.18-1a. The horizontal lines represent Bose-gas thermal estimates of the entropy per particle for a massive ($m = m_\pi$) or a massless ($m = 0$) Bose gas with a chemical potential $\mu_\pi = 0$. The horizontal variable is the number of participant nucleons for each centrality bin, as estimated using the Glauber model. It is a good quantitative measure of centrality. The systematic error of S/N in Fig. 5.18-1a is indicated by the dashed envelope lines. We note that the approximation of Brown, Panitkin, and Bertsch,[1] which neglects the radial dependence of $f(\vec{p},\vec{r})$ and uses $\langle f \rangle$ in its place, leads to a sizable overestimate of the entropy, as indicated by the gray curve in Fig. 5.18-1a.

We obtain the total pion number by integrating the pion spectra and multiply this quantity by S_π/N for each centrality to obtain the total pion entropy dS_π/dy. This is shown in Fig. 5.18-1b. The lower square shows the corresponding system entropy of all nucleons and antinucleons, as estimated using a coalescence model. The open crosses show the corresponding pion and nucleon entropies obtained by Pal and Pratt.[2] We see that total pion entropy dS_π/dy is quite linear vs. participant number N_p.

Fig. 5.18-1c shows $(dS_\pi/dy)/N_p$. We see that this quantity has a constant value of about 6.5 per participant within errors. The absence of centrality dependence in the entropy per participant suggests that there is no per-participant change in initial entropy production with collision centrality, such as might be expected if there were qualitatively different initial dynamics in central and peripheral collisions.

*See the HBT PWG web site at http://connery.star.bnl.gov/STAR/html/hbt_l

[1]D. A. Brown, S. Y. Panitkin and G. F. Bertsch, Phys. Rev. C **62**, 014904 (2000).

[2]S. Pal and S. Pratt, Phys. Lett. B **578**, 310 (2004).

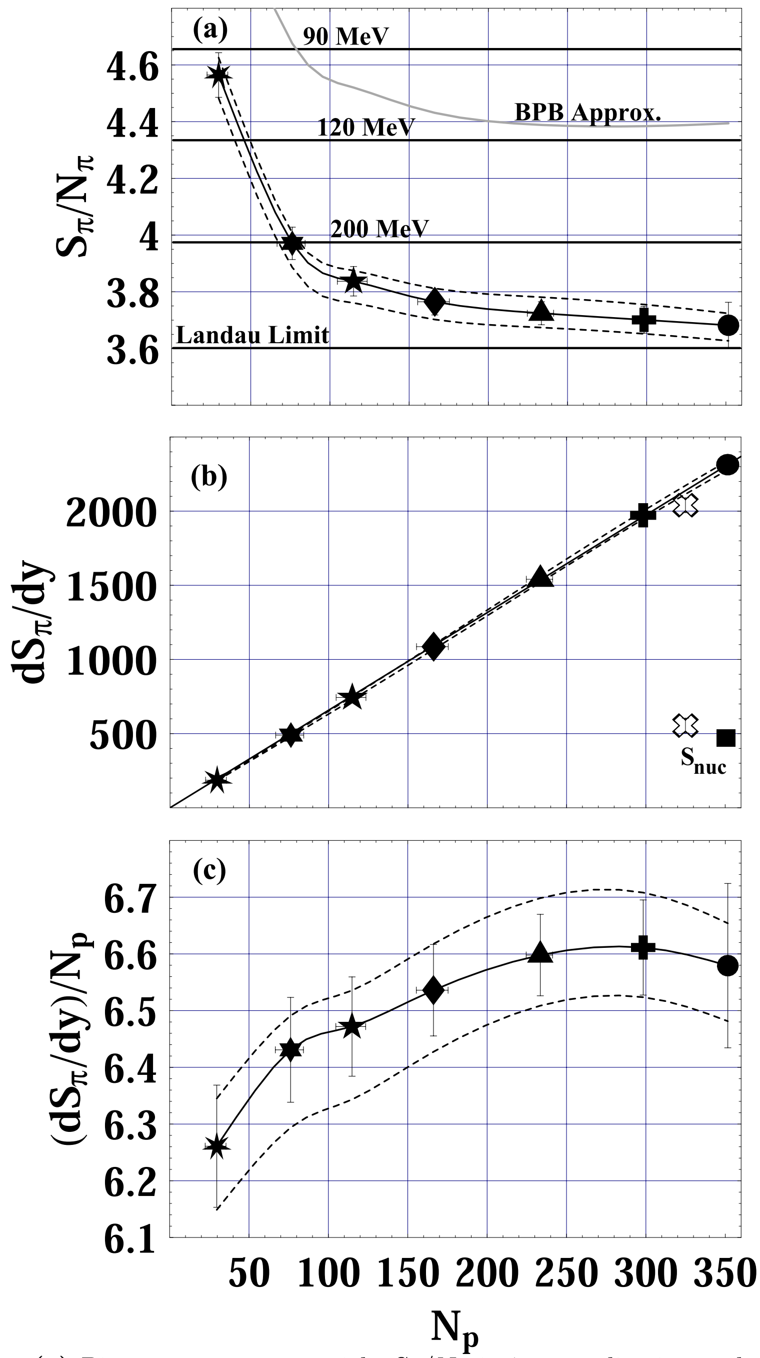

Figure 5.18-1. **(a)** Pion entropy per particle S_π/N_π in 7 centrality intervals, calculated using fits to spectra and $V_p/\sqrt{\lambda}$. Symbols are defined in text. The upper curve shows S_π/N_π using the BPB approximation. Horizontal lines show static Bose gas S_π/N_π with zero pion chemical potential and the Landau limit for massless bosons. Dashed curves in all panels indicate systematic uncertainties in $V_p/\sqrt{\lambda}$; **(b)** Total pion entropy dS_π/dy at midrapidity. Solid line is a linear fit through the origin. The square point (S_{nuc}) shows estimated total *nucleon* entropy (see text). Open crosses are entropy estimates from reference 2; **(c)** Total pion entropy per participant $(dS_\pi/dy)/N_p$ at midrapidity. Note the suppressed zero and expanded scale.

5.19 Bichsel functions for particle tracks in STAR TPC

H. Bichsel, R. J. Porter and Y. Fisyak*

The study of the ionization processes in the STAR TPC with the Fermi-Virtual-Photon method (FVP) has been expanded to the use of P10 gas (90% Ar with 10% CH_4). An improved set of optical absorption coefficients for both gases has been generated.[1] Programs permitting the calculation of simulations of ionization for full particle tracks in the TPC have been developed. Particle identification (PID) using truncated mean values of the ionization along the tracks has been simulated and has been compared with measured data from the TPC. Good agreement between calculations and measurements has been found for some parts of the observations, while there are some differences in others. A more extensive comparison should lead to improvements in the understanding of the results from the TPC.

It has been found that the dependence on particle speed $\beta\gamma$ of most probable energy losses Δ_p for track segments differs from that given by the Bethe-Bloch approximation dE/dx. Instead, "Bichsel functions" should be used.[2] Similar differences occur for truncated mean values of full tracks. This can be seen in the figure where Bichsel functions calculated with the track-program mentioned above are compared with the Bethe-Bloch function.

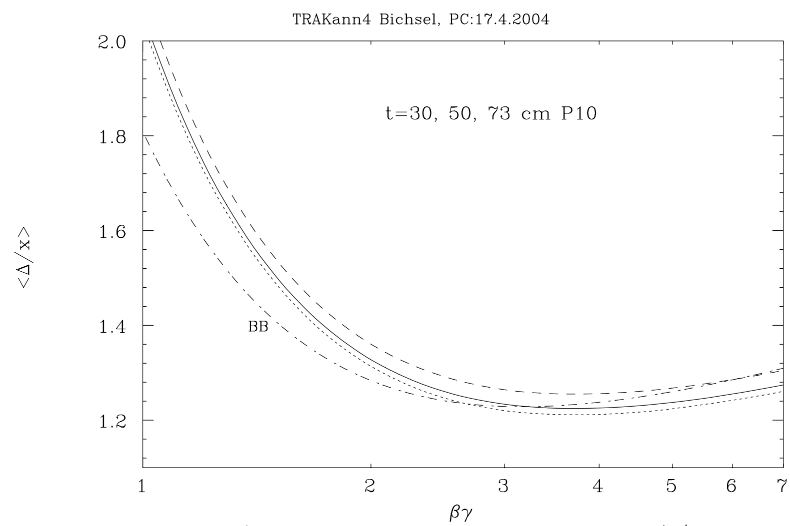

Figure 5.19-1. The dependence of truncated mean energy losses $< \Delta/x >$ on particle speed $\beta\gamma$ for tracks with length t. The Bethe-Bloch function is given by the dash-dotted line labeled BB. Three calculated Bichsel functions are shown. Solid line: $t = 73.2$ cm consisting of 11 (inner) segments with $x = 1.2$ cm and 30 [outer] segments with $x = 2$ cm. Dashed line: $t = 50$ cm consisting of 25 segments with $x = 2$ cm. This line is within 0.1% of a line (not shown) for $t = 30$ cm, with 15 segments. Dotted line: $t = 30$ cm consisting of 10 segments with $x = 1.2$ cm and 9 segments with $x = 2$ cm. At $\beta\gamma = 4$ the separation between the two $t = 30$ cm functions is 3.5 percent.

*Brookhaven National Laboratory, Upton, NY 11973.
[1]Atomic and Molecular Photoabsorption, J. Berkowitz, Academic Press, 2002.
[2]Sect. 26.2.5 of *Review of Particle Physics*, Phys. Rev. D **66**, 010001 (2002).

6 Electronics, Computing, and Detector Infrastructure

6.1 PC-based data-acquisition developments at CENPA

R. J. Seymour and H. E. Swanson

Our PC-based data-acquisition system[1] uses JAM to sort and display histograms and a C# application developed at CENPA to control the CAMAC interface and build an event data stream that is sent to JAM. Inter-process communication uses "localhost" the internal internet connection. The JAM code at the Source Forge site[2] has undergone many version changes that improved the user interface and acquisition performance. We are currently running version 1.4.

Two additional systems were added in the past year. One of these is a stand-alone system with a computer, a NIM bin and a CAMAC crate built into a roll-around rack that can be moved around the lab. It can be brought into the experiment cave or low background areas. The other is an IBM laptop computer and docking station that includes a slot for the PCI CAMAC interface. It can be taken to other accelerator facilities along with CAMAC modules and requires only the CAMAC crate to become a complete data-acquisition system. The advantages are twofold, the sort code can be written and debugged here and we don't have to use an unfamiliar data-acquisition system when running the experiment.

We have installed Eclipse, a Java development platform, on each of the computers and JAM can be run from that environment or launched as a stand alone application. Eclipse is an excellent tool for developing sort routines and in general learning the Java language. It shows syntax errors and gives suggestions on how to fix them. It also lets you browse JAM classes and methods in the context of the sort code.

At event rates greater than a few kHz the dead time can exceed 10%. ORTEC markets the CMC203 FIFO buffer that reads out FERA enabled ADCs such as the 413A into a buffer that can be read asynchronously over the CAMAC bus. We have acquired one of these modules and added a mode to the C# code which polls the buffer at a periodic rate. The observed dead time for reading 4 ADC channels at 6 kHz rate is about 3%. The CMC203 can be configured to insert the gate arrival times in the data stream which lets us measure decay rates in this low-dead-time mode.

[1] CENPA Annual Report, University of Washington (2003) p. 69.
[2] URL: jam-daq.sourceforge.net

6.2 Nanopore DNA sequencing

T. Butler, J. H. Gundlach and M. Troll*

We are continuing the development of “Nanopore Sequencing,” a novel technique for detection and analysis of DNA and RNA at the single molecule level.[1] Nanopore sequencing involves the electrically driven movement of individual, single-stranded DNA (ssDNA) or RNA molecules through a nanometer scale biological pore in a process termed “translocation” (Fig. 6.2-1). Translocation of a single molecule is observed as a transient obstruction of an ionic current that flows through the pore (Fig. 6.2-1). These transient obstructions or “blockades” characterize the physical processes underlying translocation[2] and have the potential to be utilized in a novel, ultrafast DNA sequencing method.[3]

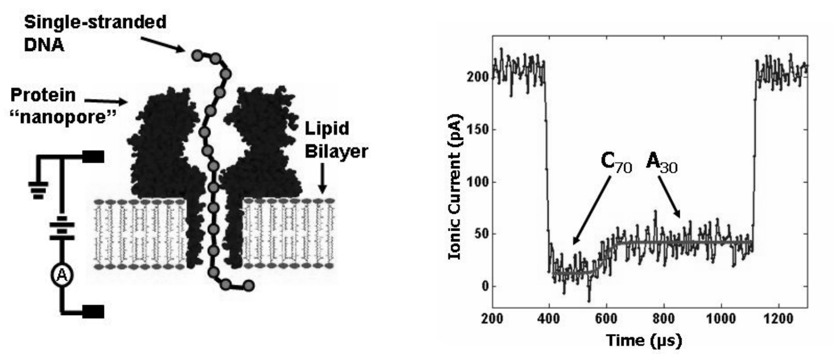

Figure 6.2-1. Schematic of single-stranded DNA translocation through biological nanopore and example ionic current blockade from $C_{70}A_{30}$ RNA block copolymer

Over the past year we have continued to develop our nanopore apparatus and have successfully reproduced many results from the literature. We have automated data acquisition and experimental control. We have taken data for the translocation of three 50 nucleotide long ssDNA homopolymers and two 50 nucleotide long RNA homopolymers. Data was analyzed with custom software developed in Matlab. Analysis revealed that differences in the characteristic blockade amplitudes of the A, C, and T ssDNA homopoymers and A RNA homopolymers are not distinguishable above instrumental noise, while that of C RNA homopolymers is distinguishable. Analysis also revealed differences in the durations of the transient blockades for the five ssDNA/RNA homopolymers. We used techniques from molecular biology to produce 100 nucleotide long RNA block copolymers consisting of 70 C bases followed by 30 A bases. Current blockades from these copolymers demonstrated a pronounced step, corresponding to the transition from the C segment to the A segment in the narrowest portion of the nanopore (Fig. 6.2-1). Quantitative analysis of the blockade signal induced by RNA copolymers is currently under way. This work has been funded by an NSF IGERT fellowship and a University of Washington Royalty Research Fund grant.

*Department of Microbiology, University of Washington, Seattle WA 98195.
[1] CENPA Annual Report, University of Washington (2003) p. 67.
[2] A. Meller, J. Phys: Condes. Matter **15**, (2003) R581-R607.
[3] J. Nakane, M. Akeson and A. Marziali, J. Phys: Condes. Matter **15**, (2003) R1365-R1393.

6.3 Electronic equipment

G. C. Harper, A. W. Myers and T.Ḋ. Van Wechel

The electronics shop personnel provided normal maintenance and repair on all laboratory electronics equipment in support of all experiments conducted at CENPA. The electronics shop also supported ongoing efforts at SNO, both from Seattle as well as on-site support at Sudbury, Ontario, Canada.

Other projects undertaken by the electronics shop include the following.

1. Designed and built several boards in support of the SNO Laser Welder.

2. Moved the SNO Deck Electronics System from the Control Room to the Deck, installed all related cabling to 40 NCD preamplifiers around the neck of the AV.

3. Constructed a new SNO NCD Pulser Distribution System and installed it at SNO in both the DECK System and the Control Room System.

4. Constructed 55 new NCD Preamps and installed them in the SNO experiment.

5. Constructed new low-voltage power-supply trays for the SNO experiment, for both underground systems (DECK System and Control Room System).

6. Constructed a preamplifier for the KATRIN experiment.

7. Constructed 10 Shaper/ADC Boards for the KATRIN experiment.

8. Constructed a second NCD Global Trigger ID Board.

6.4 NSAC - a data-acquisition and control system for the parity non-conserving neutron spin-rotation experiment

H. E. Swanson

We put together a data-acquisition system for the Parity violating neutron spin rotation experiment. The hardware consists of a 2.5 GHz Pentium 4 PC running MS Windows XP-Pro with National Instruments 64 channel multifunction DAQ and GPIB interface boards. Individual detector segments are monitored by integrating their currents in Burr Brown ACF2101 low noise integrators and reading them periodically with the ADC's. The acquisition code NSAC is a multithreaded windows application written in both Microsoft Visual C++ and National Instruments LabWindows/CVI. It extends the architecture and core functions of the EötWash data acquisition programs. This includes displaying and writing data to the hard drive, managing the starting and stopping of runs and hosting menus of user interface options. In addition to ADC data, it can integrate data from other instruments accessible by GPIB and RS232 interfaces. The system also provides the control interface for the apparatus.

A sequencer was added to synchronize reading and resetting of the integrators with changes in the fields of the polarimeter coils and the liquid-Helium configuration of the target. The sequence engine is driven from an ASCII text file that can be created or modified within the program or with an external text editor. It is hierarchical in that the first unit cycles through all its states for each state of the second unit and so on for each subsequent unit. The controlled output can be via DACs, Digital IO, a subroutine call, or a prompt for experimenter input. The sequencer is easily configured for different data-taking protocols such as measuring neutron spin-rotation or polarization products. Typically the sequencer runs continuously until the run is stopped, but it can also be configured to stop the run after its completion.

Hooks are provided to perform calculations on the raw data after the completion of a sequence. A separate display menu tree is provided to plot their results. A user interface panel allows monitoring the liquid helium levels in the target and setting the parameters required for automatic sequencing.

6.5 EötWash data-acquisition development

J. M. Borden, D. J Kapner, S. Schlamminger and H. E. Swanson

SRTWASH: The Windows 98 version of the short-range data-acquisition program continues to be used with various modifications that improved the user interface. The x, y, and z coordinates of the torsion fiber support are monitored with digital micrometers that are now read at the beginning and end of a data run. We have modified the hardware to improve the readout accuracy of the attractor index mark. The attractor's angular position is inferred from counting the number of steps sent to its stepping motor. Each time the attractor passes through the index position a bit is set that is part of the data stream. The angle obtained at the next data read was then used as a check of the absolute angle calibration. Since the period between data reads and the rate of stepping-motor pulses both affect this value we now record the angle as the index mark is passed. With typical rates the angular accuracy has increased from 0.01 degrees to 0.0015 degrees.

Work on a new data acquisition system using the National Instruments 64 channel PCI DAQ module is nearly complete. When running with very small attractor-pendulum separations seismic activity occasionally kicks the pendulum off the detector. The new system, which achieves kilohertz sample rates, should better characterize the kicked amplitude and make the damping algorithm more reliable. We plan to run both systems in parallel at first and compare their data.

EötWash-II: The data-acquisition system continues to perform reliably and there are no plans to upgrade the software to use a modern multifunction DAQ board. New algorithms were developed to damp the amplitude of the torsion pendulum and to match the speed of the turntable to the rotation rate of the fiber support when advancing to the next mirror position.

LISA: This system uses a 16-channel National Instruments DAQ board. The experimenter can configure each input channel to use the raw ADC value or to first pass it to a software lock-in amplifier and digital filter. A class calculates the filter coefficients for a 12-dB/octave Butterworth filter using the system's current sample rate and user selected time constants. Over the past year the lock-in has been carefully evaluated and its low frequency noise compares favorably with commercially available hardware models. We have implemented a PID control loop to move an attractor plate (see Section 1.8) to within a given distance of the pendulum. A digital dial indicator is read to determine the plate's position. Any deviation between this and the intended position generates an error signal which corrects the position of the plate. The position accuracy of the system is 0.0002 inches (0.005 mm). We have also added a routine to apply an arbitrary voltage waveform to the plate over the course of the measurement.

6.6 Development of the ORCA DAQ system

M. A. Howe, F. McGirt,* K. Rielage, J. Wouters* and J. F. Wilkerson

The Object oriented Real-time Control and Acquisition (ORCA) software development effort has been described in past CENPA Annual Reports[1] and has seen significant progress this year. The goal of the ORCA project is to produce a software application tool kit that can be used for quickly building flexible data acquisition systems. ORCA utilizes MacOS X as a development platform which has proven very stable.

ORCA is currently in use for several different experiments including the SNO NCD system (see Sec. 2.11) and the KATRIN beta-decay experiment (see Sec. 2.14).

A number of modules are available and support a variety of VME hardware cards including the NCD/emiT/KATRIN shaper ADC, CAEN 775 and 785 TDC, NCD Trigger, NCD/emiT 100-MHz latched clock, and several IP modules. Custom NCD hardware modules for the multiplexer readout and pulser distribution system have also been developed. The system also supports Ethernet to GPIB devices for use with digital oscilloscopes and HP Pulser hardware.

Several generic tasks have been implemented to help in the calibration and commissioning phase of experiments. A HardwareWizard was added that is capable of adjusting thresholds, gains and other hardware parameters for any number of channels that can be selected through a variety of operator-controlled logic operations. A calibration task was developed to perform an operation on a specific channel for a specific length of time before moving on to the next selected channel. This task will be used to send the log amp calibration pulse to each SNO NCD channel during data taking for calibration.

Other modules include a high voltage controller with automatic high current panic ability and a replay object capable of examining data from previous runs taken with ORCA. Also a global security function has been added so that certain modules and functions can be locked during running to prevent operators from inadvertently changing parameters that effect the data collection.

Finally, several SNO NCD experiment specific features have been implemented. The command communications interface between the current SNO DAQ software (SHaRC) and ORCA have been completed to allow for synchronized running between the PMTs and NCDs in the SNO experiment. Alarms, warnings, and high voltage status can now pass between the two systems allowing the operator to concentrate on one system at a time without being unaware of potential problems in the other. Run type coordination such as neutrino, maintenance and calibration runs are now possible. An editable tube map with NCD hardware information has also been implemented.

Future improvements include the addition of specific tasks for the KATRIN experiment and the development of Firewire to VME drivers.

---

*Los Alamos National Laboratory, Los Alamos, NM 87545.

[1]CENPA Annual Report, University of Washington (2001) p. 83; (2002) p. 81; (2003) p. 70.

6.7 Laboratory computer systems

M. A. Howe, R. J. Seymour and J. F. Wilkerson

This year again saw continuous incremental upgrades or replacements of existing systems.

Along with numerous 2.8 and 3.0 GHz generic Windows XP PCs, we have added more Linux systems. The systems supporting our RHIC work run RedHat v8.0 to match Brookhaven, and the rest of the systems have received v9.0. The RHIC group's HP-PA boxes have all been retired. Our typical newly-installed PC system runs about $700, with ever-increasing speed, memory and disk capacity.

We have one dual-processor Athlon 64 system, currently running RedHat 9.0, but slated to receive SuSe 64.

Many Macintoshes have been upgraded to dual-processor G5's.

Our cluster of VAXstation 3200GPX workstations lost two members to hardware failure, and we finally moved our primary mail server functions from one of the remaining nodes to a dedicated Linux box.
We have retired our MBD-11/VAXstation data acquisition system.
We have added a second roll-around JAM acquisition system.
We also have two JAM-capable IBM ThinkPad laptops, using docking stations to hold the PCI-based CAMAC controller card.

Our computing and analysis facility consists of:

- A mix of RedHat Linux systems, v7.3 through v9.0
- Twin dual-processor DEC/Compaq/HP Unix AlpherServer 4000s
- Two VMS/Vaxes and two VMS Alphas for "legacy" computing.
- The SNO, NCD, KATRIN and emiT groups rely upon Macintosh systems.
- Our Sun Sparcstation 20 and a pair of SunBlade 100 workstations serve CADENCE circuit design, analysis and layout duties.
- A VAXstation is the Linac and Vacuum systems' control and display system.
- Two desktop JAM acquisition and analysis systems, plus two laptops for taking to other installations.
- Although not directly used by Lab personnel, we provide co-location services for the Institute for Nuclear Theory and the Physics Nuclear Theory group in the form of one VMS VAXstation 3200. The Astronomy Department has located a 64-processor Xeon-based Beowulf cluster in our machine room.

7 Accelerator and Ion Sources

7.1 Deck and ion sources

G. C. Harper, M. A. Howe, S. K. L. Sjue and D. I. Will

With the terminal ion source in use, the injector deck is available for other research activities (see Section 7.3). Concern that LiF used to prepare neutron-capture targets might be depleted in ^{6}Li led to use of the 860 sputter ion source for crude mass spectrometry. For a test of alternate neutron-capture targets, ^{10}B was implanted using the SpIS, deck and offdeck steering magnet.

The computer code SCAN steps the steering magnet current in x from x-minimum to x-maximum, then steps once in y to scan a new line from x-maximum back to x-minimum. When y-maximum is reached a new scan is begun at y-minimum. At program startup one specifies six parameters: x-minimum, x-maximum, y-minimum, y-maximum, time interval per step, and step size. As noted in Section 7.3, SCANELP is an enhanced version of SCAN designed to save time by scanning only the inscribed ellipse within the specified rectangle.

7.2 Van de Graaff accelerator operations and development

J. F. Amsbaugh, G. C. Harper, A. W. Myers, T. D. VanWechel and D. I. Will

The tandem was entered 18 times this year. The ion species was changed during four of the openings. The #3 accelerator tube was changed during three of the openings. The tube voltage gradient was changed four times. The internal components of the TIS were all serviced during three routine servicings and the einzel lens was changed to the 2.5 cm diameter version during one of these. One opening was required to make repairs to the power lead to the TIS einzel supply and to replace the F/O connectors on the fiber optics on the terminal computer side of the telemetry link. The TIS and the foil stripper were exchanged during three openings. The electrostatic deflector supplies were either tested, repaired, or replaced during six tank openings. The electrostatic deflectors were removed and the TIS permanent magnet scheme was reinstalled during one opening. The machine was entered twice to refoil. A short in plane #55 in tube #3 was removed during one of the service openings in which a column spark problem was also solved.

Most of the problems which temporarily halted experimental use of the tandem were related to failures in the electrostatic deflector high voltage power supplies. We finally removed the deflectors entirely and returned to the operational mode in which one of a set of permanent magnets is installed for the ion species of choice. The design of a rugged power supply scheme using adequate transient suppression and potted power supplies using technology newer by 20 years has been completed. The construction of the package is complete except for the circuit boards that house the suppression circuits and connectoring scheme.

The tandem produces x-rays in bursts when the terminal is raised above 7.5 MV, an improvement from last year. The x-rays can be substantially reduced by shorting two adjacent column planes somewhere in the tube #1 region with the shorting boat. The tank must be entered to pinpoint the location of the emitting plane and then further studies of this problem must be done.

During the 12 months from April 1, 2003 to March 31, 2004 the tandem pellet chains operated 1401 hours, the SpIS 1576 hours, and the DEIS 298 hours. Additional statistics of accelerator operations are given in Table 7.2-1.

Activity Scheduled	**Days Scheduled**	**Percent of Available Time**
Molecular research, deck ion sources only	7	2
Ion implants, deck ion sources only	39	11
Nuclear physics research, deck ion sources	47	13
Nuclear physics research, terminal ion source	41	11
Subtotal, molecular or nuclear physics research	134	37
Machine development, maintenance, or crew training	136	37
Grand total	270	74

Table 7.2-1. Tandem Accelerator Operations April 1, 2003 to March 31, 2004

7.3 Progress toward UCN detectors with the 860 SpIS

A. García, G. C. Harper, S. A. Hoedl, A. Sallaska, S. K. L. Sjue and D. I. Will

We used the 860 sputter ion source (SpIS) to help manufacture ultracold neutron (UCN) detectors. This was done in two ways. We implanted ^{10}B into a 2000Å layer of vanadium evaporated onto nickel foils to make one possible UCN detector. Another possible detector is ^{6}Li in a layer of LiF evaporated onto a 2500Å thick nickel foil. We evaporated LiF onto its substrate. However, only ^{6}Li is useful to make a UCN detector, so we used the SpIS to check that the ^{6}Li was present in the LiF in its natural abundance.

We used medium grit, crystalline boron (enriched to 96% ^{10}B) mixed 1:1 with Ag to obtain our beam for boron implantation. With a detector area of about 2×10^{-4} m^2, and an absorption layer of vanadium approximately 2000Å thick, we needed to implant about 10^{18} ^{10}B's at 80 keVfor a 1:1 B/V ratio. Beam currents averaging 1μA on target require two full days to reach 10^{18} implants, so this was a time intensive process. To produce uniform implantation across the whole target, the beam was scanned by the offdeck steering magnet. We modified a program to raster the beam more efficiently, with elliptical boundaries instead of rectangular, to minimize beam time. Disregarding damaged foils and foils on which the beam was not well focused, we made four foils for UCN monitors.

The LiF detectors were created in an evaporation chamber, but we needed to use the SpIS to test the abundance of ^{6}Li. The natural abundance of ^{6}Li is 7.5%, but commercial sources could be depleted and contain far less ^{6}Li. The SpIS is good for rough mass spectrometry, because the charge to mass ratio of the ions in the beam is constant at a given magnetic field. Thus one can use the fact that the magnetic field required to tune the beam of a particular isotope is proportional to the square root of the mass. We tested the composition of the LiF by tuning the magnetic field to obtain the peak beam currents of Li$^-$, LiF$^-$, and LiF$_2$$^-$ for both ^{6}Li and ^{7}Li. Then we were able to estimate the isotopic composition from the ratios of the beam currents. The results are in the table below. The results suggest ^{6}Li is present in its natural abundance, so the LiF we used should work for the UCN detector foils.

Q/M	Expected Ion	B (Gauss)	Expected B	B Shift	Current	Li Percentage
1/6	^{6}Li$^-$	788	791.8	-2.8	17.7nA	6.8
1/7	^{7}Li$^-$	852	855.2	-3.2	240nA	93.2
1/19	^{19}F$^-$	1409	Calibration	N/A	12.7μA	N/A
1/25	^{6}LiF$^-$	1619	1616.2	2.8	3.7nA	9.7
1/26	^{7}LiF$^-$	1652	1648.2	2.8	34.3nA	90.3
1/44	^{6}LiF$_2^-$	2148	2144.2	3.8	13.7nA	8.9
1/45	^{7}LiF$_2^-$	2172	2168.2	3.6	140nA	91.1

7.4 Removal of large pieces of the old cyclotron

J. M. Borden, T. S. Cook, J. H. Elms, H. Fauska,* J. H. Gundlach, D. R Hyde, D. J. Kapner, A. W. Myers, H. Simons, D. W. Storm, D. I. Will and J. P. Will

We received funds from the College of Arts and Sciences for disposal of the low level radioactive parts of the old cyclotron. We removed the dee-stem tanks, the dees, the vacuum chamber, and the associated piping. The disposal scheme initially involved a single large box (100 cu. ft.) for removal of low level radioactive waste. There was a 17,500 lb weight limit for the box and contents. At the same time, the University Hospital was doing construction in their neutron therapy site, and had produced a significant amount of low-level radioactive demolition waste. By combining their waste with ours, we were able to share 4 of the large boxes and get about 2.5 boxes full of our own waste, while meeting the weight requirements for the boxes. In total we disposed of 27,600 lbs of metal with low-level activation.

After disassembly of the parts, they were cut into pieces that would fit into the boxes. The pieces were surveyed, as some materials were not measurably radioactive and could be disposed of by normal means. The main radioactive materials were copper and steel, both of which had measurable levels of ^{60}Co, presumably resulting from neutron capture on ^{59}Co present in those materials. As the cyclotron had not been operated since the early 80's, shorter lived activities had died out. By careful sorting of the materials, we were able to get the radioactive material into the available boxes without exceeding the weight limits.

The result of this effort was the creation of an additional 150 square feet of floor space in the old cyclotron circle room. This space is near the middle of the room and is being used mainly for the LISA development, (see Section 1.8) as well as other gravity experiments. The cyclotron magnet yoke remains, but it is relatively compact compared to the entire structure. The room has a much neater appearance besides having more space for research.

*retired staff, served as consultant.

8 The Career Development Organization: year four

T. Butler, V. M. Gehman,* K. Kazkaz, J. L. Orrell† and L. C. Stonehill

The Career Development Organization (CDO)[1] for Physicists and Astronomers at the University of Washington is finishing up its fourth successful year of activities and seminars geared toward helping students find gainful, satisfying employment after graduation. Building on the work of previous years,[2] the CDO hosted the 3^{rd} Annual Networking Day and offered a series of seminars on the wide range of careers open to Ph.D. physicists. CENPA graduate students continued to play a major role in the planning and execution of CDO-related events.

The 3^{rd} Annual Networking Day was held on November 6, 2003. The CDO identified several goals for this Networking Day, including broader departmental participation, increased contact with local companies, and student-run laboratory tours. The first goal was met with almost perfect success, and graduate student participation was up by 90% from the previous year, resulting in 16 students giving ten-minutes talks and 18 poster presentations. We started relationships with local technology companies through contacts supplied by faculty, with one result being an increase in sponsorship money to $4000, up from $3250 the previous year. Finally, the student tours were not as heavily attended as we desired, but with a shuffling of the schedule they may be more successful in subsequent Networking Days.

The Networking Day continues to provide opportunities for students to meet and introduce themselves to potential employers, as well as to apply for internships before graduation. It also served to introduce both students and employers to various resources at the University of Washington that are of interest to the wider science community.

This past year has also seen an increase in the number of seminars offered, all based around the theme of "Physicists Outside Physics". This seminar series brought in Ph.D. physicists who have been involved with work outside the traditional academic and laboratory positions:

Vic Snyder	UW Center for Career Services
Philipp K. Janert, Ph.D.	Amazon.com
Ray Warner, Ph.D.	Pacific Northwest National Laboratory
Jennifer Hodgdon, Ph.D.	Poplar ProductivityWare
Benn Tannenbaum, Ph.D.	Federation of American Scientists

Because of the success of the Networking Day and the attendance and visibility of the seminar series, the activities of the Career Development Organization are becoming established programs within the University of Washington Physics Department.

*Presently at Los Alamos National Laboratory, Los Alamos, NM 87545.
†Presently at Pacific Northwest National Laboratory, Richland, WA 99352.
[1] http://students.washington.edu/cdophys
[2] CENPA Annual Report, University of Washington, (2003) p. 76.

9 CENPA Personnel

9.1 Faculty

Eric G. Adelberger	Professor	
Hans Bichsel	Affiliate Professor	
John G. Cramer	Professor	
Peter J. Doe	Research Professor	
Hans Eggers	Visiting Scholar	
Joseph Formaggio	Research Assistant Professor	
Alejandro Garcia	Professor	
Jens H. Gundlach	Research Associate Professor	
Axsel Hallin[1]	Visiting Scientist	
Isaac Halpern	Professor Emeritus	
Blayne R. Heckel	Professor	
R.G. Hamish Robertson	Professor;	Scientific Director
Kurt A. Snover	Research Professor	
Derek W. Storm	Research Professor;	Executive Director
Thomas A. Trainor	Research Professor	
Robert Vandenbosch	Professor Emeritus	
William G. Weitkamp	Professor Emeritus	
John F. Wilkerson	Professor	
Jin Hee Yoon[2]	Visiting Scientist	

9.2 Postdoctoral Research Associates

Cristina Bordeanu
Chunhui Han
Seth Hoedl
Qingjun Liu[3]
Sean McGee
Jeffrey Reid[4]
Keith Rielage
Miles Smith[5]
Stefan Schlamminger

[1]Queen's University, Department of Physics, Stirling Hall, SNO Office, Kingston, Ontario K7L 3N6.
[2]Department of Physics, Inha University, Inchon 402-751, Korea.
[3]Presently at University of Science and Technology of China, Department of Modern Physics, Hefei, Anhu, 230026, People's Republic of China.
[4]Presently at Department of Biochemistry and Molecular Biology, One Baylor Plaza, MS: BCM125 Baylor College of Medicine, Houston, TX 77030; W. M. Keck Center for Computational and Structural Biology, Houston, TX 77005.
[5]Presently at Melbourne, Australia.

9.3 Predoctoral Research Associates

Minesh Bacrania
Ki-Young Choi
G. Adam Cox
Thomas Gadfort[1]
William Clark Griffith
Kareem Kazkaz
Jeffrey Manor[2]
Kathryn Miknaitis
Hans Pieter Mumm
John Orrell[3]
Sky Sjue
Mathew Tilley[1]
Jackson Wu[1]
Thomas Butler[1]
Ted Cook
Charles Duba
Victor Gehman[1]
Dan Kapner
Michelle Leber
Frank Marcoline
Erik Mohrmann
Noah Oblath
Anne Sallaska
Laura Stonehill
Smarajit Triambak

9.4 Research Experience for Undergraduates participants

Colin Connolly[4]
Drew Fustin[6]
Christopher West[8]
Michael Dunham[5]
Simon Slutsky[7]

[1]Department of Physics, University of Washington, Seattle, WA 98195.
[2]Left in 2003.
[3]Presently at Pacific Northwest National Laboratory, Richland, WA 99352.
[4]Department of Physics, Stanford University, Stanford, CA 94305.
[5]Department of Physics and Astronomy, University of Rochester, Rochester, NY 14627.
[6]Department of Physics and Astronomy, Drake University, 2507 University Ave., Des Moines, IA 50311.
[7]Department of Physics, Brandeis University, MB 3599, 415 South St., Waltham, MA 02454.
[8]Department of Physics, University of Florida, Gainesville, FL 32611.

9.5 Professional staff

The professional staff are listed with a description of their recent major efforts.

John F. Amsbaugh	Research Engineer	Mechanical design, vacuum systems
Tom H. Burritt	Research Engineer	Construction SNO NCD's
Gregory C. Harper	Research Engineer	Electronic and mechanical design Accelerator upgrades and operation
Mark A. Howe	Research Engineer	Software for DAQ, control systems
R. Jefferson Porter[1]	Visiting Staff	STAR analysis
Duncan J. Prindle, Ph.D.	Research Scientist	Heavy ion software
Richard J. Seymour	Computer Systems Manager	
H. Erik Swanson, Ph.D.	Research Physicist	Precision experimental equipment
Timothy D. Van Wechel	Electronics Engineer	Electronic design, construction, maintenance
Brandon Wall	Research Scientist-Engineer Assistant	SNO operation
Douglas I. Will	Research Engineer	Cryogenics, ion sources

9.6 Technical staff

James Elms	Instrument Maker
David Hyde	Instrument Maker
Allan Myers	Electronics Technician
Hendrik Simons	Instrument Maker, Shop Supervisor

9.7 Administrative staff

Barbara J. Fulton	Administrator
Kate J. Higgins	Fiscal Specialist

[1]Supported by Brookhaven National Laboratory, Upton, NY 11973.

9.8 Part Time Staff

Jesse Angle[1]	Jeremy Borden
Rogan Carr	David Crompton
Douglas Gabler[1]	Evan Goetz[1]
Danny Hinojosa[1]	Gregory Hodges
Karthik Jeyabalan[1]	Robert Kyle[1]
Emily Lemagie	Mara Lemagie
Christy McKinley	Kamil Michnicki
Quinn Minor[1]	Bryan Munro[1]
Michael Nickerson	Adam Oliver[1]
Braxton Osting	Patrick Peplowski
Shuji Uehara	Mark Wehrenberg
Matthew White[1]	Jonathan Will

[1]Left during 2003.

10 Publications

Published papers:

"Tests of the gravitational inverse square law," E. G. Adelberger, B. R. Heckel and A. E. Nelson, Ann. Rev. and Part Sci. **53**, 77 (2003).

"Neutrino studies in Mo-100 and MOON - Mo observatory of neutrinos," P.J̇. Doe *et al.*, Nucl. Phys. A **721**, 517C (2003).

"Neutral current and day night measurements from the pure D_2O phase of SNO," A. L. Hallin and the SNO Collaborators, Nucl. Phys. B Proc. Sup. **118**, 3 (2003).

"Measurement of the solar neutrino capture rate in SAGE," V. N. Gavin and the SAGE Collaborators, Nucl. Phys. B Proc. Sup. **118**, 39 (2003).

"The Majorana Ge-76 double-beta decay project," C. E. Alseth and the Majorana Collaborators, Nucl. Phys. B Proc. Sup. **124**, 247 (2003).

"Strange anti-particle to particle ratios at mid-rapidity in$\sqrt{s_{NN}} = 130$ GeV Au + Au collisions," C. Adler and the STAR Collaborators (including H. Bichsel, J. G. Cramer, D. J. Prindle and T. A. Trainor), Phys. Lett. B **567**, 167 (2003), [nucl-ex/0211024].

"Gas-phase anions containing B and N," R. Vandenbosch, Phys. Rev. A **67**, 013203-1 (2003).

"Is e^+e^- pair emission important in the determination of the ^{3}He + ^{4}He S-factor?" K. A. Snover and A. E. Hurd, Phys. Rev. C **67**, 055801 (2003).

"Directed and elliptic flow of charged pions and protons in Pb + Pb collisions at 40-A-GeV and 158-A-GeV," C. Alt and the NA49 Collaborators (including J. G. Cramer, D. J. Prindle and T. A. Trainor), Phys. Rev. C **68**, 034903 (2003), [nucl-ex/0303001].

"Net charge fluctuations in Au+Au collisions at $\sqrt{s_{NN}} = 130$ GeV," STAR Collaborators (including H. Bichsel, J. G. Cramer, D. J. Prindle and T. A. Trainor), Phys. Rev. C **68**, 044905 (2003), e-Print Archives (nucl-ex/0307007).

"Precise measurement of the $^7\mathrm{Be}(p,\gamma)^8\mathrm{B}$ factor," A. R. Junghans and the ^{7}Be Collaborators (including E. C. Mohrmann, K. A. Snover, E. G. Adelberger and H. E. Swanson), Phys. Rev. C **68**, 065803 (2003).

"Solar neutrinos from CNO electron capture," L. C. Stonehill, J. A. Formaggio and R. G. H. Robertson, Phys. Rev. C **69**, 015801 (2004), (hep-ph/0309266).

Erratum: "Midrapidity antiproton-to-proton ratio from Au+Au $\sqrt{s_{NN}} = 130$ GeV," Phys. Rev. Lett. **86**, 4778 (2001), C. Adler and the STAR Collaborators (including H. Bichsel, J. G. Cramer, D. J. Prindle and T. A. Trainor), Phys. Rev. Lett. **90**, 119903(E) (2003).

"Narrowing of the balance function with centrality in Au+Au collisions at $\sqrt{s_{NN}} = 130$ GeV,"

C. Adler and the STAR Collaborators (including H. Bichsel, J. G. Cramer, D. J. Prindle and T. A. Trainor), Phys. Rev. Lett. **90**, 172301 (2003), [nucl-ex/0301014].

"Evidence from d+Au measurements for final-state suppression of high P_T hadrons in Au+Au collisions at RHIC," STAR Collaborators (including H. Bichsel, J. G. Cramer, D. J. Prindle and T. A. Trainor), Phys. Rev. Lett. **91**, 072304 (2003), e-Print Archives (nucl-ex/0306024).

"Transverse momentum and collision energy dependence of high P_T hadron suppression in Au+Au collisions at ultrarelativistic energies," STAR Collaborators (including H. Bichsel, J. G. Cramer, D. J. Prindle and T. A. Trainor), Phys. Rev. Lett. **91**, 172302 (2003), e-Print Archives (nucl-ex/0305015).

"Three-pion Hanbury-Brown Twiss correlations in relativistic heavy-ion collisions from the STAR experiment," STAR Collaborators (including H. Bichsel, J. G. Cramer, D. J. Prindle and T. A. Trainor), Phys. Rev. Lett. **91**, 262301 (2003), e-Print Archives (nucl-ex/0306028).

"Pion-kaon correlations in central Au+Au collisions at $\sqrt{s_{NN}}$ = 130 GeV," STAR Collaborators (including H. Bichsel, J. G. Cramer, D. J. Prindle and T. A. Trainor), Phys. Rev. Lett. **91**, 262302 (2003), e-Print Archives (nucl-ex/0307025).

"Observation of an exotic S = −2, Q = −2 baryon resonance in proton-proton collisions at the CERN SPS," NA49 Collaborators (including J. G. Cramer, D. J. Prindle and T. A. Trainor), Phys. Rev. Lett. **92**, 042003 (2004), e-Print Archives (hep-ex/0310014).

"Particle-type dependence of azimuthal anisotropy and nuclear modification of particle production in Au+Au collisions at $\sqrt{s_{NN}}$ = 200 GeV," STAR Collaborators (including H. Bichsel, J. G. Cramer, D. J. Prindle and T. A. Trainor), Phys. Rev. Lett. **92**, 052302 (2004), e-Print Archives (nucl-ex/0306007).

"Azimuthal anisotropy at the relativistic heavy ion collider: the first and fourth harmonics," STAR Collaborators (including H. Bichsel, J. G. Cramer, D. J. Prindle and T. A. Trainor), Phys. Rev. Lett. **92**, 062301 (2004), e-Print Archives (nucl-ex/0310029).

"ρ^0 production and possible modification in Au+Au and p+p collisions at $\sqrt{s_{NN}}$ = 200 GeV," STAR Collaborators (including H. Bichsel, J. G. Cramer, D. J. Prindle and T. A. Trainor), Phys. Rev. Lett. **92**, 092301 (2004), e-Print Archives (nucl-ex/0307023).

"Constraints on nucleon decay via 'Invisible' modes from the Sudbury Neutrino Observatory," S. N. Ahmed and the SNO Collaborators, Phys. Rev. Lett. **92**, 102004 (2004), (hep-ex/0310030).

"Identified particle distributions in pp and Au+Au collisions at $\sqrt{s_{nn}}$ = 200 GeV," STAR Collaborators (including H. Bichsel, J. G. Cramer, D. J. Prindle and T. A. Trainor), Phys. Rev. Lett. **92**, 112301 (2004), e-Print Archives (nucl-ex/0310004).

"Measurement of the total active ^{8}B solar neutrino flux at the Sudbury Neutrino Observatory with enhanced neutral current sensitivity," S. N. Ahmed and the SNO Collaborators, Phys. Rev. Lett. **92**, 181301 (2004).

Papers submitted or to be published:

"Thoughts about nanodosimetry," H. Bichsel, submitted to Adv. Quantum Chem.

"Backgrounds to sensitive underground experiments," J. A. Formaggio and C. J. Martoff, Ann. Rev. Nucl. and Part. Sci., Invited review, to be published.

"Correlation analysis with scale-local entropy measures," J. G. Reid and T. A. Trainor, submitted to J. Phys. A, mat-ph/0304010.

"Kaon production and kaon to pion ratio in Au + Au collisions at $\sqrt{s_{NN}} = 130$ GeV," C. Adler and the STAR Collaborators (including H. Bichsel, J. G. Cramer, D. J. Prindle and T. A. Trainor), submitted to Phys. Lett. B, [nucl-ex/0206008].

"Centrality and pseudorapidity dependence of charged hadron production at intermediate P_T in Au+Au collisions at $\sqrt{s_{NN}} = 130$ GeV." STAR Collaborators (including H. Bichsel, J. G. Cramer, D. J. Prindle and T. A. Trainor), submitted to Phys. Rev. C, e-Print Archives (nucl-ex/0404020).

"Photon and neutral pion production in Au+Au collisions at $\sqrt{s_{NN}} = 130$ GeV," STAR Collaborators (including H. Bichsel, J. G. Cramer, D. J. Prindle and T. A. Trainor), submitted to Phys. Rev. C, e-Print Archives (nucl-ex/0401008).

"Production of charged pions and hadrons in Au+Au collisions at $\sqrt{s_{NN}} = 130$ GeV," STAR Collaborators (including H. Bichsel, J. G. Cramer, D. J. Prindle and T. A. Trainor), submitted to Phys. Rev. C. e-Print Archives (nucl-ex/0311017).

'Transverse momentum fluctuations in nuclear collisions at 158 AGeV," NA49 Collaborators (including J. G. Cramer, D. J. Prindle and T. A. Trainor), submitted to Phys. Rev. C, e-Print Archives (hep-ex/0311009).

"Comment on 'Electromagnetic dissociation of ^{8}B and the astrophysical S-factor for ^{7}Be$(p,\gamma)^8$B'," K. A. Snover, A. R. Junghans and E. C. Mohrmann, Phys. Rev. C, accepted for publication.

"Sub-millimeter tests of the Gravitational Inverse Square Law," C. D. Hoyle, D. J. Kapner, B. R. Heckel, E. G. Adeleberger, J. H. Gundlach, U. Schmidt and H. E. Swanson, submitted to Phys. Rev. D.

"Azimuthally sensitive HBT in Au+Au collisions at $\sqrt{s_{NN}} = 200$ GeV," STAR Collaborators (including H. Bichsel, J. G. Cramer, D. J. Prindle and T. A. Trainor), submitted to Phys. Rev. Lett. e-Print Archives (nucl-ex/0312009.

"Event-by-Event P_T fluctuations in Au-Au collisions at $\sqrt{s_{NN}} = 130$ GeV," STAR Collaborators (including H. Bichsel, J. G. Cramer, D. J. Prindle and T. A. Trainor), submitted to Phys. Rev. Lett. e-Print Archives (nucl-ex/0308033).

"Lambda and anti-lambda production in central Pb-Pb collisions at 40-A GeV, 80-A GeV and 158-A GeV," T. Anticic and the NA49 Collaborators (including J. G. Cramer, D. J. Prindle and T. A. Trainor), Submitted to Phys. Rev. Lett. e-Print Archive: nucl-ex/0311024.

"Pion, kaon, proton and anti-proton transverse momentum distributions from p+p and d+Au collisions at $\sqrt{s_{NN}} = 200$ GeV," STAR Collaborators (including H. Bichsel, J. G. Cramer, D. J. Prindle and T. A. Trainor), submitted to Phys. Rev. Lett. e-Print Archives (nucl-ex/0309012).

"Production of e^+e^- pairs accompanied by nuclear dissociation in ultra-peripheral heavy ion collision," STAR Collaborators (including H. Bichsel, J. G. Cramer, D. J. Prindle and T. A. Trainor), submitted to Phys. Rev. Lett. e-Print Archives (nucl-ex/0404012).

"Rapidity and centrality dependence of proton and anti-proton production from Au+Au collisions at $\sqrt{s_{NN}} = 130$ GeV," STAR Collaborators (including H. Bichsel, J. G. Cramer, D. J. Prindle and T. A. Trainor, submitted to Phys. Rev. Lett. e-print Archives [nucl-ex/0306029).

"Azimuthally sensitive HBT in Au+Au collisions at $\sqrt{s_{NN}} = 200$ GeV," STAR Collaborators (including H. Bichsel, J. G. Cramer, D. J. Prindle and T. A. Trainor, to be published in Phys. Rev. Lett. e-Print Archives (nucl-ex/0312009.

"Cross sections and transverse single-spin asymmetries in forward neutral pion production from proton collisions at $\sqrt{s} = 200$ GeV," STAR Collaborators (including H. Bichsel, J. G. Cramer, D. J. Prindle and T. A. Trainor, to be published in Phys. Rev. Lett. e-Print Archives (hep-ex/0310058).

"Multi-strange baryon production in Au-Au collisions at $\sqrt{s_{NN}} = 130$ GeV," STAR Collaborators (including H. Bichsel, J. G. Cramer, D. J. Prindle and T. A. Trainor, to be published, Phys. Rev. Lett. e-Print Archives (nucl-ex/0307024).

"emiT: An apparatus to test time reversal invariance in polarized neutron decay," H. P. Mumm and the emiT Collaborators (including A. García, L. Grout, M. Howe, L. P. Parazzoli, R. G. H. Robertson, K. M. Sundqvist and J. F. Wilkerson), submitted to Rev. Sci. Instrum., arXiv:nucl-ex/0402010.

"New tests of the strong equivalence principle and of the inverse square law," E. G. Adelberger, *Proceedings of XXV Johns Hopkins Workshop 'A Relativistic Spacetime Odyssey'*, to be published.

Invited talks, abstracts and other conference presentations:

"A mini Big-Bang," H. Bichsel, Invited Lecture at Chiang Mai University, Chiang Mai, Thailand, January, 2003.

"SNO: Looking beyond the Sun," J. A. Formaggio, Invited talk, *Nnbar Workshop*, Bloomington, IN, February, 2003.

"Solar neutrinos: Current implications and future pssibilities," J. F. Wilkerson, Invited talk, *Neutrino Horizons - Off the Axis Lecture Series*, Fermilab, Batavia, IL, March, 2003.

"A search for time reversal violation in neutron beta decay," H. P. Mumm and the emiT Collaborators, *Nuclear Science Advisory Committee Review*, Oak Ridge National Laboratory, Oak Ridge, IL, March, 2003.

"Nanopore DNA sequencing," J. H. Gundlach, seminar, University of Washington, Seattle, WA, April, 2003.

"The year of the Neutrino," J. A. Formaggio, Colloquium, Duke University, Durham, NC, April, 2003.

"A place in the Sun for the neutrino," "If they have mass, why can't you tell me what it is?" and "Neutrinos - the road ahead," R. G. H. Robertson, *The Page Lectures*, Yale University, New Haven, CT, April, 2003.

"A place in the Sun for the neutrino," R. G. H. Robertson, *Herzfeld Lecture*, Catholic University, Washington, DC, April, 2003.

"A place in the Sun for the neutrino," R. G. H. Robertson, Colloquium, Ohio State University, Columbus, OH, April, 2003; University of California, San Diego, CA, May, 2003; Brattain Memorial Lectures, Whitman College, Walla Walla, WA, October, 2003; Stuart Freedman Festschrift, University of California, Berkeley, CA, January, 2004; Los Alamos National Laboratory, Los Alamos, NM, February, 2004.

"Science intersections at a National Underground Science and Engineering Laboratory," J. F. Wilkerson, Invited Plenary Talk, *Conference on Intersections of Particle and Nuclear Physics*, New York, NY, May, 2003.

"$\overline{v}_e$ and the Sudbury Neutrino Observatory," J. L. Orrell, *Conference on the Intersections of Particle and Nuclear Physics: CIPANP2003*, AIP Conference Proceedings **698**, 275 (2003); New York, NY, May 2003.

"Neutral current measurement at the Sudbury Neutrino Observatory: Past and future," S. McGee, *Northwest Section Meeting of the APS*, Portland, OR, May, 2003.

"Short-range tests of Newton's Inverse Square Law," D. Kapner, E. Adelberger, J. Gundlach, B. Heckel and E. Swanson, *Northwest Section Meeting of the APS*, Portland, OR, May, 2003.

"The STAR time projection chamber (TPC)," H. Bichsel, *Northwest Section Meeting of the APS*, Portland, OR, May, 2003.

"Status of the neutral current detector array at SNO," G. A. Cox, *Northwest Section Meeting of the APS*, Portland, OR, May, 2003.

"The emiT experiment: A search for time reversal invariance violation in polarized neutron beta decay," H. P. Mumm and the emiT Collaborators, *XI International Seminar on Interactions of Neutrons with Nuclei*, Dubna, Russia, June, 2003.

"^{7}Be$(p,\gamma)^8$B and the solar p-p chain," K. A. Snover, A. R. Junghans, E. C. Mohrmann, T. D. Steiger, E. G. Adelberger, J. M. Casandjian, H. E. Swanson, L. Buchmann, A. M. Laird, S. H. Park and A. Zyuzin, Invited paper, *Proc. 1st Yamada Symp. on Neutrinos and Dark Matter* in Nucl. Phys., Nara, Japan, June, 2003 (http://ndm03.phys.sci.osaka-u.ac.jp/proc/index.htm).

"Pion phase space density and the RHIC entropy crisis," J. G. Cramer, paper presented at the *STAR Physics Analysis Workshop*, Lawrence Berkeley National Laboratory, Berkeley, CA, June, 2003.

"SNO II: Salt strikes back," J. A. Formaggio, Invited talk, *Weak Interactions in Particle and Nuclei*, Trento, Italy, June, 2003.

"SNO II: Salt strikes back," and "Continuing the hunt for the sterile neutrinos," J. A. Formaggio, Invited talk, *5th International Workshop on Neutrino Factories and Superbeams, NuFACT'03*, Columbia University, New York, NY, June, 2003.

"The new Seattle-TRIUMF ^{7}Be$(p,\gamma)^8$B S-factor determination," A. R. Junghans, E. C. Mohrmann, K. A. Snover, T. D. Steiger, E. G. Adelberger, J. M. Casandjian, H. E. Swanson, L. Buchmann, A. M. Laird, S. H. Park and A. Zyuzin, *Proc. 8th Internat. Workshop On Topics in Astroparticle and Underground Physics, TAUP 2003*, University of Washington, Seattle, WA, September, 2003.

"Recent results from SNO and other solar neutrino experiments," R. G. H. Robertson, Invited Talk, *Proc. 8th Internat. Workshop On Topics in Astroparticle and Underground Physics International Conference, TAUP 03*, University of Washington, Seattle, WA, September, 2003.

"New determination of the ^{7}Be$(p,\gamma)^8$B S factor," A. R. Junghans, E. C. Mohrmann, K. A. Snover, T. D. Steiger, E. G. Adelberger, J. M. Casandjian, H. E. Swanson, L. Buchmann, A. M. Laird, S. H. Park and A. Zyuzin, *Proc. 6th Internat. Conf. on Radio. Nuclear Beams (RNB6)*, Argonne, IL, September, 2003.

"Weak interactions and fundamental symmetries with rare isotopes," A. García, *Proc. 6th Internat. Conf. on Radio. Nuclear Beams (RNB6)*, Argonne, IL, September, 2003, accepted for publication.

"Revealing nature's secrets with gravity," J. H. Gundlach, *Symposium on the Future of Gravitational Physics and Astronomy*, Albert Einstein Institute, Potsdam, Germany, September, 2003.

"Measurement of the gravitational constant, " J. H. Gundlach, colloquium, Montana State University, Bozeman, MT, September, 2003.

"Notes about straggling ("Landau") functions," H. Bichsel, *Invited lecture at Workshop 'Innovative Detectors for Supercolliders'*, Erice, Sicily, September, 2003.

"Search for the ^{8}B$(2^+) \rightarrow {}^8$Be(0^+) ground-state transition," M. Bacrania, *Rare Isotope Accelerator Summer School 2003*, East Lansing, MI, August, 2003; Poster, *Radioactive Nuclear*

Beams 6, Argonne National Laboratory, Argonne, IL, September, 2003.

"Particle identification at STAR-TPC with ionization measurements, H. Bichsel, *Invited lecture at 8^{th} International Conference on Advanced Technology and Particle Physics*, Villa Olmo, Como, October, 2003.

"Results from the salt phase of the SNO experiment," J. A. Formaggio, Invited talk, *Weak Interactions and Neutrinos Workshop - 2003, WIN 03*, Lake Geneva, WI, October, 2003.

"Entropy and phase-space density at RHIC," J. G. Cramer for the STAR Collaborators, Invited paper presented at *Second Warsaw Meeting on Particle Correlations and Resonances in Heavy Ion Collisions*, Warsaw, Poland, October, 2003, to be published in Nucleonica.

"MEGA: A low-background radiation detector," K. Kazkaz, C. E. Aalseth, T. W. Hossbach, V. M. Gehman, J. D. Kephart and H. S. Miley, *Proceedings of IEEE Nuclear Science Symposium and Medical Imaging Conference (NCC-MIC) 2003*, Portland, OR, October, 2003 to be published in IEEE Transactions on Nuclear Science, June, 2004. (manuscript ID TNS-00202-2003.R1).

"Sudbury Neutrino Observatory neutral current detector acquisition software overview," M. A. Howe, G. A. Cox, P. J. Harvey, F. McGirt, K. Rielage, J. F. Wilkerson and J. M. Wouters, *Proceedings of IEEE Nuclear Science Symposium and Medical Imaging Conference (NCC-MIC) 2003*, Portland, OR, October, 2003, to be published in IEEE Transactions on Nuclear Science, June, 2004.

"Sudbury Neutrino Observatory neutral current detector readout system," G. A. Cox, poster presentation, *Proceedings of IEEE Nuclear Science Symposium and Medical Imaging Conference (NCC-MIC) 2003*, Portland, OR, October, 2003, submitted for publication to *IEEE Transactions on Nuclear Science.*

"University of Washington lab report to SNEAP," G. C. Harper, *Symposium for Northeastern Accelerator Personnel, SNEAP, 2003*, IReS, Strasbourg, France, October, 2003.

"Production of a radioactive ion beam at the University of Washington," G. C. Harper, *Symposium for Northeastern Accelerator Personnel, SNEAP, 2003*, IReS, Strasbourg, France, October, 2003.

"Big G," J. H. Gundlach, seminar, Stanford University, Palo Alto, CA, October, 2003.

"Gravity on the test bench: Torsion balance renaissance," J. H. Gundlach, colloquium, University of Washington, Seattle, WA, November, 2003.

"Two-dimensional scale dependence of P_T fluctuations in 200 GeV Au-Au collisions," T. A. Trainor and the STAR Collaborators, American Physical Society, Tucson, AZ, Oct. 2003, Bull. Am. Phys. Soc. **48**, No. 8, 25 (2003), Session BD.

"Two-dimensional scale dependence of net-charge and total-charge number fluctuations in 200 GeV Au-Au and p-p collisions," D. J. Prindle and the STAR Collaborators, American

Physical Society, Tucson, AZ, Oct. 2003, Bull. Am. Phys. Soc. **48**, No. 8, 25 (2003), Session BD.

"Centrality, scale and energy dependence of P_T fluctuations at RHIC and SPS," T. A. Trainor and the STAR Collaborators, American Physical Society, Tucson, AZ, Oct. 2003, Bull. Am. Phys. Soc. **48**, No. 8, 25 (2003), Session BD.

"Testing the isobaric multiplet mass equation," S. Triambak, A. Garcia, G. Hodges, A. Sallaska and C. West, American Physical Society, Tucson, AZ, Oct. 2003, Bull. Am. Phys. Soc. **48**, No. 8, 29 (2003), Session BF.

"A search for solar electron antineutrinos at the Sudbury Neutrino Obsevatory," J. Orrell and the SNO Collaborators, American Physical Society, Tucson, AZ, Oct. 2003, Bull. Am. Phys. Soc. **48**, No. 8, 39 (2003), Session CD.

"Radioactive background measurements in the neutral current detector array at SNO," G. A. Cox and the SNO Collaborators, American Physical Society, Tucson, AZ, Oct. 2003, Bull. Am. Phys. Soc. **48**, No. 8, 39 (2003), Session CD.

"Precision measurements of astrophysically interesting reaction cross sections," P. Peplowski, C. Bordeanu, J. Manor, K. A. Snover and D. W. Storm, American Physical Society, Tucson, AZ, Oct. 2003, Bull. Am. Phys. Soc. **48**, No. 8, 49 (2003), Session 8P.

"Shielding the multi-element germanium array and segmented enriched germanium assembly," K. Kazkaz and the Majorana Collaborators, American Physical Society, Tucson, AZ, Oct. 2003, Bull. Am. Phys. Soc. **48**, No. 8, 97 (2003), Session HG.

"Radioactive beam development at the University of Washington tandem accelerator facility," M. Bacrania, *UW Physics Career Development Organization Networking Day*, Seattle, WA, November, 2003.

"Pion interferometry and RHIC physics," J.Ġ. Cramer for the STAR Collaborators, Invited paper presented at *IX Mexican Workshop on Particles and Fields Physics Beyond the Standard Model*, Universidad de Colima, Colima, Mexico, November, 2003.

"Event structure at RHIC from p-p to Au-Au," T. A. Trainor, *Workshop on Quark Coalescence and Recombination*, Institute for Nuclear Theory, University of Washington, Seattle, WA, December, 2003.

"How do you weigh a neutrino? Double beta-decay," J. F. Wilkerson, *Invited Public Address to the South Dakota Joint Legislative Committees and SD Public TV*, Pierre, SD, January, 2004.

"The pion entropy and phase space density of Au+Au collisions at $\sqrt{s_{NN}} = 130$ GeV at RHIC," J. G. Cramer for the STAR Collaborators, poster presentation, *The Seventeenth International Conference on Ultra-Relativistic Nucleus-Nucleus Collisons (Quark Matter 2004)*, Oakland, CA, January, 2004.

"Soft and semi-hard components in $p - p$ collisions at $\sqrt{s_{NN}} = 200$ GeV," R. J. Porter, poster presentation, *The Seventeenth International Conference on Ultra-Relativistic Nucleus-Nucleus Collisons (Quark Matter 2004)*, Oakland, CA, January, 2004.

"Extracting two-particle correlations from fluctuation measurements," D. J. Prindle, poster presentation, *The Seventeenth International Conference on Ultra-Relativistic Nucleus-Nucleus Collisons (Quark Matter 2004)*, Oakland, CA, January, 2004.

"Large-scale two-particle p_T correlations in Au+Au collisions at $\sqrt{s_{NN}} = 200$ GeV obtained by inversion of $\langle p_T \rangle$ fluctuation scale dependence," D. J. Prindle, poster presentation, *The Seventeenth International Conference on Ultra-Relativistic Nucleus-Nucleus Collisons (Quark Matter 2004)*, Oakland, CA, January, 2004.

"Some comments on TPC tracking," H. Bichsel, *Invited lecture at ALCPG 2004 Winter Workshop*, SLAC, Stanford, CA, January, 2004.

"Measuring Newton's gravitational constant G," J. H. Gundlach, Indiana University, Bloomington, IN, February, 2004.

"Was Newton right? New Tests of the Inverse Square Law," B. R. Heckel, colloquium, University of Victoria, Victoria, Canada, February, 2004.

"Solar neutrinos - The dawning of a nu era," J. F. Wilkerson, Invited Talk, *AAAS Meeting*, Seattle, WA, February, 2004.

"Weighing the Neutrino," J. F. Wilkerson, Invited Talk, *APS Neutrino Study Workshop*, Pasadena, CA, February, 2004.

"Looking through the 'veil of hadronization': Pion entropy & PSD at RHIC," J. G. Cramer, plenary session invited paper presented at the *STAR Collaboration Meeting*, California Institute of Technology, Pasadena, CA, February, 2004.

"Event structure at RHIC from p-p to Au-Au," T. A. Trainor, *20th Winter Workshop on Nuclear Dynamics*, Trelawny Beach, Jamaica March, 2004.

"Preparation for space: Torsion balance fundamental physics experiments", J. H. Gundlach, *Fundamental Physics in Space: 2004 NASA/JPL Workshop*, Solvang, CA, April, 2004.

Conference presentations by collaborators of CENPA personnel:

"Strangeness production in heavy ion collisions at SPS energies," NA49 Collaborators (including J. G. Cramer, D. J. Prindle and T. A. Trainor), *Proceedings of the International Europhysics Conference on High Energy Physics*, Aachen, Germany, July 2003, submitted to JHEP, e-Print Archives (hep-ex/0311010).

"Large-scale two-particle number correlations in soft and semihard 200 GeV p-p collisions," R. J. Porter and the STAR Collaborators, American Physical Society, Tucson, AZ, Oct. 2003, Bull. Am. Phys. Soc. **48**, No. 8, 25 (2003), Sessin BD.

“Systematic studies in the emiT time reversal violation experiment,” L. Broussard and the emiT Collaborators, American Physical Society, Tucson, AZ, Oct. 2003, Bull. Am. Phys. Soc. **48**, No. 8, 3, 49 (2003), Session 8P.

“Pion interferometry from pp and d-Au collisions at RHIC,” T. Gutierrez and the STAR Collaborators (including H. Bichsel, J. G. Cramer, D. J. Prindle and T. A. Trainor), poster presented, *The Seventeenth International Conference on Ultra-Relativistic Nucleus-Nucleus Collisons (Quark Matter 2004)*, Oakland, CA, January, 2004, e-Print Archives (nucl-ex/0403012)

“Anisotropic flow in the forward directions,” M. Oldenburg and the STAR Collaborators, (including H. Bichsel, J. G. Cramer, D. J. Prindle and T. A. Trainor), poster presented, *The Seventeenth International Conference on Ultra-Relativistic Nucleus-Nucleus Collisons (Quark Matter 2004)*, Oakland, CA, January, 2004, e-Print Archives (nucl-ex/0403007).

“Azimuthal anisotropy: the higher harmonics,” A. Poskanzer and the STAR Collaborators (including H. Bichsel, J. G. Cramer, D. J. Prindle and T. A. Trainor, parallel session contributed paper, *The Seventeenth International Conference on Ultra-Relativistic Nucleus-Nucleus Collisons (Quark Matter 2004)*, Oakland, CA, January, 2004, to be published in Nuclear Physics, e-Print Archives (nucl-ex/0403019)

“Highlights from STAR,” K. Schweda and the STAR Collaborators (including H. Bichsel, J. G. Cramer, D. J. Prindle and T. A. Trainor), plenary session invited paper, *The Seventeenth International Conference on Ultra-Relativistic Nucleus-Nucleus Collisons (Quark Matter 2004)*, Oakland, CA, January, 2004, to be published in Nuclear Physics.

“STAR measurements of open charm production in d-Au collisions $\sqrt{s_{NN}}$ =200 GeV,” A. Tai and the STAR Collaborators (including H. Bichsel, J. G. Cramer, D. J. Prindle and T. A. Trainor), plenary session invited paper, *The Seventeenth International Conference on Ultra-Relativistic Nucleus-Nucleus Collisons (Quark Matter 2004)*, Oakland, CA, January, 2004, to be published in Nuclear Physics.

10.1 Degrees Granted, Academic Year, 2003-2004

A search for an Electron Antineutrino Signal in the Sudbury Neutrino Observatory, John Laurence Orrell (2004).